Strål säkerhets myndigheten
Swedish Radiation Safety Authority

Authors: Iradj Sattari-Far
Mikael Lorentzon

Research

2011:05

Overview and Evaluation of the NESC Projects for Fracture Assessments of Nuclear Components

Report number: 2011:05 ISSN: 2000-0456
Available at www.stralsakerhetsmyndigheten.se

SSM perspective

Background

The Network for Evaluation of Structural Components (NESC) was started in 1993 and since then six different projects have been carried out. A seventh NESC-project is still in progress. The overall objective of these projects has been to study the reliability of the entire process of structural integrity assessment within an international framework. The network is coordinated by the European Commission's Joint Research Centre (JRC) in Petten, Netherlands, and involves a large number of participants from different countries, including Sweden.

Objectives of the project

The main purpose of this Swedish study was to identify and compile all the NESC-results that are of particular importance to the safety assessment of components with cracks and to the determination and evaluation of in-service inspection intervals.

Results

The report presents a collection of the main features of each NESC-project including material characterization, crack configurations, loadings, fracture assessments and important observations. It also provides a comparison of different codes used in fracture prediction during the NESC-I test. Some important conclusions and recommendations for each of these projects can be found at the end of the report.

Future needs for research

At present there is no need for further research in this area.

Project information

Project leader at SSM: Kostas Xanthopoulos
Project number: SSM 2008/30, 2037012-25

Strål
säkerhets
myndigheten
Swedish Radiation Safety Authority

Authors: Iradj Sattari-Far and Mikael Lorentzon, Inspecta Nuclear AB,
Stockholm, Sweden

2011:05

Overview and Evaluation of the NESC Projects for Fracture Assessments of Nuclear Components

Date: February 2011
Report number: 2011:05 **ISSN:** 2000-0456
Available at www.stralsakerhetsmyndigheten.se

This report concerns a study which has been conducted for the Swedish Radiation Safety Authority, SSM. The conclusions and viewpoints presented in the report are those of the author/authors and do not necessarily coincide with those of the SSM.

SSM 2011:05

TABLE OF CONTENT

SUMMARY

The overall objective of the NESC network has been to examine the reliability of the entire process of structural integrity assessment within an international framework. Within this network, six projects were conducted under the period of 1993-2008. The main targets of these projects were:

NESC-I: This project evaluated the interactions among various technical disciplines applied to the integrity assessment of a large-scale thermally shocked spinning cylinder experiment. The cylinder test was designed to simulate selected conditions associated with an ageing flawed reactor pressure vessel.

NESC-II: This project was on brittle crack initiation, propagation and arrest of shallow cracks in clad vessels under PTS loading. The results of this project underlined the conservatism of existing defects assessment procedures for shallow RPV flaws.

NESC-III: This project was to quantify the accuracy of structural integrity assessment procedures for defects in dissimilar welds. The project was built around the conducted ADIMEW-project to share its overall objectives and to provide additional input.

NESC-IV: This project was an experimental/analytical program to develop validated analysis methods for transferring fracture toughness data generated on standard test specimens to shallow flaws in reactor pressure vessel welds subject to biaxial loading in the lower-transition temperature region.

NESC-V: This project aimed to develop a European multi-level procedure for handling of thermal fatigue phenomena in the nuclear power plant components. It also aimed to create a database of service and mock-up data for better understanding of thermal fatigue damage mechanisms.

NESC-VI: This project was an extension of the NESC-IV project. Embedded subclad racks in beam specimens under uniaxial loading were studied to study the transferability of fracture toughness data between different crack configurations.

This report gives an overview report of these six NESC projects. The reports cover the main features of each project including; crack configurations, loading, material characterization, fracture assessments and important conclusions. Also given in this report is a comparison of different codes in fracture prediction of the NESC-I test. Based on this review study, some important conclusions and recommendations useful for the Swedish NPP are given.

PREFACE

The Network for Evaluation of Structural Components (NESC) was launched in 1993 to undertake large-scale collaborative projects capable of serving as international benchmarks for validating the total structural integrity process. The network is coordinated by the European Commission's Joint Research Centre (JRC) in Petten, Netherlands, and including nuclear power plant operators, manufacturers, regulators, service companies, and R&D organizations from different countries.

Under period of 1993-2008, six NESC project have been conducted. The overall objective of these NESC projects has been to study the reliability of the entire process of structural integrity assessment within an international framework. Simulation of PTS transient loading of a flawed RPV represents a logical choice for the focus of that study because of the substantial structural assessment challenges posed by the problem. The objective was accomplished through NESC-I by organising the assessment process into component disciplines and examining topics that included NDE accuracy and reliability, material properties data requirements, test measurement techniques, and appropriate levels of complexity for thermal/structural analyses and fracture assessments. The effectiveness of those disciplines in fulfilling their functions was evaluated using data generated during all phases of a highly structured program.

An important goal of the NESC projects has been to reach a better understanding of the inter-dependencies among the component disciplines. In addition, results from those evaluations have been used:

- To identify deficiencies within current techniques that could benefit from further research.
- To identify important areas of uncertainty in the assessment process.
- To identify methodologies that are effective in application and make recommendations on best practice techniques.
- To explore the levels of conservatism within the existing structural integrity codes and standards, and where appropriate, to provide input for development of improved versions.

The main targets of the NESC projects were:

NESC-I: This project evaluated the interactions among various technical disciplines applied to the integrity assessment of a large-scale thermally shocked spinning cylinder experiment. The NESC-I spinning cylinder test was designed to simulate selected conditions associated with an ageing, flawed reactor pressure vessel subjected to severe pressurised thermal shock loading

NESC-II: This project was on brittle crack initiation, propagation and arrest of shallow cracks in a clad vessel under PTS loading. The results of this project underlined the conservatism of existing defects assessment procedures for shallow RPV flaws, and indicated the resistance to severe thermal shocks of degraded material containing simulated flaws.

NESC-III: This project studied the accuracy of structural integrity assessment procedures for defects in dissimilar welds. The NESC-III project was built around the conducted ADIMEW project to share its overall objectives and to provide additional input on a contribution-in-kind basis.

NESC-IV: This project was an experimental/analytical program to develop validated analysis methods for transferring fracture toughness data generated on standard test specimens to shallow flaws in reactor pressure vessel welds subject to biaxial loading in the lower-transition temperature region.

NESC-V: This project aimed to develop a European multi-level procedure for handling of thermal fatigue phenomena in the nuclear power plant components. It also aimed to create a database of service and mock-up data for better understanding of thermal fatigue damage mechanisms.

NESC-VI: This project was an extension of the NESC-IV project. Embedded subclad racks in beam specimens under uniaxial loading were studied to study the transferability of fracture toughness data between different crack configurations.

The main features of these six NESC projects are given in Table 1.

Table 1: Main information of the NESC projects.

	Defect geometry	Loading	Test temp. (^{o}C)	Duration
NESC-I	Deep surface and subclad cracks in thick cylinders	PTS	From 290 to 5	1993-2001
NESC-II	Shallow surface and subclad cracks in thick cylinders	PTS and axial tension	From 300 to 20	1999-2003
NESC-III	Surface cracks in dissimilar welds of pipes	Uniaxial bending	300	2001-2006
NESC-IV	Shallow surface and subclad cracks in beams	Uniaxial and biaxial bending	Between -100 and -40	2001-2006
NESC-V	Different types	Thermal fatigue	Between 64 and 280	2003-2006
NESC-VI	Shallow subclad cracks in beams	Uniaxial bending	Room temp.	2006-2008

For the NESC projects, different Task Groups were set up to carry out the work as follows:

TG1 - Inspection/Non-Destructive Evaluation (NDE)
TG2 - Material Properties
TG3 - Structural Analysis
TG4 - Instrumentation
TG5 - Co-ordination
ETF - Evaluation Task Force
DEAG - Destructive Examination Advisory Group

This report aims to give an overview description of all six NESC projects conducted so far. The report gives a collection of the main features of each project including; crack configurations, loading, material characterization, fracture assessments and important observations. Based on this review study, some conclusions and recommendations that may be useful for the Swedish nuclear power plants are given.

1 The NESC-I project

The NESC-I project was the first and the longest project among the six NESC projects that have been performed so far. It took more than 8 years (1993-2001) to conduct all the tasks within the project. NESC-I was sponsored jointly by the UK Health and Safety Executive (HSE) and the European Commission (EC). The countries participating in NESC-I were predominantly European (Austria, Belgium, Finland, France, Germany, Italy, Netherlands, Spain, Sweden, Switzerland, United Kingdom), along with Japan and the United States. Within those countries, more than 50 organisations have contributed to the NESC-I project since the launch of NESC in 1993.

1.1 GENERAL ASPECTS

The NESC-I project was the first and the longest project among the six NESC projects that have been performed so far. It took more than 8 years (1993-2001) to conduct all the tasks within the project. NESC-I was sponsored jointly by the UK Health and Safety Executive (HSE) and the European Commission (EC). The countries participating in NESC-I were predominantly European (Austria, Belgium, Finland, France, Germany, Italy, Netherlands, Spain, Sweden, Switzerland, United Kingdom), along with Japan and the United States. Within those countries, more than 50 organisations have contributed to the NESC-I project since the launch of NESC in 1993.

The project was focused on the total process of structural integrity assessment as applied to a fracture experiment involving a large, heated cylindrical specimen containing sharp defects (cracks) at or near the inner surface. A unique feature of the project was the inclusion of NDE as an integral part of a large-scale PTS fracture experiment, thus highlighting the influence of inspection data on RPV integrity assessments performed by structural analysts. A schematic of the different phases within the NESC-I project is shown in Fig. 1.1.

The NESC-I project covered the manufacture, testing, materials characterisation, instrumentation, non-destructive and destructive examinations, and structural/fracture assessments of the test cylinder. It tried to give an integrated assessment of the test, including an evaluation of interdisciplinary factors, relevance to reactor transients, technology transfer to nuclear and non-nuclear plant, and implications for national codes and standards.

Installation of different defects in the test cylinder was carried out by MPA-Stuttgart, Framatome and JRC/AEAT. All information regarding the fabrication, size and location of the defects was maintained secret throughout the pre-test and post-test NDE trials organised within the project.

Details of the activities conducted within the NESC-I project are given in Refs [I-1]-[I-6].

1.2 CRACK GEOMETRY AND LOADING

The test cylinder was manufactured from halves taken from the SC-4 and SC-6 (A 508 class 3) forgings previously tested at AEAT, with the yielded material machined from the inner surface. The specimen was welded in Germany, clad internally with austenitic steel in France, and finally heat-treated and machined in the UK. A total of 18 defects of varying sizes and types were introduced into the inner surface of the cylinder as below:

- Five Class A EDM notches were fabricated prior to the cladding process.
- Three large fatigue defects were included.
- Ten cracks were installed sub-clad in two groups to simulate cold and hot cracks.

Five of these defects were analysed through the project. Information of these defects are given in Fig. 1.2.

Post-weld and post-clad heat treatments of the NESC-I cylinder were conducted to essentially preserve the material and fracture toughness properties of SC-4 and SC-6. The pre-test inspection phase was conducted in a manner similar to that of the PISC trials to evaluate the effectiveness of current and proposed NDE procedures.

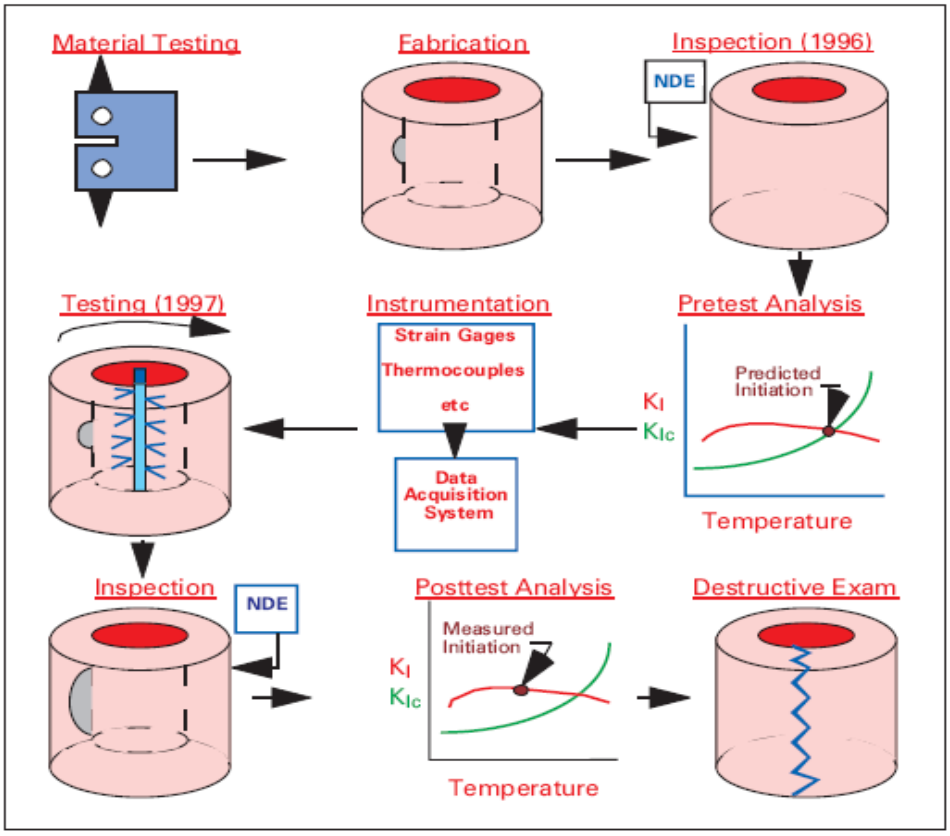

Fig. 1.1: Schematic of different phases within the NESC-I project.

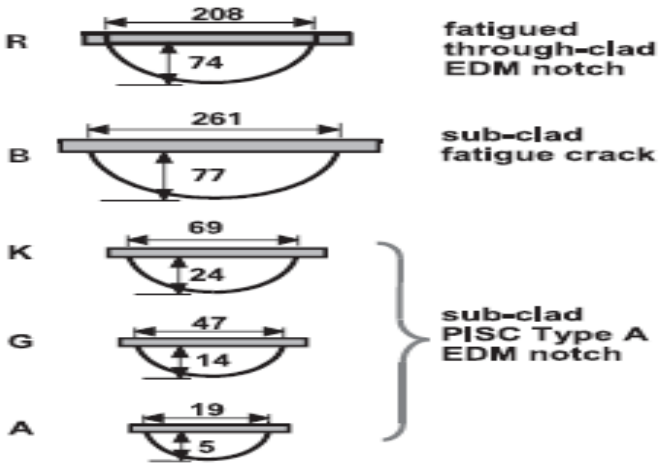

Fig. 1.2: Defects considered in the fracture assessment analysis of NESC-I.

The test was conducted by AEAT in March 1997. The facility suspended the specimen about its axis of revolution and was capable of rotational speeds up to 2500 rpm. Prior to start of the test, the cylinder was heated uniformly to upper-shelf temperatures (293 °C). The planned thermal shock was applied by a water spray quench (2 °C) of the inner surface which was initiated when the cylinder reached a rotational

speed of 2,100 rpm. The quench continued for 12 minutes during which time the rotational speed was increased to a maximum of 2,400 rpm. A step change in output from certain strain gages was observed between 213 and 217 s and implied that the large through-clad flaw had experienced cleavage initiation at one end.

After the test, the large defects were opened at low temperature (in liquid nitrogen) to permit metallographic/fractographic studies of the fracture surfaces. Selected smaller notches were also opened for study, while others were left unopened and evaluated using high-quality X-ray images of the individual blocks. These examinations confirmed that the large through-clad flaw exhibited ductile tearing in the base and clad/HAZ material, which tripped to cleavage at one end under the clad/HAZ layer. The cleavage event arrested following a total flaw extension of approximately 12-15 mm just below the clad/HAZ region, thus confirming that a major objective of the experiment had been achieved. An unexpected result from these studies was the identification of substantial regions of intergranular fracture around the large sub-clad defect.

The main features of the thermal transient scenario used for the fracture assessments of the NESC-I test are in Fig. 1.3.

1.3 MATERIAL CHARACTERIZATION

The Materials Task Group (TG2) of NESC was responsible for conducting a comprehensive materials characterisation-testing programme to determine the physical, mechanical and fracture toughness properties of the forging, heat-affected zone (HAZ) and cladding of the cylinder specimen. Those data provided an essential part of the required input for thermal, structural and fracture mechanics analyses that were carried out by the Structural Analysis Task Group (TG3) during the pre-test and post-test phases of the project. TG2 focused on the following objectives:

- Provide adequate and reliable data as required by the Structural Analysis Task Group to carry out thermal/structural/fracture analyses of the cylinder;
- Study constraint effects on fracture toughness of the forging material;
- Evaluate the effects of an extra tempering treatment (post-weld heat treatment) on fracture toughness of the forging material and on the properties of the cladding and heat-affected zone;

The NESC-I cylinder specimen was fabricated from A 508 Class 3 steel subjected to a non-standard heat treatment to simulate radiation embrittlement of an RPV steel. The fabrication process utilised the remaining arcs of the previously tested cylinders SC-4 and SC-6. Summaries of the fabrication histories for these test cylinders and the chemical compositions of the base and cladding materials are given in Table 1.1.

Mechanical and thermal properties

Miniature tensile specimens were taken from the clad layer in the L orientation with respect to the welding direction. Tensile specimens were drawn from the HAZ in the L orientation referenced to the main forming direction during forging. The HAZ layer varied in thickness from 5 to 10 mm and the specimens were extracted at slightly different depths to sample material in four distinguishable categories defined for the HAZ. Properties of Young's Modulus, Poisson ratio, coefficient of thermal expansion, thermal conductivity, specific heat capacity and density were determined at temperatures of 25 °C and 300 °C. Linear relations approximating the temperature dependence of the elastic and thermal properties are given in Table 1.2.

Initial temperature:	290 °C
Quenching temperature:	5 °C
Initial spinning speed:	2100 rpm
Final spinning speed:	2280 rpm
Acceleration time:	5 minutes
Total test time:	12 minutes

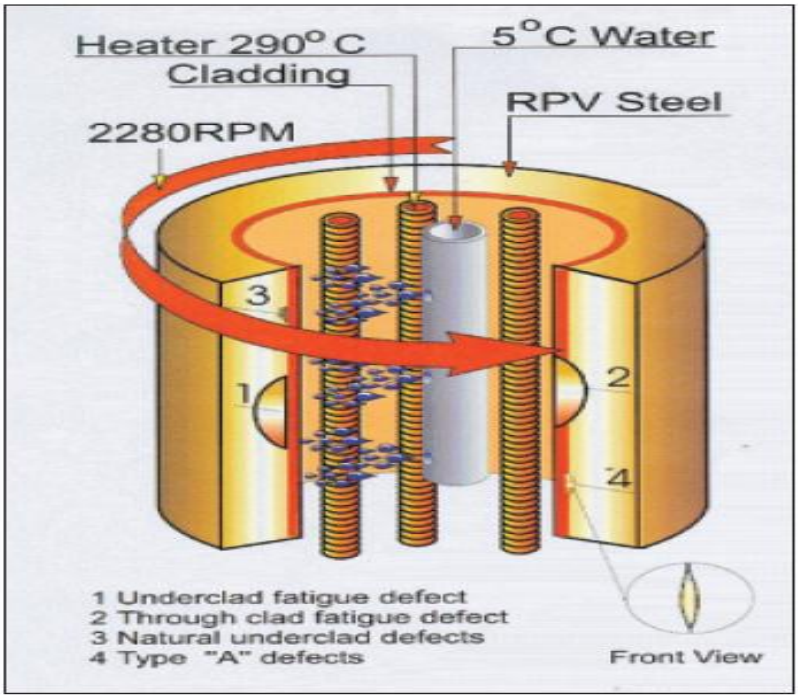

Fig. 1.3: Schematic of the NESC-I spinning cylinder test.

Table 1.1: History of test cylinders SC-4 and SC-6.

- Forging produced by Forgemasters Engineering, UK
- Heat treatment
  - Austenization: 6 h at 950 °C
  - Quench: Water quench from 950 °C
  - Temper: 8 h at 580°C ± 10°C
- Spinning cylinder tests at AEA Technology, Risley, UK
  - Quench, initial temperature: 300 °C
  - maximum rotational speed: 530 rpm (SC-4); 2000 rpm (SC-6)
  - maximum heat transfer coeff.: 22,000 W/m °C

	C	Si	Mn	S	P	Cr	Mo	Ni
Base Material	0.23	0.23	1.32	0.011	0.012	0.08	0.50	0.73
Cladding	0.025	1.50	2.0	0.025	0.03	19.0	-	10.0

Table 1.2: Temperature dependence of elastic and thermal properties for the NESC-I materials.

Property		Base/HAZ	Cladding
Young's Modulus, E	(GPa)	211.7 - 0.0682T (°C)	150.2 - 0.0862T (°C)
Poisson ratio, ν		0.28	0.28
thermal conductivity, κ	(W/m °C)	40.6 - 0.0097T (°C)	13.9 + 0.018T (°C)
specific heat capacity, c_p	(kJ/kg °C)	$4.1x10^{-4}T + 0.432$	$4.1x10^{-4}T + 0.432$
coefficient of thermal expansion, α	(μm/m °C)	11.6 + 0.014T (°C)	15.7 + 0.0096T (°C)
density, ρ	(kg/m³)	7800 (20 °C) 7720 (290 °C)	7720 (20 °C) 7610 (290 °C)

True stress versus true plastic-strain curves were constructed from tensile test data as functions of temperature for the base forging, HAZ and clad layers. The tensile tests were performed at 20 °C, 150 °C and 300 °C in an air environment. Mean curves fitted to the tensile data are depicted in Fig. 1.4.

Hardness measurements and optical microscopy were performed to determine the shape and thickness of the cladding and HAZ. The thickness of the HAZ varied in the range from 5 to 10 mm. Curves depicted in Fig. 1.5 illustrate the elevation in hardness measured across the maximum HAZ width position. Hardness values in the thin part of the HAZ were slightly higher than those in the thickest part.

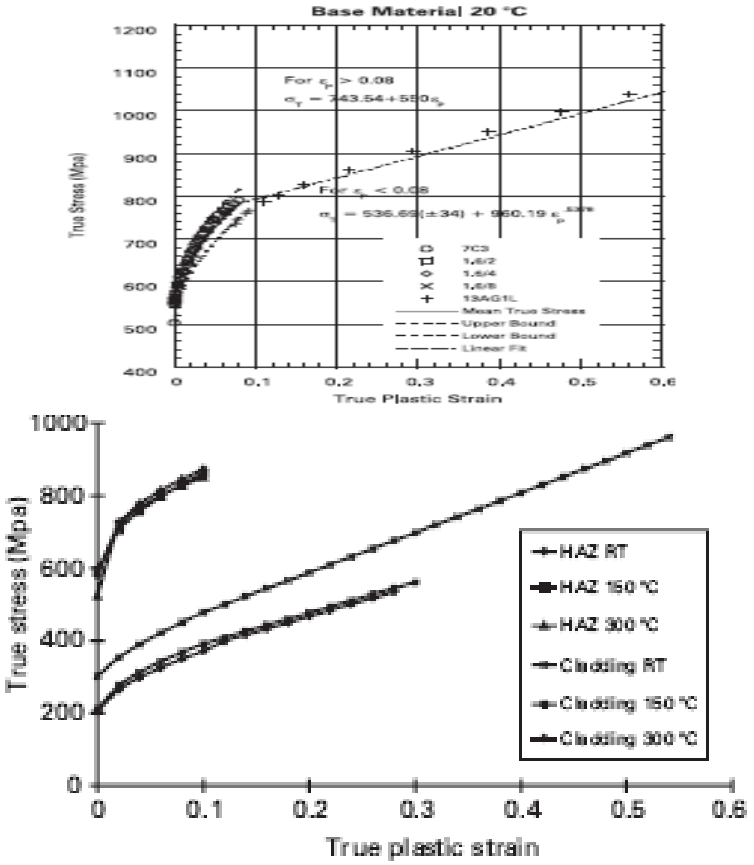

Fig. 1.4: True stress - true plastic strain curves of the NESC-I materials.

Fracture toughness testing

Static fracture toughness testing was carried out using the ESIS P2-92 and ASTM 1152-87 standards applied to CT specimens and three-point bend specimens (thickness of 2.5, 5, 10 and 25 mm). The fracture toughness data were analysed by the Master Curve Approach. Fracture toughness curves of the base material corresponding to the 5, 50 and 95 percent fracture probabilities are given in Fig. 1.6.

The Master Curve reference temperature for the base metal and the HAZ were determined to be To = 68 °C and 16 °C, respectively. Tests were also conducted on the base material using three-point bend specimens (thickness of 25 mm) with a/W ratios of 0.1 and 0.5 to study shallow crack effects on cleavage fracture toughness in the transition temperature region. The shallow crack data generated from the a/W = 0.1 specimens implied a transition temperature of To = 32 °C.

The J-resistance data for the cladding, HAZ and base metal were determined according to the ESIS P2-92 procedure utilising the single specimen technique that allows for crack growth. Testing was conducted by ECN, ENEL and IWM. The fracture toughness data for each material in terms of J- Δa curves are given in Fig. 1.7.

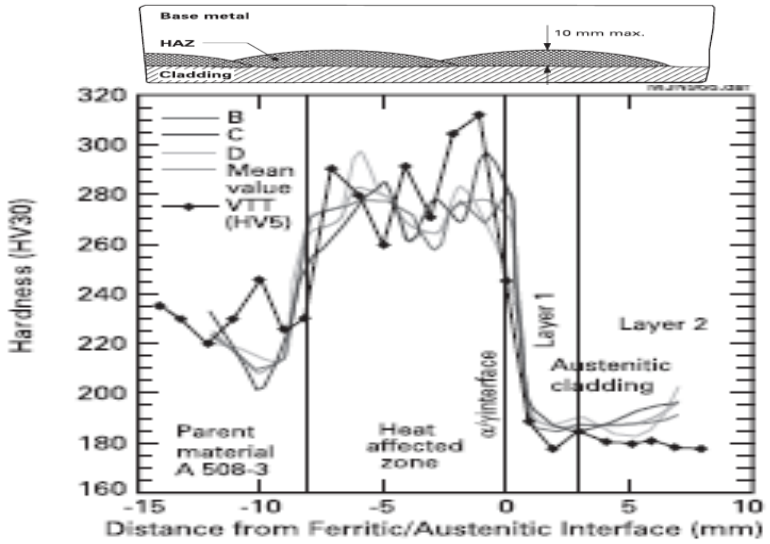

Fig. 1.5: Hardness distribution measured across the cladding/HAZ in the NESC-I cylinder.

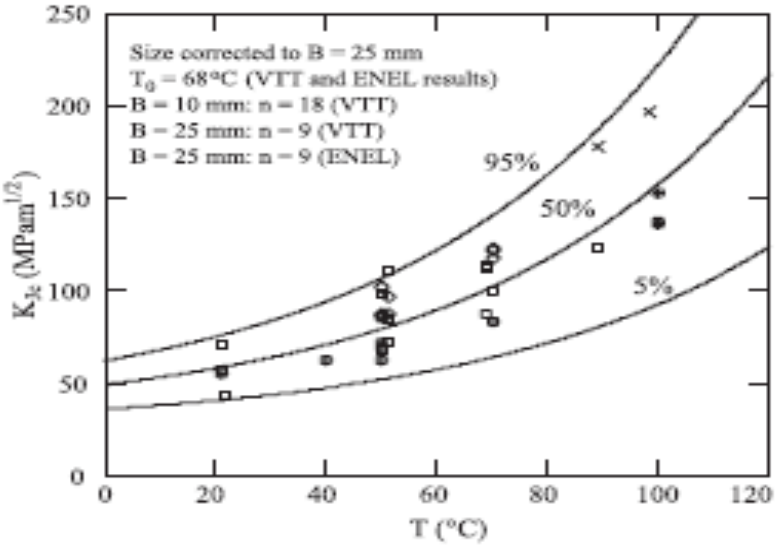

Fig. 1.6: Static fracture toughness of the base metal with specimen thickness 10 mm and 25 mm.

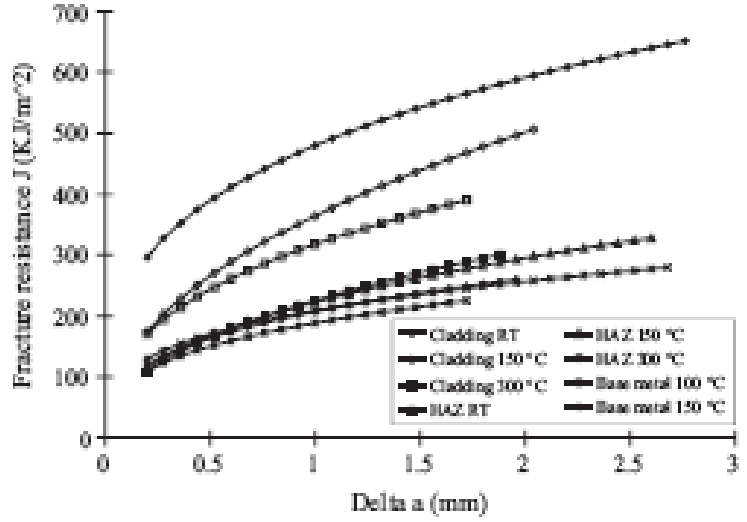

Fig. 1.7: Mean *J-Δa* curves for the base metal, HAZ and cladding.

1.4 FRACTURE ANALYSIS

The Structural Analysis Group (TG3) of the project organised pre-test analyses both simplified and sophisticated analytical techniques. After the test was performed, the TG3 members conducted post-test analyses that included the influencing factors in fracture assessment of the defects.

Pre-test analysis

A series of thermal, structural and fracture mechanics analyses were performed to generate pre-test predictions for defect behaviour during the proposed spinning cylinder test. These analyses were based on the defect dimensions recorded during the inspection trials conducted by TG1 and on the material properties database developed by TG2. Predictions were given in terms of the extent of crack growth by ductile tearing and the time to cleavage initiation during the thermal shock transient. The analysis matrix included those defects in the cylinder that were perceived to have significance for the structural integrity assessment process.

The pre-test analyses focused on five defects shown in Fig. 1.2. Comparisons of thermal and stress analyses performed for the pre-test analysis matrix are provided in Fig. 1.8. It showed very good agreement in the temperature results, and rather good agreement in the stress results. Differences in the stress distributions near the inside surface of the cylinder are due to variations in approach to modelling of the clad and HAZ regions.

Fig. 1.9 showed the prediction of ductile tearing and cleavage fracture mechanisms in the form of K versus crack tip temperature curves for a finite-element model of through-clad defect R. It includes the cleavage fracture toughness confidence curves (5-95%) from small-specimen data and the ductile tearing toughness curves corresponding to 0.1, 0.5 and 2 mm crack growth. No brittle fracture initiation was expected at P9 because only the decreasing branch of KI intersects the scatter band of cleavage fracture toughness, indicating a warm pre-stressed condition. Furthermore, comparison of the applied KI curve for point P6 with the fracture toughness confidence curves implies a high probability of cleavage fracture initiation after approximately 150 s.

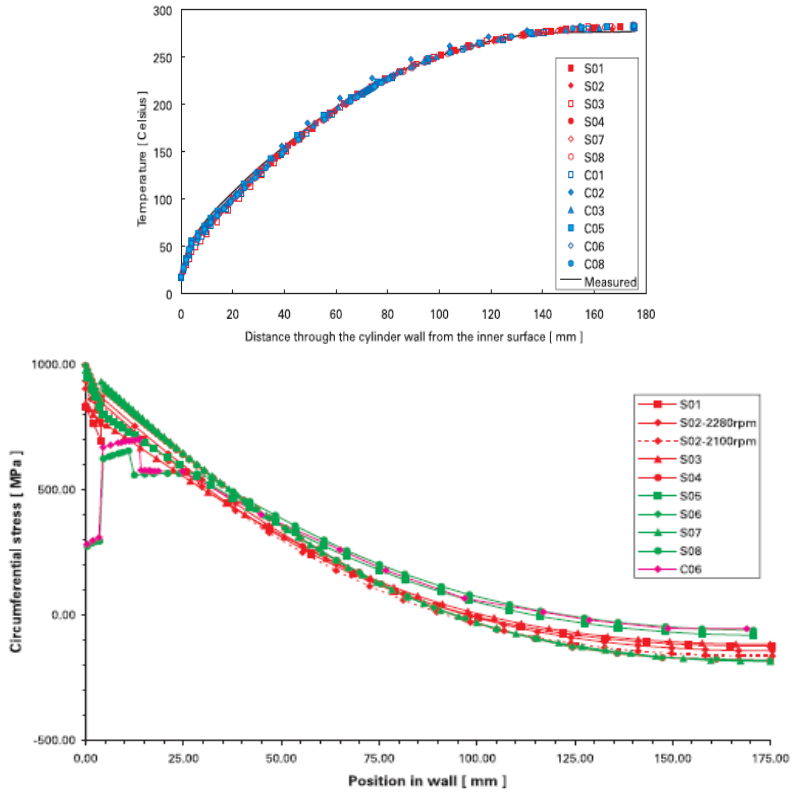

Fig. 1.8: Through-wall temperature and circumferential stress distributions computed at 300 seconds into the transient obtained from the pre-test analyses.

Fig. 1.10 depicts a summary of fracture assessments performed for the large through-clad defect R at (or near) the HAZ/base metal interface. It was observed that the spread in results for the simplified approaches is larger than that for the 3-D finite-element analyses. The pre-test fracture assessments predicted that the large defects in the spinning cylinder would initiate in the base metal immediately beneath the HAZ and extend in the axial direction; no cleavage extension was predicted in the radial direction (i.e., into the cylinder wall).

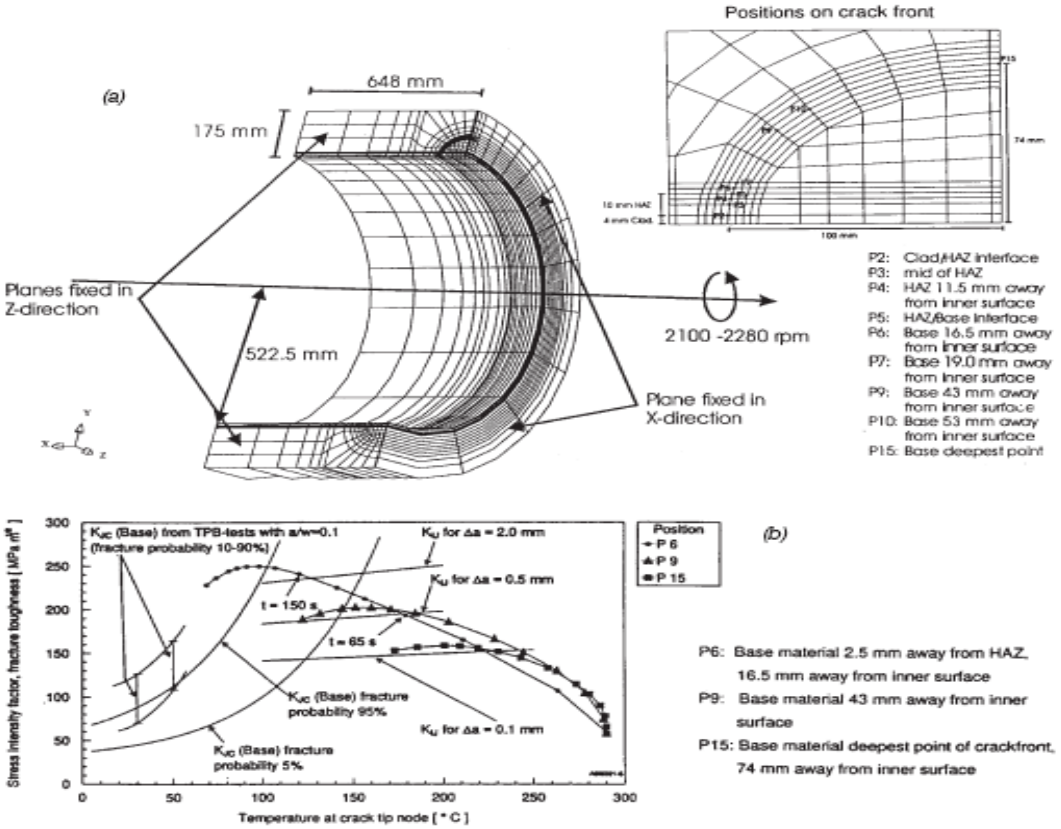

Fig. 1.9: Pre-test fracture assessment of different crack front positions in base metal of defect R.

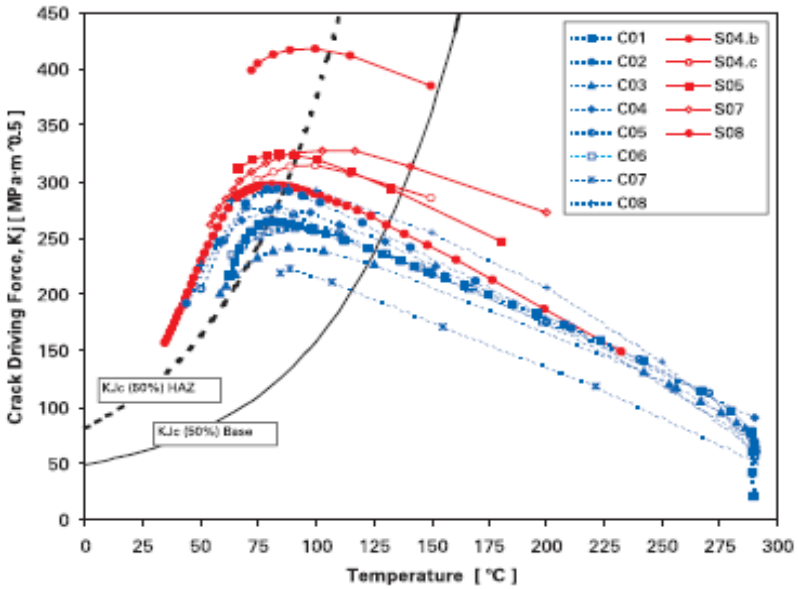

Fig. 1.10: Computed stress-intensity factor versus crack-tip temperature at HAZ/base metal interface of defect R in the pre-test analyses.

Post-test analysis

Post-test analyses incorporated the loading conditions recorded during the test and the initial defect dimensions determined during the destructive examination of the cylinder. Fracture assessments were carried out both in the context of a Master Curve methodology and a coupled cleavage-ductile local approach formulation. Consideration was given to other factors that were likely to have influenced behaviour of the large defects during the thermal shock transient.

The majority of the post-test studies exploited the Master Curve description of material toughness to infer the probability of a cleavage event. A schematic drawing of the idealised defect R is shown in Fig. 1.11. The two near-surface crack tips are asymmetrically sited in 'narrow' HAZ (nominally 5mm) as seen on the left and 'wide' HAZ (nominally 10mm) as seen on the right. Results of the analyses on these two defects are briefly given below:

Master Curve analysis of surface defect R

- At point 6 located 11.5 mm below surface in BM and near HAZ/BM interface, the results predict a failure probability of Pf = 1.0; the temperature range is such that ductile tearing would be expected before failure by cleavage. The actual behaviour was that no cleavage was observed, although several millimetres of tearing occurred at this point. The amount of ductile tearing was predicted to be greater than 5 mm, based on data at 150 °C.

- At point located 16.5 mm below surface at cleavage initiation site, the results indicate Pf = 1.0 for probability of cleavage fracture. The actual event at this point was initiation of a cleavage fracture after some 3 mm of stable tearing.

- At point located 28 mm below surface, the results predicting low cleavage probability and ~4 mm of stable tearing are consistent with observed behaviour.

- At position located approximately 70 mm below the surface, the results predict zero probability of cleavage initiation; the temperature is sufficiently high that only ductile tearing would be expected. The actual fracture surface shows small cleavage facets close to the base of the crack.

The K-T of defect R at different positions along the crack front are shown in Fig. 1.12.

Maste Curve analysis of defect B

This required estimates of K, T under peak driving force conditions since no cleavage event could be identified. Results from the conducted analyses provided some evidence of possible constraint effects up to a distance approximately 14 mm into the cylinder wall, i.e. up to the HAZ/BM interface. At a point 9 mm below the surface (in the middle of the HAZ), predictions were for stable tearing in excess of 5 mm, followed by a cleavage event (Pf = 1.0). While no cleavage occurred, ductile tearing up to 4.5 mm was observed.

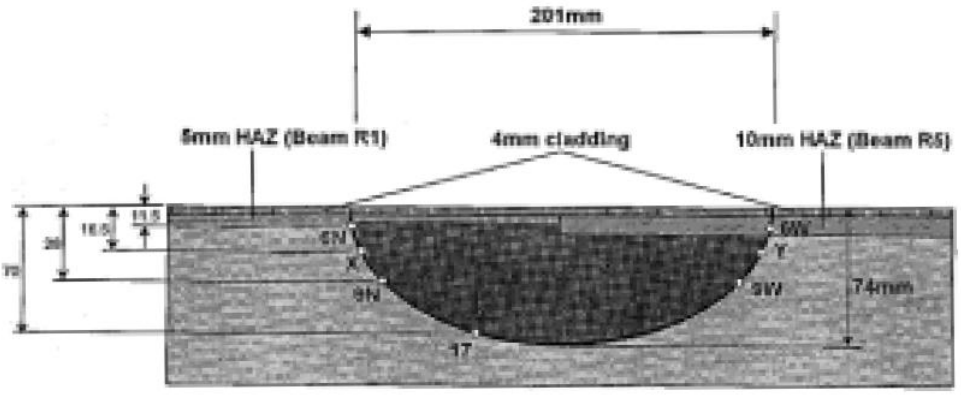

Fig. 1.11: Schematic drawings of the through-clad defect R.

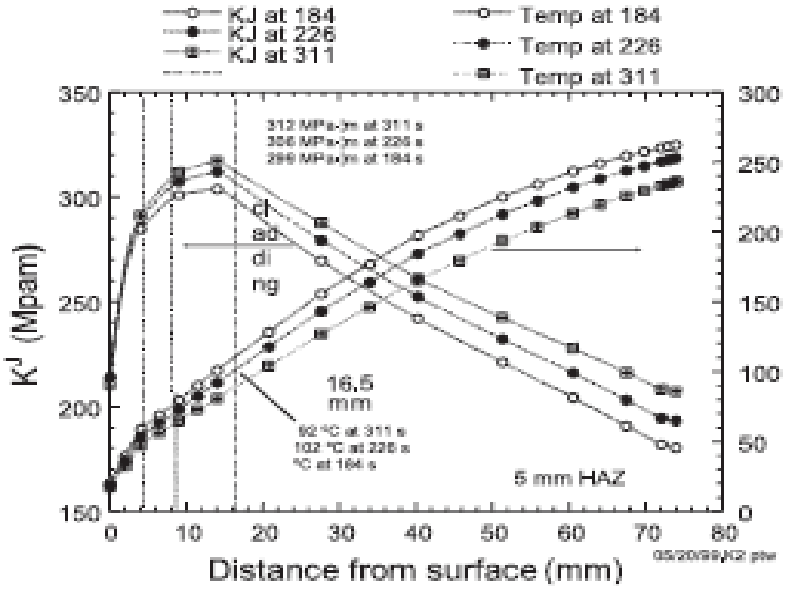

Fig. 1.12: Driving force transients for the through clad defect R assuming a narrow 5 mm HAZ.

1.5 SOME IMPORTANT OBSERVATIONS

Structural assessment of the local cladding failure

The analysis indicated that the cladding above subclad defect B experienced very high circumferential stresses and high levels of plastic deformation during the test. For the cladding above the deepest point of the defect, these stresses were sufficiently high to produce conditions for plastic collapse and rupture. These calculations are consistent with the extent of deformation and failure actually incurred by the cladding over defect B during the experiment.

Constraint Effects

Constraint is a key factor in the transferability of fracture toughness data generated on standard specimens to defects in actual components. The conventional approach of applying fracture data relevant to plane strain (i.e., high constraint conditions) may introduce an unnecessary level of conservatism in many situations.

Constraint consideration of the test indicated that the low-constraint region extends just beyond the HAZ/BM interface. That prediction is reasonably consistent with the observation that no cleavage initiation occurred close to the HAZ boundary in either of the defects R and B, although it would have been expected from computed failure probabilities based on deep-notch fracture toughness data.

Gradients in material properties

The fact that defect R did not initiate in cleavage at the wide HAZ end, although it was predicted to do so prior to t = 311 s, cannot be explained satisfactorily either in terms of reduced crack-tip constraint at that location compared with position X, or by the modest reduction in the driving force due to the increased HAZ thickness. Instead the absence of a cleavage event is thought likely to be linked to the fact that even below the HAZ, the toughness will decrease gradually back to the nominal base material level. Where the HAZ is deepest, this region could have extended over the region in which a cleavage event was anticipated. Post-test examinations confirm that the base material hardness was modified to a depth of approximately 10 mm below the visible HAZ boundary.

Evidence For Warm Pre-Stressing Effects

In PTS analysis of RPVs, warm pre-stressing (WPS) effects refer to the delaying of cleavage initiation in

the latter stages of the transient during which both the crack driving force and the temperature are decreasing. Since the NESC-I test was designed to achieve a cleavage event at the large defects, care was taken to avoid WPS by choosing a lower starting temperature and by accelerating the spin velocity at an appropriate moment to maintain an increasing crack driving force.

The fact that the desired cleavage event was achieved at the large through-clad defect R shows that WPS effects were absent (or not significant) at that position at the moment of initiation. Therefore, the assessment of the role of WPS was limited to areas where no cleavage occurred, i.e. in the BM of the cylinder wall located away from the HAZ/BM interface.

Cladding Effects

In terms of structural analysis, the cladding is important in several ways:

- The severity of the PTS can be diminished on account of the lower thermal conductivity of the austenitic clad with respect to the ferritic BM.
- Beneficial warm pre-stressing effects (WPS) are more likely since the crack driving force reaches a maximum at a higher temperature.
- The presence of cladding above sub-clad defects can mechanically impede their opening.
- The clad residual stresses arising from thermal mismatch can influence the driving force estimates.
- For many codes and standard assessment procedures, the cladding mechanical properties cannot be taken into account, however the overall assumed defect depth must include the clad thickness. For small sub-clad defect this can be a significant penalising factor.

The defect B has been simulated as both a through- and sub-clad flaw to quantify this beneficial influence of the cladding on crack driving forces in the near-surface region. It was shown that an intact cladding above defect B reduces the local crack driving forces by up to 24%.

Destructive examination

Crack extension was observed along the entire crack front of defect R. Initial tearing was followed by a significant local cleavage event in the region just below the clad HAZ, as can be seen in the upper part in Fig. 1.13. In this region, the maximum crack extension was measured to be 17 mm. The point of initiation for this cleavage event is about 16.5 mm below the clad surface. The subsequent SEM examination confirmed that the initial extension was by ductile tearing before the cleavage event was triggered. Within the HAZ little ductile tearing is evident. However, a finger of brittle intergranular fracture can be seen in Fig. 1.13 that propagated in the axial direction of the cylinder; this may be linked to a more brittle segregated zone.

Crack extension occurred along the entire initial crack front in the large sub-clad defect B, as illustrated schematically in Fig. 1.14. The maximum crack extension of 15 mm had occurred just below the HAZ. At the deepest part of the defect, the crack extension was up to 4.5 mm. At the end of the defect, the mechanism of extension was mainly intergranular cracking, whereas at the opposite end it was initially intergranular, followed by evidence of ductile tearing. At deeper positions of the defect front the ductile tearing mode became predominant. Along the tip of the fatigue defect there was evidence of a large stretch zone, indicating that a considerable driving force was needed to initiate the crack advance.

Codes and standards approach

Defects found during manufacture or in service are normally assessed using the rules of the appropriate national design or defect assessment code. These rules are designed to yield pessimistic results, so that an adequate safety margin can be maintained in service. They are therefore not suitable for best estimate test

predictions. Summary results of the assessments based on the different codes and standards are given in the following table. Some conclusions and issues related to these assessments are given below:

- There is a surprising measure of agreement between the different codes, despite the differences in methodology. All agree in predicting very shallow acceptable defects.
- All the assessments predict very small allowable defect depths, in the range 1 mm to 9 mm deep. These contrast with behaviour during the test, in which only limited crack growth took place from defects 75-80 mm deep.
- The pessimism in the code assessments is due both to overestimates in the crack driving force and to the use of pessimistic material properties for shallow cracks.
- Code-based methods are more pessimistic when applied to the near-surface regions of defects than when applied to the maximum depth points. The pessimism of code-based methods applied to shallow sub-clad defects is excessive.
- For large surface defects through the cladding, standard assessment techniques provide a good estimate of crack driving force at the maximum depth point, although care must be taken defining the defect position and dimensions.
- For smaller sub-clad defects, standard assessment methods are very pessimistic compared with cracked body analyses. This is caused primarily by the assumption that the cladding is ineffective, which is manifestly untrue.
- Most code assessments deliberately use lower bound fracture data, either as measured 5% failure probability curves or as a lower bound design curve. Clearly this introduces pessimism, but it is necessary pessimism. Some codes then require additional safety factors on this lower bound data.

Constraint effects are difficult to quantify, so are generally ignored in code assessments. They affect shallow defects and the near surface regions of large defects.

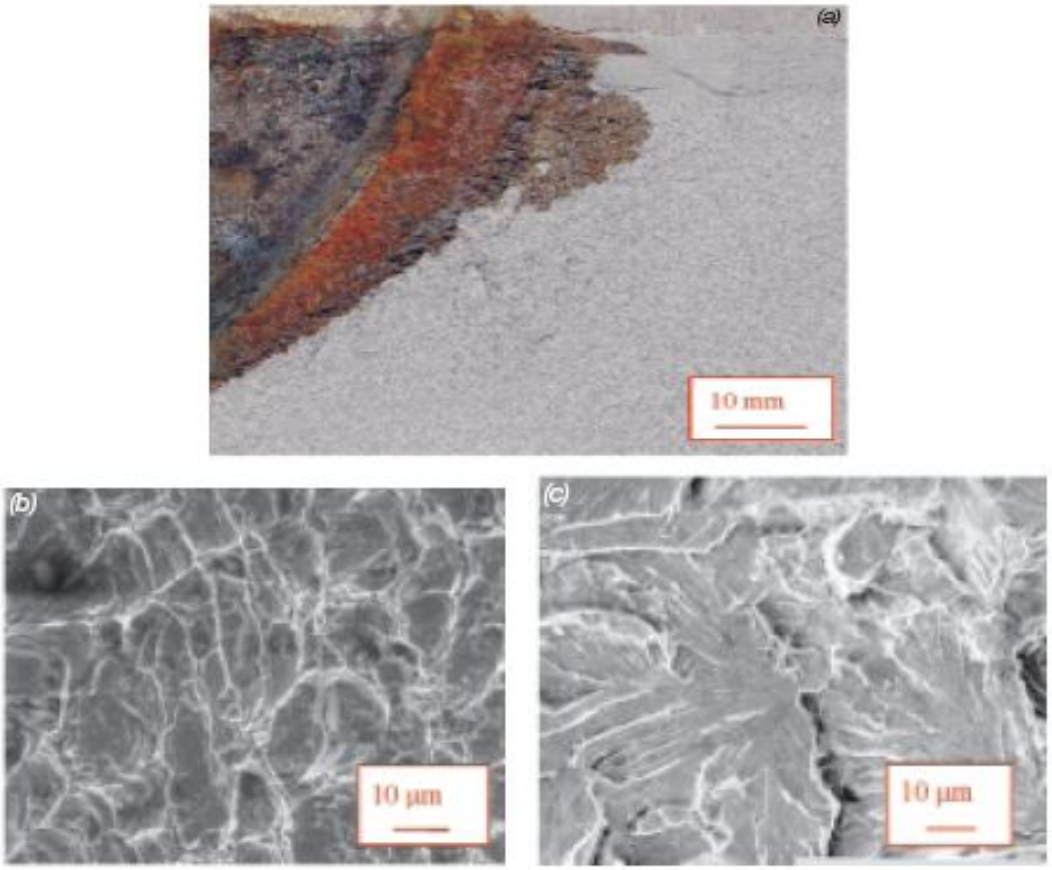

Fig. 1.13: Fracture surface of defect R showing the crack propagation and cleavage event site.

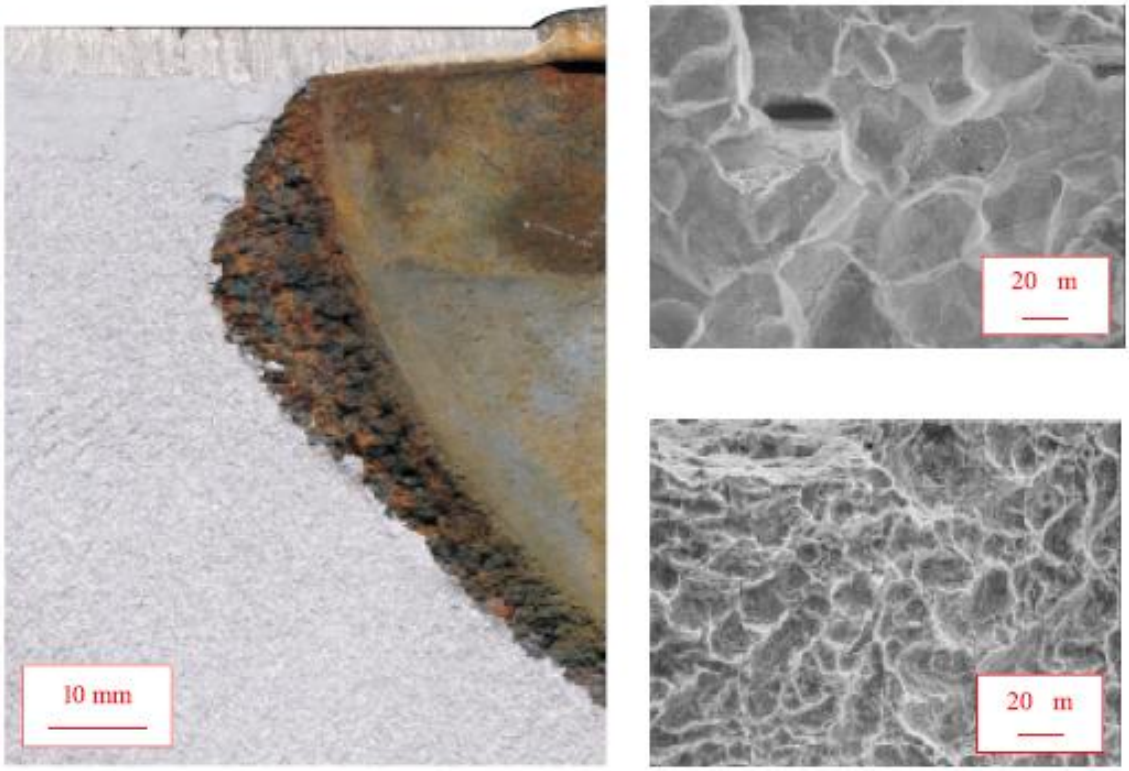

Fig. 1.14: Detail of the fracture surface of defect B showing the area of maximum extension.

Item	R6	SKIFS 1994:1	KTA	ASME XI	PD 6493:1991	RCCM/RSEM
Initial screening used?	No	No	No	Yes – all defects fail	No	No
Thermal and stress analysis methods	Elastic FE using ABAQUS, from BE NESC-1 pre-test prediction	Elastic FE using ADINA, from IWM/PreussenElektra NESC-1 pre-test prediction.	Elastic FE using ADINA, from IWM/PreussenElektra NESC-1 pre-test prediction.	Elastic, using FAVOR code – spin simulated within FAVOR by an equivalent pressure	Elastic FE using ABAQUS, from BE NESC-1 pre-test analyses.	Elastic, using CALORI Therman Analysis using finite differences, Stress Analysis using analytical formulations
Stress components	Primary Spin stress Secondary thermal shock stress No weld residual stress	Primary Spin stress Secondary thermal shock stress No weld residual stress	Spin and Thermal shock, with no distinction between primary and secondary loads No weld residual stress	Equivalent pressure and Thermal shock, with no distinction between primary and secondary loads No weld residual stress	Primary Spin stress Linearised secondary thermal shock stress 150 MPa weld residual stress	No distinction between Primary and Secondary Stresses, No weld residual stress
Handling of cladding	Present in thermal and stress analyses. Removed for fracture assessment	Present in thermal and stress analyses Considered in fracture assessment	Present in thermal and stress analyses Removed for fracture assessment	*? not clear*	Present in thermal and stress analyses. Removed for fracture assessment	Present in thermal and stress analyses. Present in Under-clad fracture assessments
Flaw model	Surface semi-elliptic defect a/2c=0.333 (3:1)	Surface semi-elliptic defect, a/2c~0.333	Surface semi-elliptic defect, a/2c=0.16 (6:1)	Surface semi-elliptic defect, a/2c=0.42	surface semi-elliptic defects, a/2c=0.5, 0.16	Surface semi-elliptic defect, a/2c=0.333 Elliptic defect buried beneath cladding
Assessment points	Surface point (applied to clad interface) and maximum depth	Surface point and maximum depth	Surface point and maximum depth	Near-surface (20□) and maximum depth	Maximum depth only	Surface, maximum depth, and bi-metallic interface

Item	R6	SKIFS 1994:1	KTA	ASME XI	PD 6493:1991	RCCM/RSEM
SIF calculation method	R6Code software– 8th order polynomial, defect in cylinder	SACC software (solution based on Newman-Raju with up to 3rd order polynomial fit)	Newman-Raju	FAVOR code – *3rd order polynomial fit?*	CrackWise software(uses Newman-Raju with linearised stresses)	CALORI code
J estimation method	R6 Rev 3 Option 1	R6 Rev 3 Option 1	LEFM with SSY correction	None – LEFM	Based on R6 Rev 2, Option 1	LEFM with plasticity correction
consideration of structural collapse.	R6Code, global collapse	SACC, global collapse	None	None	CrackWise, *local collapse*	None
Metal temperature assumptions	At clad interface and max depth	Appropriate to tip position	Appropriate to position	Appropriate to position	Appropriate to position	Appropriate to position
Yield strength	345 MPa (ASME)	345-302 MPa (ASME)	500 MPa	Not used	458 MPa	NESC-1 data, with temperature variation
Fracture toughness	NESC-1 deep crack 5% failure probability lines for HAZ (surface point) and Base (max depth) Lower bound ductile initiation and 2mm tearing from NESC-1 data	Base: K_{Ia} based on RT_{NDT}=101°C – K_{Ia}^{max} is 220 MPa√m HAZ: K_{Ia} based on RT_{NDT}=50°C Clad K_i=186 down to 122	NESC-1 base material shallow flaw 50% failure probability with safety factor	ASME K_{IC} (emergency/faulted), RT_{NDT}=115□C NESC-1 deep crack 5% failure probability lines for base material	NESC-1 deep crack 50% failure probability lines for base material NESC-1 shallow crack 50% failure probability lines for base material	Base: K_{IC} from RCCM code with RT_{NDT}=101□C. Cladding: NESC-1 data
Failure criteria	>2mm tearing on upper shelf Cleavage initiation	Clad initiation ASME K_{Ia} in HAZ and base.	Cleavage initiation	Cleavage initiation	Cleavage initiation Crack arrest also considered	Cleavage initiation in base material Tearing *initiation* in the cladding

Item	R6	SKIFS 1994:1	KTA	ASME XI	PD 6493:1991	RCCM/RSEM
Handling of WPS	Allowed if no prior tearing	Not mentioned	Allowed – no comment on prior tearing	Not mentioned	Not mentioned	Not allowed
Safety Factors	None specified	Flow stress = 2.4Sm, not standard R6 K_i – √2 for emerg/fault, √10 for norm/upset Lr – 1.2 for emerg/fault, 2.4 for norm/upset	1.5 on K_{IC}	√2 on toughness curve	None specified	*Based on RCCM code* *(Appropriate code is RSEM: at present Safety Margins are under discussion)*
Final critical/acceptable flaw size	Surface point: 6.8 mm Max depth: 1.8 mm (emergency/faulted)	Emergency/faulted: 5.7 mm Normal/Upset: 1.2 mm	9 mm with WPS 3 mm no WPS 14 mm no WPS, No SF	1.2 mm (ASME Kic/√2) 1.5 mm (KJC 5% /√2)	a/2c=0.5: 2 mm a/2c=0.16: 4 mm (deep crack data, cleavage initiation)	Less than 1 mm

2 The NESC-II project

2.1 GENERAL ASPECTS

The tests planned in NESC-II simulated an irradiated material. The combination of the shallow defect geometry, the loading configuration and the low toughness material condition presented a distinct challenge from that addressed in the NESC-I experiment, while allowing the network to build on experience of the lessons learned for applying an integrated assessment approach.

The testing concept utilises a thick-walled hollow cylinder that was welded at both ends to the grips of a 100 MN tensile testing machine. In addition to axial load, the specimens were loaded by internal pressure (pressurised water up to 300 bar and 300°C). The thermal shock cooling was achieved by spraying cold water evenly over the inner surface of the cylindrical specimen.

In 1996 a project was launched with the sponsorship of the German Federal Government, first under the control of the Ministry for Education and Research (BMBF), and later taken over by the Ministry for Economics and Technology (BMWi). The planned tests were to show the influence of the cladding on the behaviour of cracks in the base material in the transition regime of fracture toughness under the PTS loading. The programme foresaw two tests: the first, denoted NP2, would be carried out on a test component containing a fully circumferential sub clad crack. The second, NP1, would contain two semi-elliptical surface breaking defects.

In July 1998 MPA-Stuttgart contacted the NESC Network Management to propose that these two PTS experiments be adopted as the core of a new NESC project. It was foreseen that NESC participation could provide:

- Important additional data concerning the influence of the clad/HAZ region on the fracture behaviour of shallow through and sub-clad defects, the size and geometry of which have great relevance to RPV assessment for emergency cooling transients i.e. PTS.
- Additional experience with material characterisation and fracture toughness measurements in RPV material subject to cladding processes.
- Further confirmation of the predictive capabilities of fracture mechanics and micromechanics analysis methods applied to this type of problem
- Further confirmations about the sizing capabilities of NDE methods applied to through-clad and sub-clad defects in RPV materials.

Details of the activities conducted within the NESC-II project are given in Refs [II-1]-[II-4].

2.2 CRACK GEOMETRY AND LOADING

Two cylinder test pieces were designed to meet the test objectives. One cylinder with the designation NP1 contained two semi-elliptic through clad circumferential cracks. The other cylinder with the designation NP2 contained one circumferential crack buried under the cladding. Fig. 2.1 shows the geometry information of these two cylinders.

For static loading, a tensile testing machine with a maximum load of 100 MN was built at MPA Stuttgart in 1979. For the case of pressurized thermal shock (PTS) loading a test loop was designed for the 100 MN testing machine. Within this test facility large-scale hollow cylindrical specimens up to an outer diameter of 800 mm and a wall thickness of 200 mm could be heated up on the outer surface up to 350°C and could be quenched on the inner surface with water of ambient temperature. Simultaneously an axial

force of up to 100 MN loaded the specimen. The test loop was designed for internal pressure up to 35 MPa (350 bar). The flow rate was up to 17.2 litters/sec.

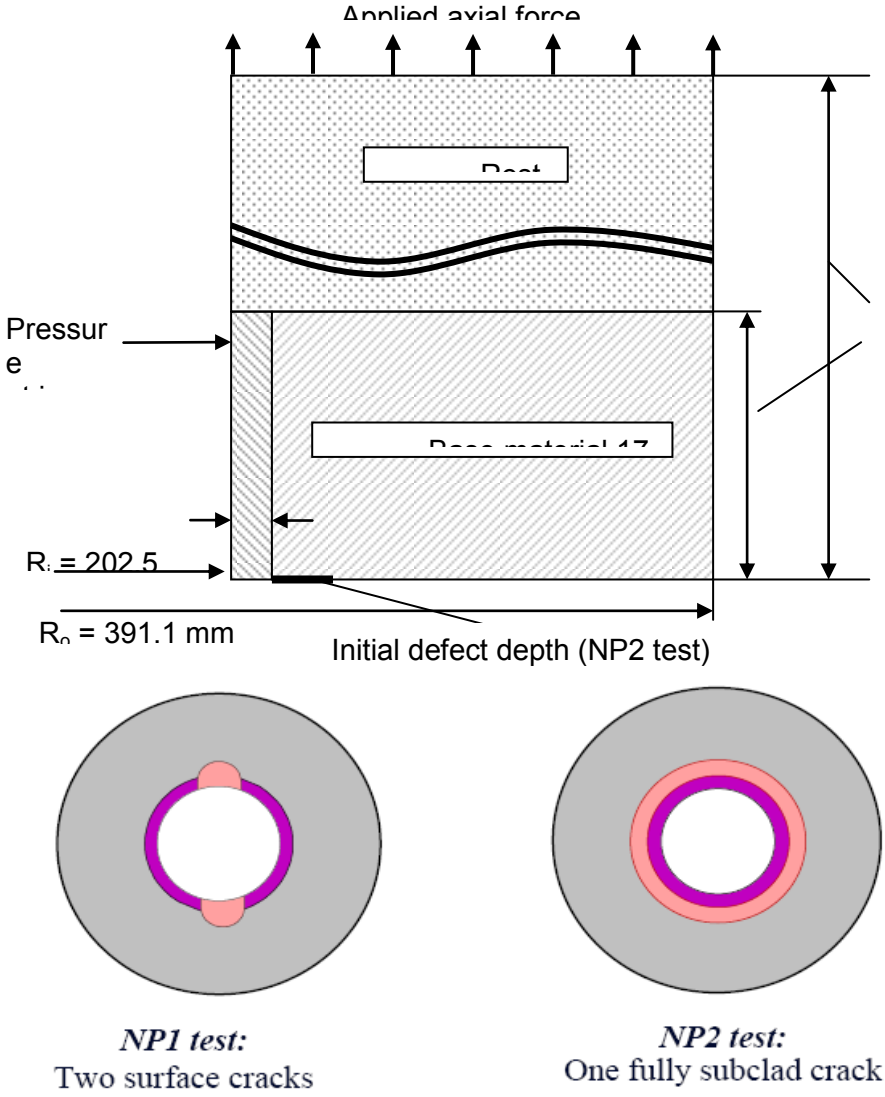

Fig. 2.1: Geometry of specimen NP1 and NP2.

A model material KS22 was available at MPA, which could be heated treated to suitably modify the mechanical properties. A series of experiments were performed to optimise the heat treatments. The chosen heat treatment for the actual material before cladding was to austenitise at 1000 ^{o}C for 8h and oil quench, then to temper at 680^{o}C for 16h and air cool followed by 710^{o}C for 13h with a final air cool.

The test cylinders and reserve pieces were clad and heat treated as a single component. The cladding direction was parallel to the axis of the test cylinders. The curvature of the test cylinder required the use of 30 mm strips of clad material instead of 60 mm strips. The cladding was welded in two layers with a total thickness of 8 mm. Subsequently the stress relief heat treatment was made at 650^{o}C for 6.5 h. Therefore no change in mechanical properties was expected. Heating and cooling between the various stages was made smoothly with temperature changes not higher than 20 K/h. In addition, in the case of the NP2 test piece, a fatigue crack was inserted before cladding. There was no change of crack geometry in the base material after welding and stress relief heat treatment.

In specimen NP1 the final crack depth of notch A was 23.8 mm and of notch B 19.6 mm. The crack length was 63 mm for notch A and 59 mm for notch B. These dimensions have been determined at the

broken crack section after the thermal shock test. Both defects were sealed to avoid the intrusion of water during quench. The average depth of the pre-fatigued notch in specimen NP2 is 8 mm, so the crack tip is located beneath heat affected zone in unaffected base material. The measurement was done with an ultrasonic method before the PTS test, and confirmed with measurements after the PTS test.

Both NP1 and NP2 tests were run in a similar manner. The specimens were filled with water and were then heated up to foreseen starting temperature level and profile, as assumed in the pretest analyses. During the heating phase the system was pressurised to avoid boiling. Then the high pressure pumps were started. The external force was applied. The electrical heating was switched off to avoid any malfunction of the readings. By switching the valves the flow changed from the bypass branch to the specimen branch. Quench of the inner surface then started.

The internal pressure in specimen NP1 was 7.8 MPa during the test. Slight changes of about 0.1 MPa occurred in the very first stage of quenching. The external force was kept constant at 20 MN for about 2000 sec after start of quench. Fig. 2.2 shows the temperature profile in the wall of the cylinder for various time steps. The influence of the different conductivity of the austenitic cladding and the ferritic base material may be seen near the inner surface. The cladding acts to insulate the base material and therefore leads to a shallower overall thermal gradient than without cladding. The measurement of the acoustic emission did not show any events pointing to crack initiation.

The internal pressure in specimen NP2 was 5.8 MPa during the test. Slight changes of about 0.1 MPa occurred in the very first stage of quenching. The external force was kept constant at 43 MN for about 1800 sec after start of quench.

2.3 MATERIAL CHARACTERIZATION

The material used for the NP1 and NP2 components was type “17 MoV 8 4 mod”, machined from the cylinder used in the previous NT3 PTS experiment, which in turn was fabricated from the K22 model material, designed to simulate the end-of-life condition of RPV welds. The major difference between the material used for the NP1 and NP2 components and the NT3 cylinder was the deposition of a two-layer cladding and the subsequent stress relief heat treatment. The composition of the base and clad materials is shown in Table 2.1. Fig. 2.3 shows the hardness profile across a radial section of the clad cylinder.

After the NP2 test, the specimen was cut into 24 segments. Material was set aside for fracture testing from between cuts 5 and 7 i.e. the region of the specimen in which the extent of crack extension was greatest. This material is denominated “NP2”. Lastly, reference is made to the so-called rest material or extension material. This was the 508 Cl.2 steel used to extend the cylindrical test section to the grips inserted in the test machine.

Physical and mechanical properties

Fig. 2.4 shows the physical and mechanical parameters of the base and cladding materials at different temperatures. For the base material, the reference temperature is 35^{o}C, which implies that the value given for α is the total thermal expansion coefficient between the stated temperature and the reference temperature. The properties of the cladding material are based on investigations within the NESC-I project. In this case the thermal expansion coefficient data are total values with respect to ambient (25°C). The elastic modulus values for the base material and the cladding material are also given in Fig. 2.4. The Poissons ratio is assumed constant at 0.3.

Tensile testing was performed on specimens from the base and cladding materials to provide stress-strain curves as input to the finite element fracture models. The plastic strain versus stress data at 20, 150 and 300°C are shown in Fig. 2.4.

Charpy impact energy data for the 17MoV 8 4 mod base material and the heat affected zone (HAZ) induced by the cladding process are compared in Fig. 2.5. The data were labelled as being from NP1, in the LS & TL orientation and NP2 in the LS orientation for the base material and LS for the HAZ

material. It was observed that for the base material, there was essentially no difference between the data from the NP1 and NP2 series or between the data in the LS and TL orientations. Analysis of the combined data set showed the 41J temperature, TE41, to be 116.1ºC.

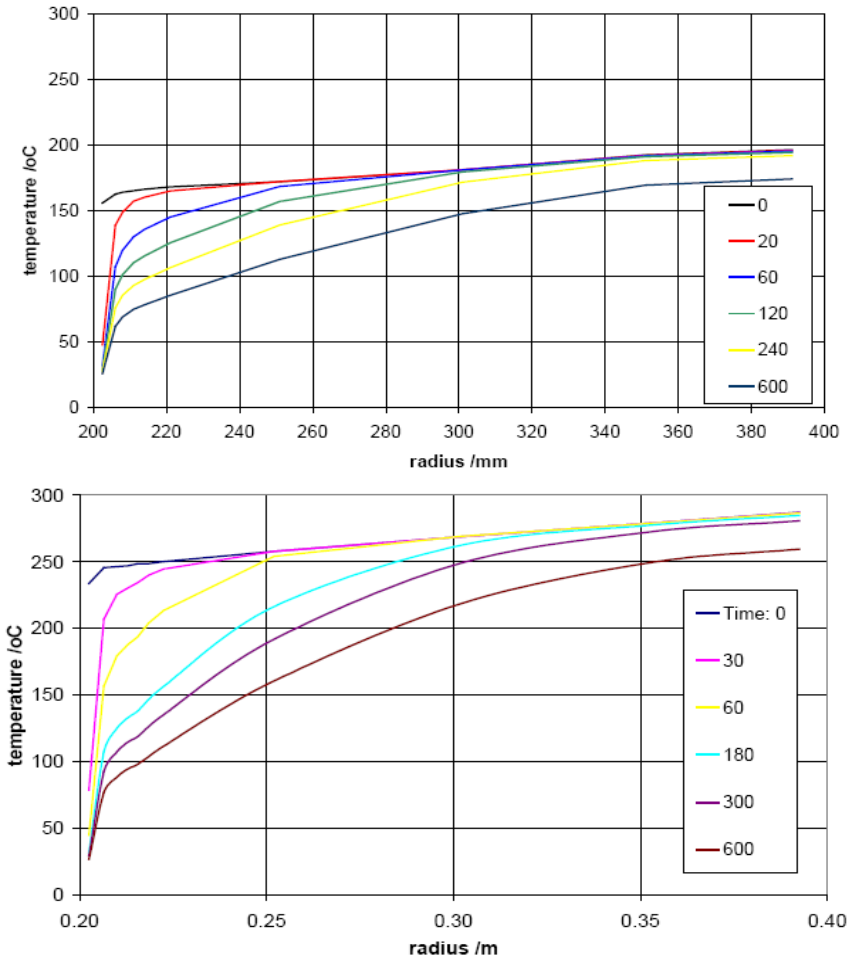

Fig. 2.2: Temperature profiles for test NP1 (above) and test NP2 (below) during the tests.

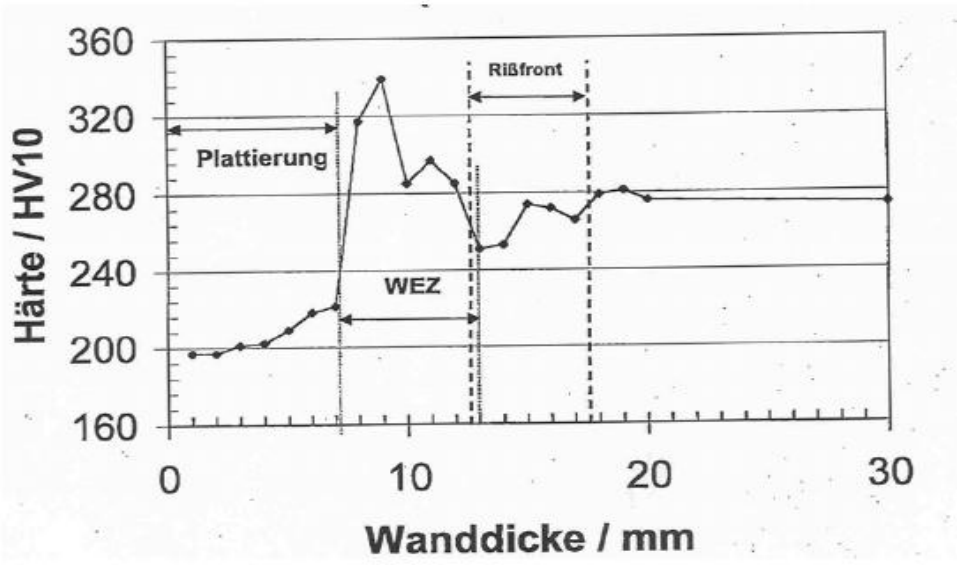

Fig. 2.3: Hardness profile across the clad and base material.

Table 2.1: Composition of base 17 MoV 8 4 mod and clad materials.

Element	*Content (wt %)*		
	Base	Clad Layer 1	Clad Layer 2
	17 MoV 8 4 mod	X2 CrNiNb 24 12	X2 CrNiNb 24 12
Carbon	0.17	0.018	0.017
Silicon	0.30	0.31	0.20
Manganese	0.59	1.66	1.77
Phosphorus	0.014	0.01	0.012
Sulphur	0.018	0.007	0.008
Chromium	0.32	23.12	20.20
Molybdenum	1.03		
Nickel	0.25	11.4	10.7
Aluminium	<0.01		
Vanadium	0.35		
Copper	0.11	0.03	0.02
Tin	<0.01		
Cobalt	0.02	0.03	0.05
Arsenic	0.03		
Niobium		0.78	0.66
Tantalum		0.02	0.02
Iron	bal	bal	Bal

Fracture toughness testing

Fracture toughness testing was conducted at MPA, VTT and IWM laboratories. A brief presentation of these results including considerations of the Master Curve methodology and constraint is given below.

MPA supplied the project with existing data for the NT3 material and results of testing performed on the NP material. For the NT3 material, compact, C(T), specimens of a range of thicknesses between 15 and 50mm were tested using both deeply notched (a/W ~ 0.5) and shallow notch (a/W ~ 0.1) specimens. For the NP material, a/W ~ 0.55 (10×20 and 20×20 SE(B) specimens were tested. All these specimens were 20% side-grooved. The data provided were toughness, K_{Jc}, at specimen fracture and K_{Ji}, toughness at 'true' initiation, based on measurements of stretch zone width (SZW) on the specimen surfaces. After the NP1 and NP2 tests, the results of a limited amount of HAZ toughness testing on Charpy-size, 10×10 SE(B), specimens of NP material also became available. These data provide further evidence of the higher toughness properties of HAZ relative to base material. The MPA results are given in Table 2.2.

VTT conducted fracture toughness testing on 20% side-grooved 10×10 SE(B) specimens over a range of temperatures. Twenty deeply notched (a/W ~ 0.5) and seven shallow notch (a/W ~ 0.1) specimens were tested. The crack propagation direction in these specimens was circumferential. Deep notch specimens were tested at ~-50ºC, room temperature (22ºC), ~50ºC and ~150ºC. Shallow notch specimens were tested at room temperature only. The Master Curve analysis of fracture toughness data from the different laboratories and the determined T_0–values are shown in Fig. 2.6.

Analysis of the VTT and IWM data for shallow notch (a/W = 0.1), low constraint yielded a T_o estimate of 28.5ºC. This represents a shift in T_o of -37ºC with respect to the value determined for the deep notch (a/W=0.5) specimens and is attributed to constraint loss effects. A very similar shift was observed in the NESC-I materials testing.

Thermo-physical properties of the 17 MoV84 base

Temp. [°C]	c_p [J/g°C]	□ [g/cm^3]	□ [W/m°C]	□□[1/°C]
92	0.47	7.80	42.4	1.23 x10^{-5}
178	0.51	7.77	38.3	1.29 x10^{-5}
293	0.55	7.74	36.7	1.36 x10^{-5}
384	0.58	7.71	35.6	1.39 x10^{-5}
490	0.64	7.67	33.4	1.43 x10^{-5}
588	0.70	7.63	31.6	1.45 x10^{-5}
692	0.84	7.60	27.8	1.46 x10^{-5}

Thermo-physical properties of the Type 347 cladding

Temp. [°C]	c_p [J/g°C]	□ [g/cm^3]	□ [W/m°C]	□□[1/°C]
25	0.48	-	14.36	1.61 x10^{-5}
150	0.52	-	16.59	1.65 x10^{-5}
250	0.55	-	18.55	1.70 x10^{-5}
300	-	-	-	1.73 x10^{-5}

Young's Modulus Data for cladding and base

Temperature (°C)	Cladding	Base material
20	152	210
150	139	201
250	127	-
300	-	191

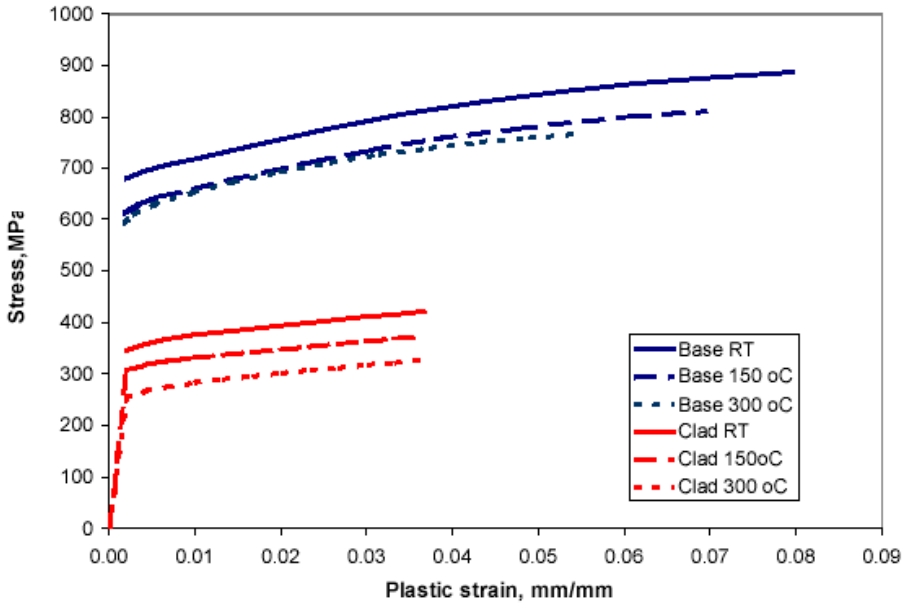

Fig. 2.4: Stress-plastic strain curves for the base and clad materials.

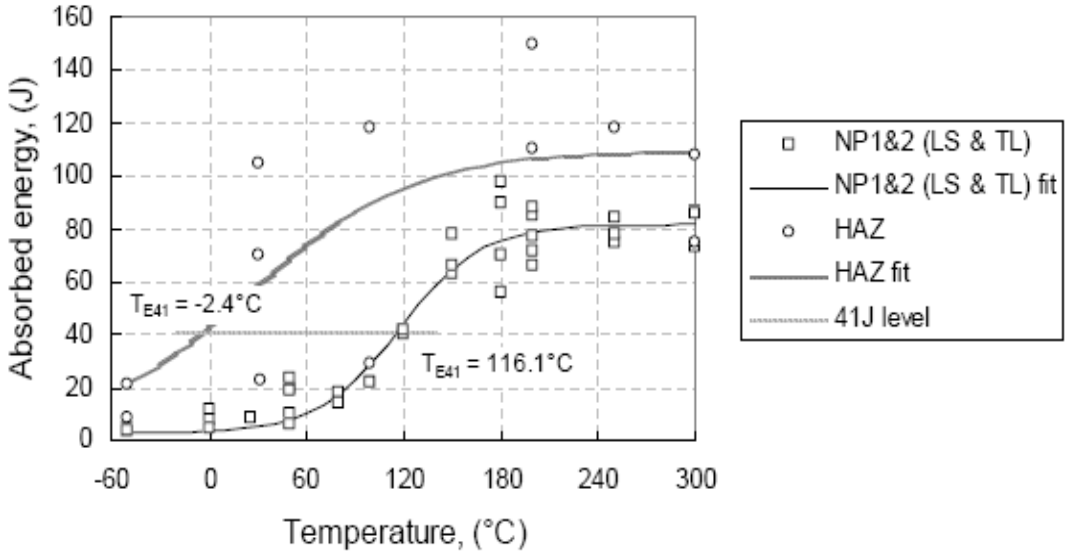

Fig. 2.5: Comparison of the Charpy impact energy data for the base material and the HAZ.

Table 2.2: Fracture toughness data of the NP material conducted by MPA.

Specimen	Temp. [°C]	E [GPa]	Str. zone [mm]	J_i [N/mm]	K_{Ji} [MPa√m]	J_c [N/mm]	K_{Jc} [MPa√m]	Section [mm²]
NP1 HA1	23	210	0.016	22	71	50	107	10x20
NP1 HA8	50	216	0.026	18	65	66	125	10x20
NP1 HA6	75	216	0.025	27	80	75	133	10x20
NP1 HA2	100	216	0.029	22	72	58	117	10x20
NP1 HA5	150	200	0.044	37	90			10x20
NP1 HA3	200	200	0.032	28	78			10x20
NP1 HA4	300	190	0.037	42	94			10x20
NP1 AA4	23	210	0.008	18	64	18	64	20x20
NP1 AA2	50	210	0.024	19	66	55	113	20x20
NP1 AA5	75	216	0.023	22	72	32	87	20x20
NP1 AA1	100	216	0.032	31	86	50	109	20x20
NP1 AA3	150	200	0.031	37	90			20x20

For the specimens taken from the HAZ material, only five toughness data were available, including two 'no failures'. All results were above the E1921 K_{Jc} limit criterion. Ignoring this limitation, a T_o value of about 4ºC can be determined, which implies a shift of - 62ºC with respect to the NP base material. This agrees with the Charpy data for the HAZ (which show a reduction of TE41 of approximately 118ºC) and indicates that the HAZ is considerably tougher than the base material.

Comparison of ASME RT_{NDT} and RT_{To} curves

At the request of several members of TG3, the representation of the fracture toughness transition curve using the ASME reference temperature parameters RT_{NDT} and RT_{To} was also considered.

Determination of RT_{NDT} posed a problem for the 17 MoV 8 4 mod material, since no drop weight tests had been made i.e. no T_{NDT} value was available. However by combining the three sets of Charpy absorbed energy data for base material, it was possible to develop a curve based on the lowest datum at each of a number of test temperatures. This is in accordance with the method described in the ASME Code, Section 3, Sub-Section NB2331(a) to determine the temperature at which 68J is absorbed.

Alternatively, the RT_{To} parameter defined in Code Case N-629 as T_o + 19.4°C may also be considered. For the NP material, this yields RT_{To} = 85°C. The corresponding RT_{To} and RT_{NDT} transition curves are shown in Fig. 2.7. It is seen that the curve based on RT_{NDT} is a very conservative bound to the transition regime toughness data.

MPA NP data	T_0 = 60.1°C
VTT NP data	T_0 = 63.2°C
IWM NP2 data	T_0 = 76.3°C
All NP data combined	**T_0 = 65.6°C**

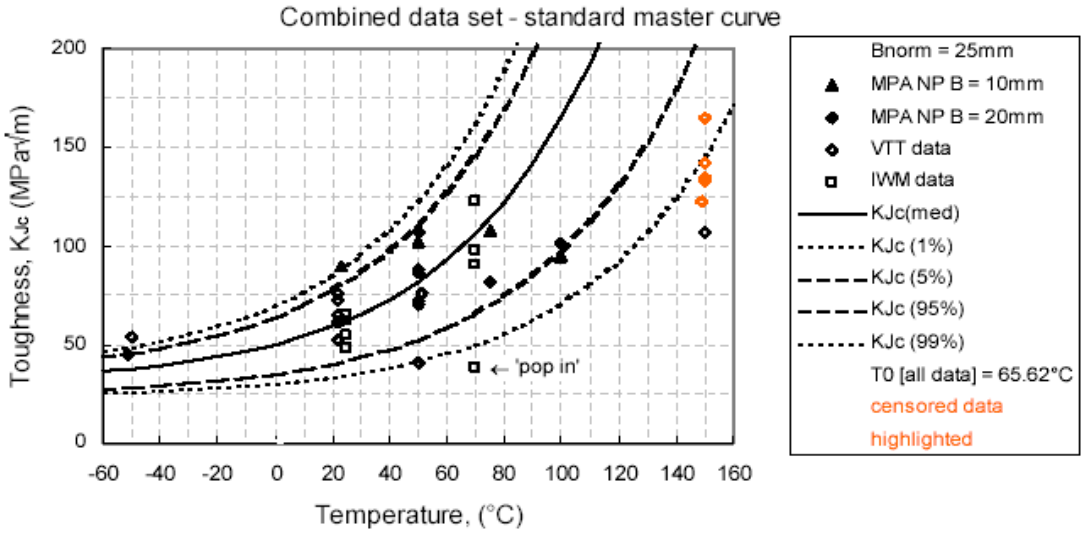

Fig. 2.6: Master Curve analysis of data from deep cracked specimens of the base material.

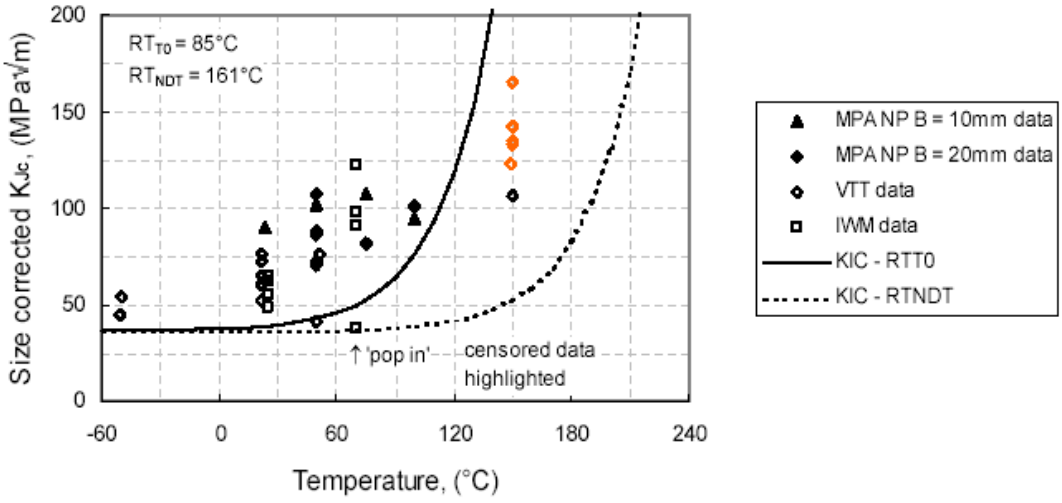

Fig. 2.7: Comparison of the ASME fracture toughness curves referenced to RT_{NDT} and RT_{To}.

2.4 FRACTURE ANALYSIS

Pre-test analyses were performed, leading to recommendations concerning the test conditions of NP1 and NP2 tests. After the tests, post-test analyses were conducted based on a problem definition of the tests. The post-test analyses are briefly described below.

The fracture analyses of the two problems were conducted using refined elasto-plastic cracked body finite element analyses as well as simpler so-called engineering methods. The refined models are assumed to give accurate solutions of the relevant parameters such as crack driving forces and constraints against plasticity. The refined cracked body analyses conducted by the different partners were very similar with respect to finite element meshing, assumed defect geometry, analysis procedure and calculation of crack driving forces.

All partners modelled the subclad defect problem as an axisymmetric problem. The IWM model used the maximum depth, 10.5mm, in the analysis whereas all other partners used the average crack depth 8 mm. For the problem NP1, double symmetry was assumed and only one eighth of the vessel was modelled. The defect A being the most critical one was modelled using more or less its exact geometry. The heat conduction and stress analyses were conducted separately. The thermal analysis was first performed using the prescribed thermal transients and the resulting temperature distributions were subsequently imposed in the mechanical analysis to generate thermal stresses along with the mechanical loads. The elastic-plastic stress intensity factor, K_J was used to predict the failure probability. The *J*-integral was calculated using 2D or 3D domain integrals and assuming deformation plasticity. BE conducted a thorough investigation using so-called engineering approaches, in particular the British R6-method. In the R6 analyses the so-called simplified secondary load assumption was adopted and crack driving forces were calculated using weight function technique. In addition the French RSE-M and the American ASME XI methods were also used to a smaller extent. The following gives a brief description and discussion of the post-test analyses.

Analysis of the circumferential sub-clad defect (NP2)

The post-test problem definition contained a transient definition for the test that specified a more severe fluid temperature transient than in the pre-test definition coupled with considerably reduced inner surface heat transfer coefficients (the peak heat transfer coefficient was 2.9 kW/m2K compared to 15kW/m2K in the pre-test definition). BE, IWM and Framatome performed post-test analyses of the NP2 transient using ABAQUS. The analyses from the different partners were very similar. Fig. 2.8 depicts the measured and computed temperature histories at the inner and outer surface and at the location of the deep crack tip. It is obvious that the actual test cylinder cooled faster near the inner surface than predicted by thermal analyses using the data from the problem definition. This discrepancy at the inner surface is believed to be linked to either uncertainty of the actual heat transfer or temperature transient at the surface. BE used constant heat transfer coefficients in the analyses whereas Framatome did not make this assumption, but both approaches resulted in the same inconsistency at the inner surface. BE adopted also the pre-test inner surface fluid temperature definition with a constant heat transfer coefficient and this gave a much better prediction of temperatures near the inner surface. This suggests that the temperature discrepancy for the inner surface was primarily due to uncertainty in the transient.

Five organisations produced non-linear cracked body finite element post-test analyses of the NP2 test; BE, MPA DNV and IWM, all using ABAQUS; and Framatome, using SYSTUS. Table 2.3 presents details of these analyses. The agreement between post-test analyses from the different partners is very good. The IWM analysis used the maximum crack size of 10.5 mm rather than the mean crack size of 8 mm chosen by the other analysts.

The crack driving force at the two crack tips computed by DNV is shown in Fig. 2.9 versus time into transient at the crack tip respectively. The crack driving force is higher for the deep crack tip than for the one located in the clad/HAZ interface. The HAZ is also generally tougher than the base material and crack growth is therefore primarily expected to occur at the deep tip.

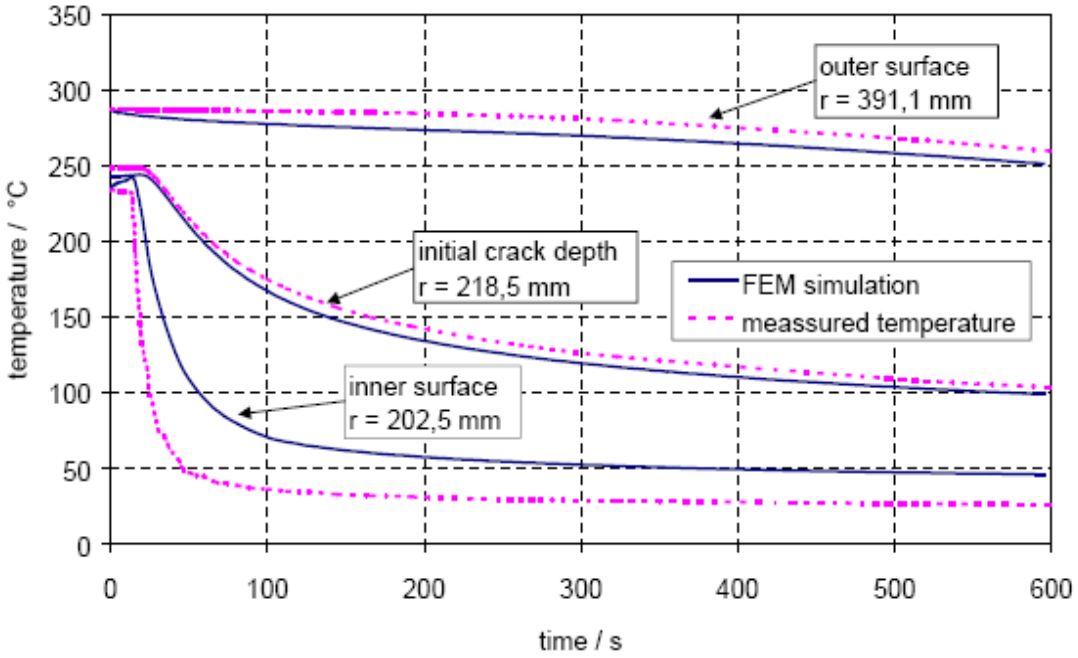

Fig. 2.8: Comparison between calculated and measured temperature data for NP2.

Table 2.3: Summary of peak crack driving forces predicted by NP2 post-test analyses.

Organisation	*Code*	*Peak crack driving force at deepest tip (MPa √m)*	*Temperature (°C)*	*Time (s)*	*Notes*
BE	ABAQUS	97.7	127.5	310	8 mm crack
DNV	ABAQUS	96.1	126	310	8 mm crack
Framatome	SYSTUS	104	124	?	8 mm crack
IWM	ABAQUS	115	129		10.5 mm crack
		(100)	(~124-125)		(scaled to 8 mm)
First test event			145	186	
DNV	ABAQUS	95	146	190	
BE	ABAQUS	92	147	180	
MPA	ABAQUS	72	147	?	Believed to use pre-test constant properties

Analysis of the semi-elliptical through-clad defects (NP1)

The inner surface temperature transients specified in the pre and post-test definition documents were very similar. However, the inner surface heat transfer coefficient for the post-test transient was much lower than that assumed prior to testing. The computed temperature distributions reproduced the measured temperatures fairly well when the post-test definitions were used.

The predictions from the different refined non-linear cracked body analyses were as expected very similar when the same data was used. In the presentation of results and discussion below, results from only one partner will often be shown, knowing that the other partners had very similar results if not stated otherwise.

Three organisations performed non-linear cracked body analyses of the NP1 test. They were DNV, IWM and Framatome. This problem is more complicated to analyse since the crack tip loading varies along the front in the model. The defect A was considered to be the most critical one and was the adopted defect in conjunction with double symmetry in the analyses. Agreement between the three predictions at the deepest point was impressive as can be seen in Fig. 2.10. Only DNV reported the variation of crack driving force around the crack front, and their predictions for the HAZ 11 mm beneath the inner surface, and cladding 1.9 mm beneath the inner surface, are compared with the deepest point in Fig. 2.11. It can be seen that the crack driving force in the near-surface region is somewhat higher than at the maximum depth position. As mentioned above, the toughness of the HAZ is expected to be higher than for the base material so crack extension, if it occurs, is most likely at the deepest point.

DNV Consulting have made estimates of the level of constraint along the crack fronts using different constraint theories. Fig. 2.12 depicts the computed variation of different constraint parameters along the crack front in NP1. The DNV analyses predicted virtually no constraint loss for NP1 except close to the inner surface where constraint loss was predicted.

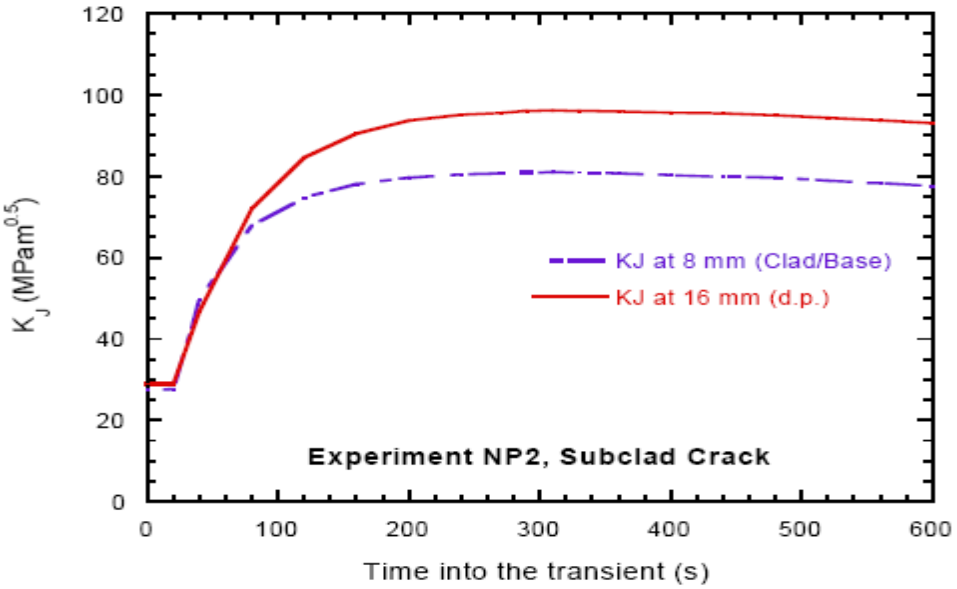

Fig. 2.9: Computed applied K_J of the NP2 subclad defect at two crack tip positions.

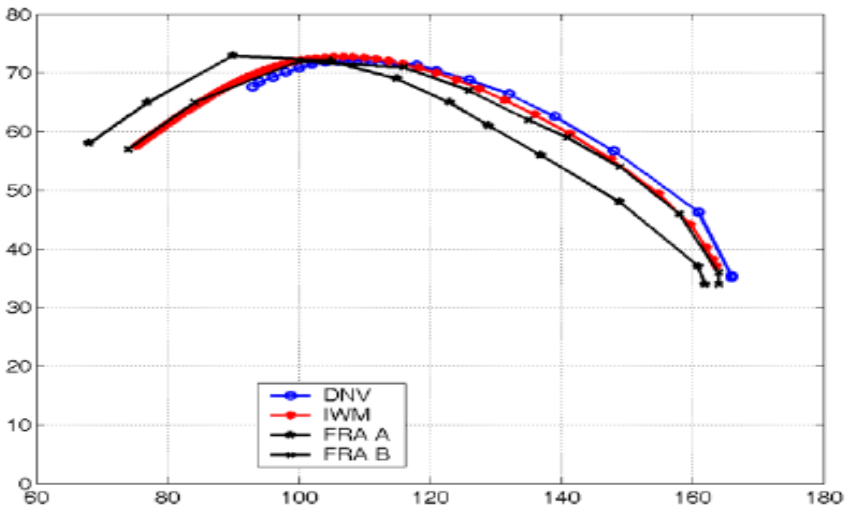

Fig. 2.10: Variations of applied K_J as function of temperature from the post-test predictions for NP1.

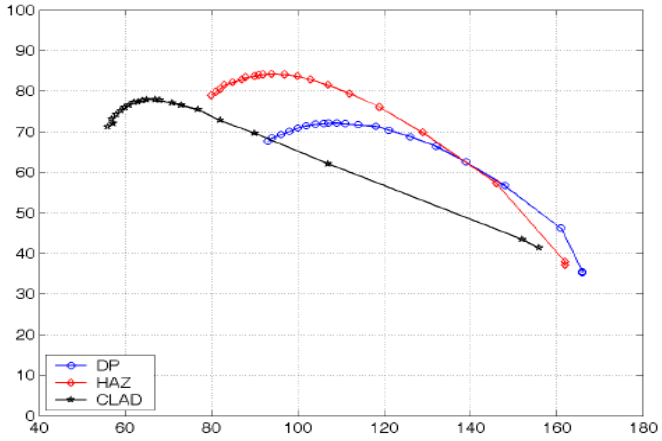

Fig. 2.11: Comparison of DNV predictions for applied K_J as function of temperature at deepest point, in the HAZ, and in the cladding for NP1.

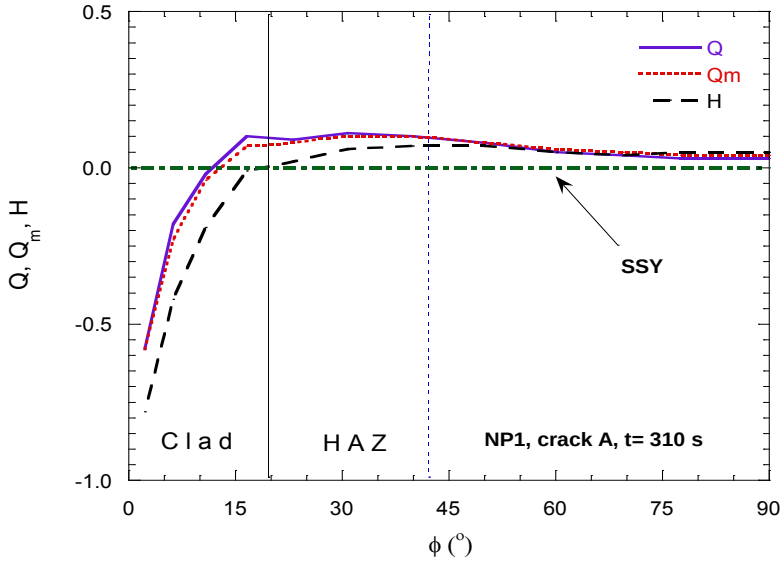

Fig. 2.12: Variations of the constraint parameters *Q*, *Qm* and *H* along the crack front of Defect A of the NP1 cylinder at 310 seconds into the test, the from DNV post-test analysis.

2.5 SOME IMPORTANT OBSERVATIONS

Failure assessment based on the R6 and Swedish SKIFS methods

Simple engineering methods may be used either for best-estimate predictions or for failure avoidance assessments. Two organisations conducted failure avoidance assessments of the NESC-II tests:

1. BE performed R6 assessments using the approach adopted in the UK.
2. DNV performed assessments using the SACC analysis program to the Swedish SKIFS 1994:1 code [SKIFS, 1994].

Both assessments made use of stress and temperature predictions from best estimate uncracked body finite element analyses already performed by the participants as part of the post-test analysis campaign. They therefore used NESC-II specific material properties and transient definitions. The two assessments examined complementary aspects of these three areas. The key assumptions of the BE and DNV assessments are compared in Table 2.4. The DNV assessments are discussed below.

The assessment performed by DNV treated the cladding as present for the purpose of calculating stresses and modelling the defects, but took no account of cladding or HAZ toughness. A single defect model was used for each test, namely a buried defect for NP2 and a surface elliptic defect for NP1. The variables examined were the *J*-estimation scheme, the fracture toughness response, and the overall safety factor on toughness:

- ✓ The crack driving force was estimated using simple elastic SIF's (referred to as "ASME"), and procedures broadly equivalent to the simple and inelastic R6 methods.
- ✓ The fracture toughness response was modelled by the Standard Master curve at 50% failure probability, size corrected to 25 mm and 60 mm for NP1, and to 25 mm and 1373 mm for NP2. Obviously these curves differ somewhat from those used by BE. The ASME K_{Ia} curve was also used with the pre-test estimate of RT_{NDT}. This combination is slightly more pessimistic than the K_{Ic} curve used by BE.
- ✓ The standard ASME XI safety factors on fracture toughness were used, in addition to a safety factor of 1.0.

Table 2.4: Comparison of R6 and SKIFS failure avoidance assessments of NESC-II tests.

Item	R6	SKIFS 1994:1
Thermal and stress analysis methods	Elastic FE using ABAQUS, from BE post-test best-estimate analyses	Elastic and elastic-plastic FE using ABAQUS, from DNV post-test best-estimate analyses
Stress components	Primary axial load Secondary thermal shock stress No weld residual stress	Primary axial load Secondary thermal shock stress No weld residual stress
Handling of cladding	Present in thermal and stress analyses. Both present and removed for defect models Both present and ignored for material fracture toughness	Present in thermal and stress analyses Present in defect model Ignored for material fracture toughness
Flaw model	**NP1**: circumferential semi-elliptic defect in cylinder, a/c=0.65 (defect A) **NP2**: buried defect in plate and extended circumferential surface defect in cylinder	**NP1**: circumferential semi-elliptic defect in cylinder, a/c=0.65 (defect A) **NP2**: buried defect in plate
Assessment points	**NP1:** "Surface" point and maximum depth **NP2:** maximum depth point	**NP1:** more onerous of surface point and maximum depth **NP2:** maximum depth point
SIF calculation method	R-Code software– 8th order through-wall polynomial.	SACC software
J estimation method	R6 Rev 4 Option 1	R6 Rev 3 Option 1. None (LEFM) for pure ASME XI
Handling of secondary stresses	Elastic, R6 simple ρ method	Elastic, SACC simple ρ method Elastic-plastic, SACC inelastic method
consideration of structural collapse.	R-Code, global collapse	SACC, global collapse
Metal temperature assumptions	Inner surface or clad/HAZ interface for "surface" point Maximum depth	At surface and maximum depth
Yield strength	NP1: 600 MPa (best-estimate) NP2: 595 MPa (best estimate)	Not stated – presumably best-estimate data
Fracture toughness	**NP1:** Modified Master curve, NP forging material, 5% failure probability, 60 mm size correction. Standard Master Curve, HAZ, 5% failure probability, 25 mm size correction **NP2:** Modified Master curve, NP forging material, 5% failure probability, 400 mm size correction. **Both:** ASME K_{Ic} curve, RT_{NDT}=161°C Lower bound ductile initiation and 2mm tearing (implicit – not actually used)	**NP1:** Standard Master curve, NP forging material, 50% failure probability, 25 mm and 60 mm size correction. **NP2:** Standard Master curve, NP forging material, 50% failure probability, 25 mm and 1373 mm size correction. **Both:** ASME K_{Ia} curve, RT_{NDT}=140°C – K_{Ia}^{max} is 220 MPa√m
Failure criteria	Cleavage initiation. >2mm tearing on upper shelf (not invoked). $L_r<L_r^{max}$ (not invoked)	Cleavage initiation.
Handling of WPS	Allowed if no prior tearing	Not allowed
Safety Factors	None	√2 for emergency/faulted conditions, √10 for normal/upset conditions, both on fracture toughness No information given on plastic collapse

3 The NESC-III project

3.1 GENERAL ASPECTS

Defect tolerance of Dissimilar Metal Welds (DMW) is an important issue when assessing found defects and at planning of In-Service Inspection (ISI) of nuclear power plants components. Inspection difficulties, variability of material properties and residual stresses all combine to create problems for structural integrity assessment. In general, those welds are made of austenitic stainless steels or Ni-base alloys (e.g. Inconel 182), and typically occur at piping connections to reactor pressure vessel nozzles, main circulation circuits, steam generators and pressurizers. However, under specific conditions cracking may occur. One prominent corrosion mechanism affecting austenitic stainless steels and Ni-base alloys, which has been of significant economic concern to the industry, is Stress Corrosion Cracking (SCC). This damage mechanism results from the localized attack of the grain boundaries of a susceptible material under load in BWR- and PWR-environment. The grain boundary regions undergo attack and cracks are formed. The cracks typically propagate with little or no evidence of plastic deformation. Most nuclear power plants in Sweden have been in operation for a period of at least twenty years and cracking due to stress corrosion or fatigue cannot be excluded. Leakage and failure of the component are possible events over time. It is thus important to be able to accurately assess the safety margin against failure.

The NESC III-project has the main objectives to:

1) Quantify the accuracy of structural integrity assessment procedures for defect-containing dissimilar metal welds.

2) Participate in the design and evaluation of a unique large-scale test to determine the actual behaviour under load of a defect in a dissimilar metal weld of industrial scale.

3) Address critical issues including: inspection performance, laboratory-scale fracture testing on welds and potential benefits of advanced fracture modelling.

Within the NESC III/ADIMEW-project *(Assessment of aged piping DIssimilar MEtal Weld integrity)*, a defect containing pipe component of industrial size composed of a 316L austenitic steel welded to an A508 ferritic steel was tested under four-point bending load at service temperature (300 ˚C). The ADIMEW-test was performed at EdF Les Renardieres, Fontainebleau, France, in mid-July 2003. The experiment provides a unique opportunity to increase the understanding of defect tolerance of dissimilar metal welds and validate simplified engineering fracture assessment methods.

In order to verify the load at initiation of crack extension, the experiment has been analysed with 3D, elastic-plastic, finite element calculations using commercial FE-codes. The critical defect size was also analysed using the R6-method implemented in the software SACC.

Details of the activities conducted within the NESC-III project are given in Refs [III-1]-[III-5].

3.2 CRACK GEOMETRY AND LOADING

The most important features of the crack configuration and test conditions of NESC-III are given below.

Mock-up geometry

The ADIMEW-test specimen consists of a bimetallic pipe, made of four pipe sections as shown in Figs. 3.1 to 3.3 below. The mock-up section has been extended on each side with pipe sections to a final pipe length of about 7 m. The extension pipes, made of carbon high strength steel, have the same diameter and

thickness as the mock-up section. The notch is located approximately 285 mm (offset) from the symmetry axis.

Fig. 3.1: Four-point bending assembly used by EdF at Les Renardieres in France.

Details of the weld geometry and dimensions of the pipe sections are shown in Figs. 3.3 and 3.4. The thickness of the pipe is 51 mm and its external diameter is 453 mm. The defect, a notch of 17 mm depth at the outer surface, see Fig. 3.4, was inserted by electro-erosion in the first buttering layer (309L) parallel to the fusion line and at a distance of about 1.5 mm from the ferritic material. The width of the notch is about 0.4 mm and the notch-tip radius is 0.2 mm.

The experiment showed ductile material behaviour without brittle fracture of the component. A stable crack extension of around 25 mm along the weld fusion line was obtained before the displacement controlled test was stopped.

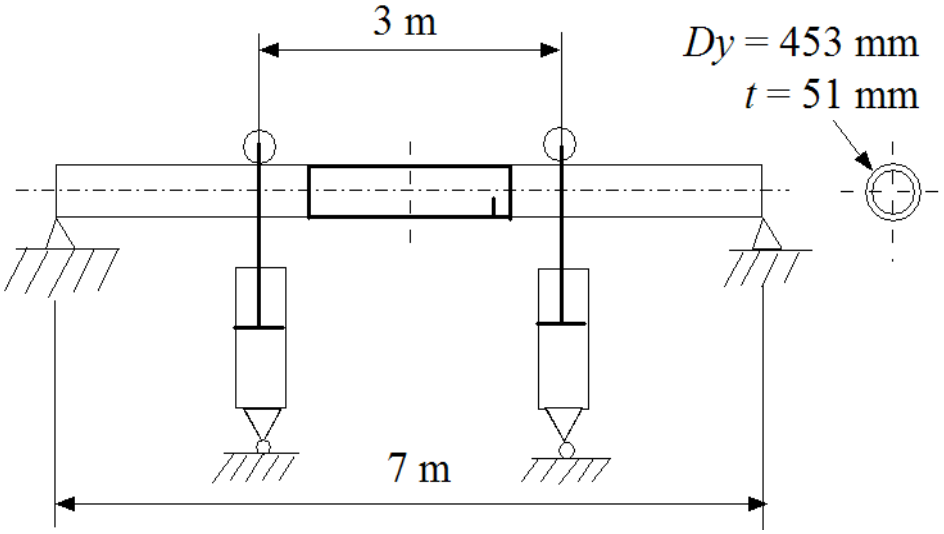

Fig. 3.2: A schematic illustration of the ADIMEW-test.

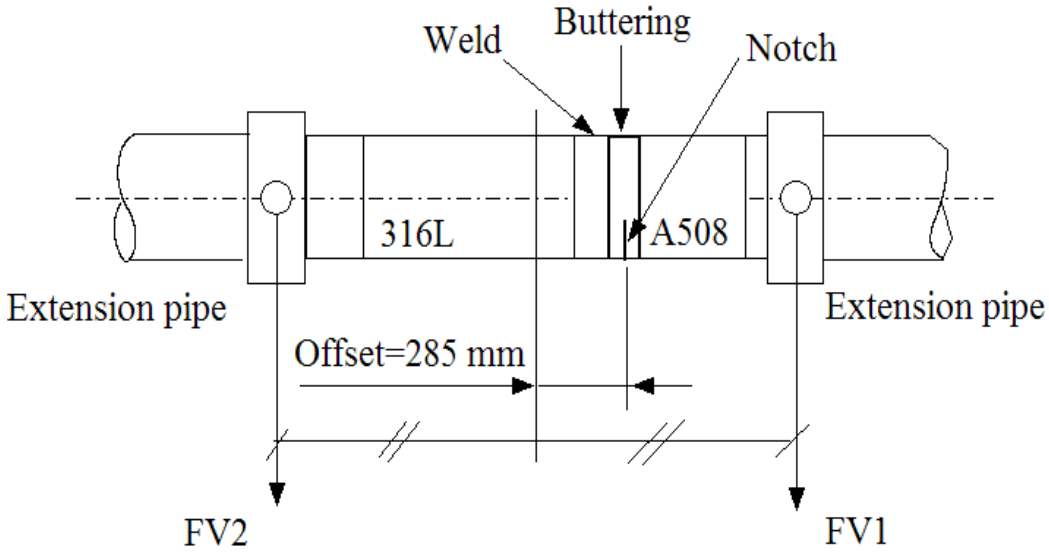

Fig. 3.3: Mock up geometry of the ADIMEW-test.

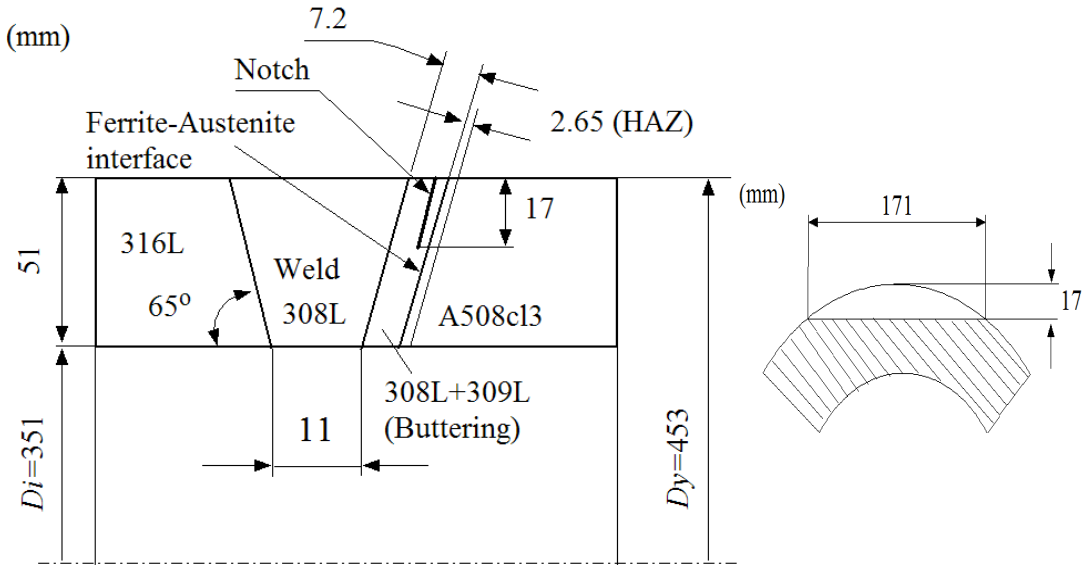

Fig. 3.4: Details of the dissimilar metal weld geometry.

3.3 MATERIAL CHARACTERISATION

The material data used in all FEM calculations are given in Table 3.1 – 3.3. The stress-strain curves used in the FEM analyses are plotted in Figs. 3.5 to 3.7.

Table 3.1: Material properties for the base material 316L used in the FEM analysis.

Temperature [ºC]	***E* – modulus [GPa]**	***ν* [-]**	**Yield Strength [MPa]**	***α*** [$\cdot 10^{-6}$/°C]
20	189	0.285	294	16.4
100	185	0.29	271	16.8
200	176	0.293	240	17.2
300	170.5	0.295	213	17.7
400	162	0.31	185	18.1
500	151	0.315	150	18.4
600	144	0.315	130	18.7

Table 3.2: Material properties for the base material A508 used in the FEM analysis.

Temperature [ºC]	***E* – modulus [GPa]**	***ν* [-]**	**Yield Strength [MPa]**	***α*** [$\cdot 10^{-6}$/°C]
20	207.2	0.285	513	11.22
100	202	0.2875	483	11.79
200	195	0.29	471	12.47
300	187.5	0.29	463	13.1
400	180	0.295	430	13.72
500	125	0.305	400	14.32
600	70	0.315	300	14.5

Table 3.3: Material properties the weld material 316L used in the FEM analysis.

Temperature [ºC]	***E* – modulus [GPa]**	***ν* [-]**	**Yield Strength [MPa]**	***α*** [$\cdot 10^{-6}$/°C]
20	189	16.4	416	16.4
100	185	16.8	392	16.8
200	176	17.2	362	17.2
300	170.5	17.7	333	17.7
400	162	18.1	306	18.1
500	151	18.4	272	18.4
600	144	18.7	252	18.7

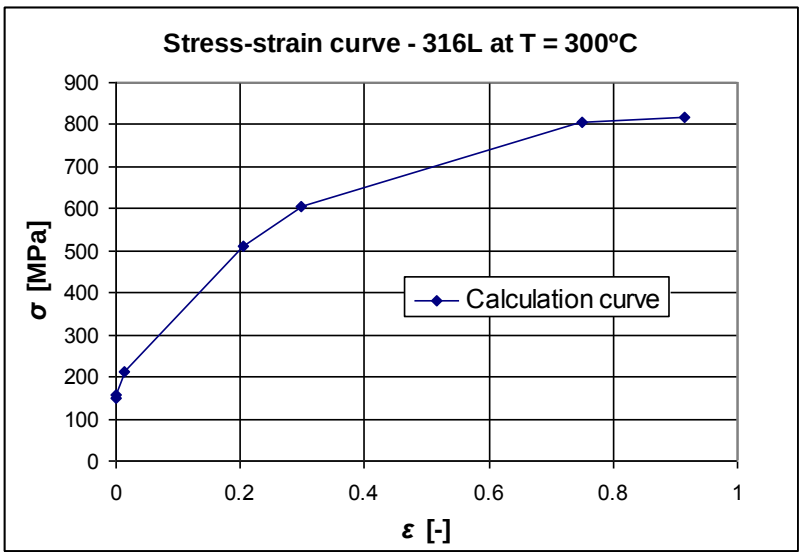

Fig. 3.5: True stress-strain curve estimated from tensile test for 316L at T = 300ºC.

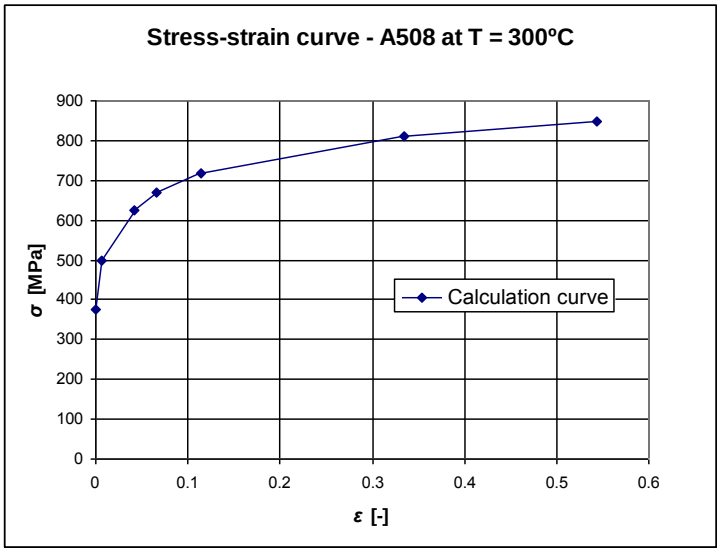

Fig. 3.6: True stress-strain curve estimated from tensile test for A508 at T = 300ºC.

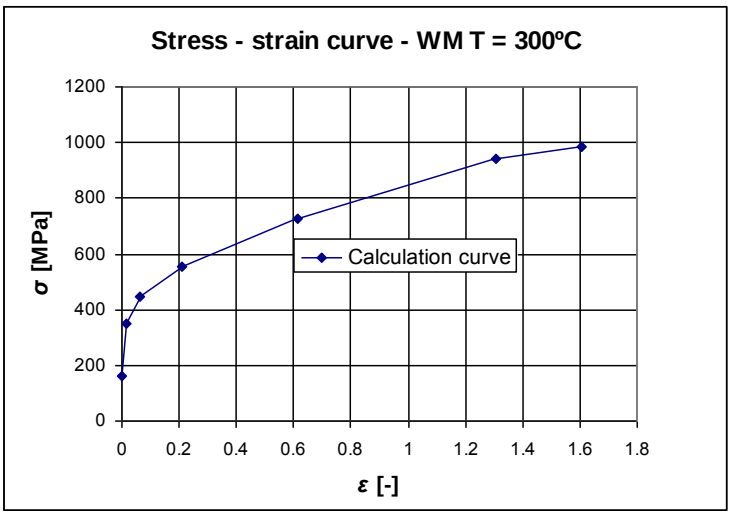

Fig. 3.7: True stress-strain curve obtained from tensile test for weld material at T = 300ºC.

3.4 FRACTURE ANALYSIS

Analyses based on the R6-method (option 1) was conducted in order to perform engineering analyses of the critical defect size for the bending moment at crack initiation, M_{init}=1.80 MNm. The software SACC was used in the analyses.

There are two basic failure modes assessed by the R6-method: plastic collapse and fracture. The R6-approach consists of evaluating two parameters, K_r and L_r, dependent on the applied loads, material properties, and the geometry, including crack size and shape.

The defect geometry is approximated by a part circumferential, semi elliptical, external surface crack, see Fig. 3.8. The dimensions of the pipe geometry are in agreement with those described in Fig. 3.4.

The defect geometry considered is perpendicular to the pipe axis. The crack length/depth aspect ratio was fixed to 10 in all analyses.

In all cases analysed here, the fracture toughness data of the weld metal is assumed to be J_{Ic} = 156 N/mm. The defect is analysed with three different strength properties; that is the yield strength and tensile strength of the 316L parent pipe material, the weld metal and the ferritic material, respectively. It is motivated that failure is competing at two positions of the pipe; ductile fracture at the defect in the buttering and plastic collapse of the austenitic 316L pipe.

In order to verify the influence of weld residual stresses on the critical defect size, a single case was studied with axial weld residual stresses after PWHT and at 300 ºC. The distribution of these stresses is shown in Fig. 3.9.

The results from the R6-analyses are presented in Figs. 3.10 to 3.13, in terms of Failure Assessment Diagrams (FAD). The circles in the figures correspond to a crack depth of 17 mm.

A summary of the calculated critical defect sizes, corresponding to initiation for the applied moment of 1.8 MNm, is presented in Table 3.4 for five cases.

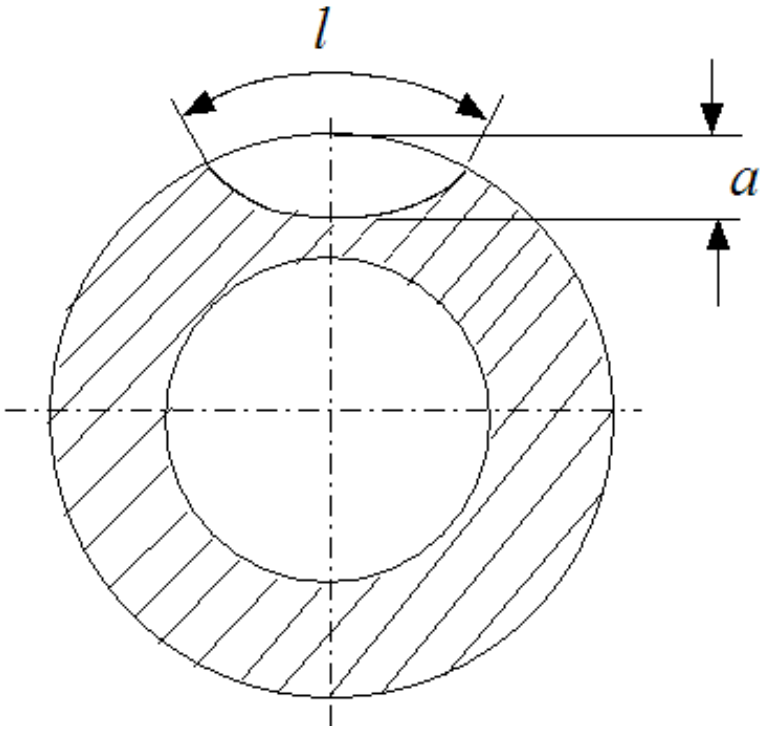

Fig. 3.8: Approximating defect geometry used in the R6-analysis.

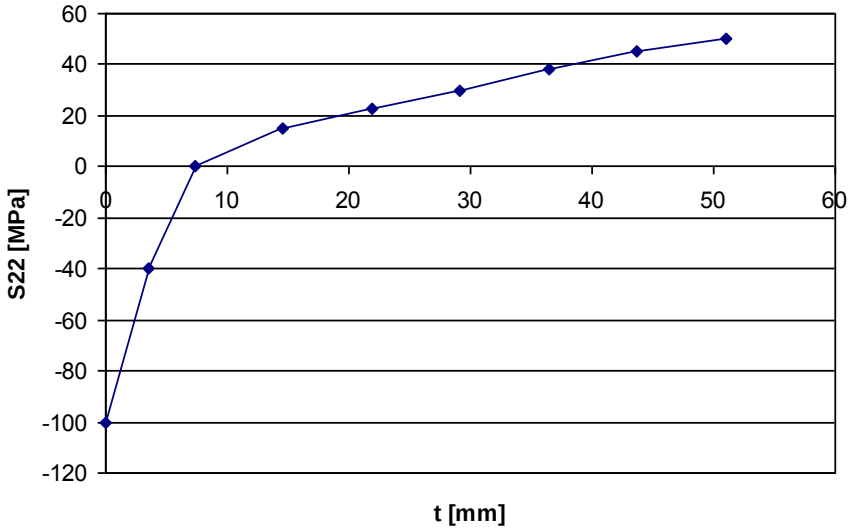

Fig. 3.9: Axial residual stress through the thickness after PWHT and at the temperature 300 ºC. The coordinate t = 51 mm corresponds to the outer surface of the pipe section.

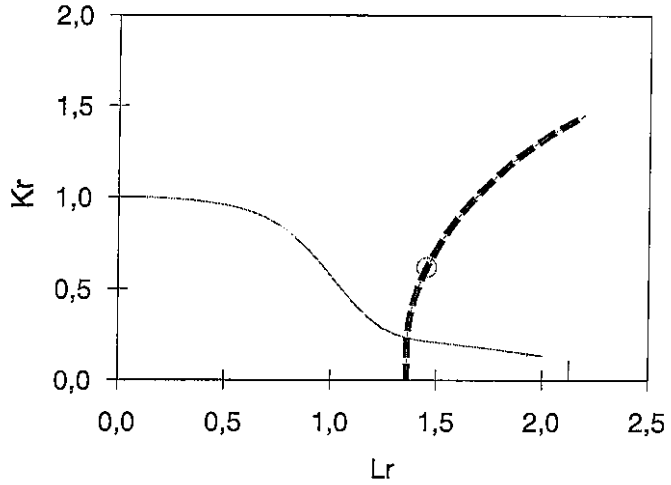

Fig. 3.10: FAD for J_{Ic} = 156 N/mm and the strength properties of the 316L parent pipe material. The load used corresponds to the bending moment M_{init} = 1.80 MNm.

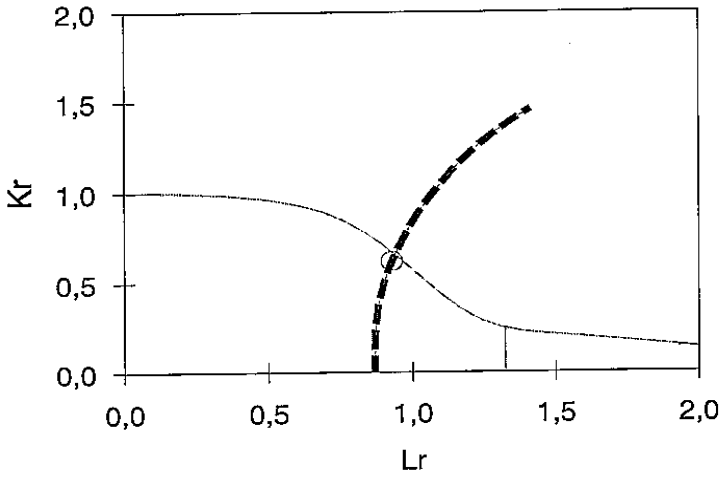

Fig. 3.11: FAD for J_{Ic} = 156 N/mm and the strength properties of the weld metal. The load used corresponds to the bending moment M_{init} = 1.80 MNm.

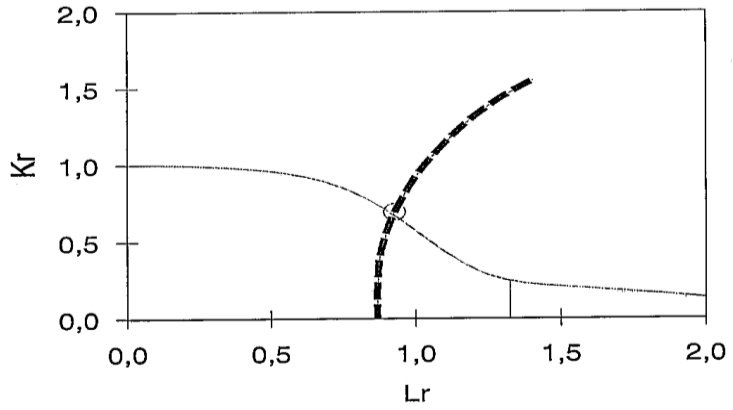

Fig. 3.12: FAD for J_{Ic} = 156 N/mm and the strength properties of the weld metal. The load used corresponds to the bending moment M_{init} = 1.80 MNm. Weld residual stresses according to [9] have been considered.

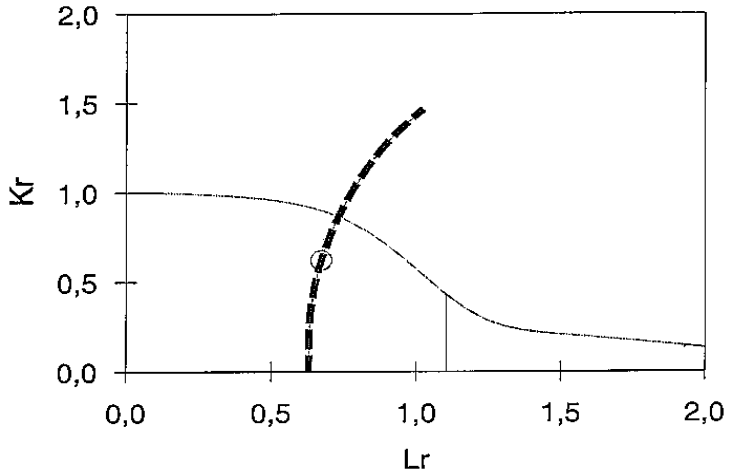

Fig. 3.13: FAD for J_{Ic} = 156 N/mm and the strength properties of the Ferritic base metal (A508) . The load used corresponds to the bending moment M_{init} = 1.80 MNm.

Table 3.4: Critical defect sizes for different strength properties and residual stress, as calculated with the R6-method for the applied bending moment M =1.80 MNm.

Case	Yield properties at 300 ºC		Fracture toughness		Residual stresses included	Critical crack depth a [mm]	Critical crack length l [mm]
	Material	σ_f [MPa]	J_{Ic} [N/mm]	K_{Ic} [MPa√m]			
1	316L	333	156	170	No	**3.1**	31.0
2	Weld Metal	387	156	170	No	**18.4**	185.1
3	Weld Metal	387	156	170	Yes	**16.4**	165.1
4	Ferritic Base Metal (A508)	552	156	170	No	**25.1**	252.2
5	316L	333	3*156	293	No	**8.6**	86

The flow stress σ_f is calculated as the mean value of the yield and tensile strength of the material. The relevant case for evaluation of crack extension from the notch in the buttering is of course the case 2 or 3, having the yield and tensile strength of the weld metal. The results for case 3 and comparison to the FE-analyses shows that the R6-procedure results in a good determination of the defect size at onset of crack growth. The result of a critical defect depth of 16.4 mm is very close to the effective depth of 17 mm.

By comparing case 2 and 3, it is obvious that the weld residual stresses only have a minor influence on the critical defect size for this weld. This is expected since the weld residual stresses at 300 ºC are low, due to an efficient Post Weld Heat Treatment (PWHT). In addition it could be noted that numerical investigations has shown that the relative contribution from secondary stresses to J should decrease rapidly for high values of primary loads (Lr).

As discussed above, for the bending moment at onset of crack extension from the inserted defect in the buttering, we will also have extensive yielding of the 316L parent pipe. The 316L material has the lowest yield properties of the materials. Note that plastic deformation in the 316L pipe is restrained somewhat close to the junction to the weld material. Thus plastic collapse is expected in a section away from the location of the defect.

A common recommendation when assessing defects at weld junctions is to use the fracture toughness of the material where the crack-tip is located, and to use the lowest yield stress properties of all materials at the weld junction. This is motivated by the fact that fracture is governed by a local process at the crack-tip, and plastic collapse is a more global process. The case 1 analysis above, assuming the fracture toughness of the weld material and flow properties of the 316L material, predicts failure for a surface defect of 3 mm depth only. In case 5 the fracture toughness JIc is increased by a factor of three, and still ductile tearing is predicted for a defect size as small as 8.6 mm. This indicates that it is a very conservative assessment to assume the lowest data of all involved materials, as in case 1, when assessing a crack in the buttering.

The result indicates that the mixed mode loading is not of major importance for assessment of the 25º inclined crack. Note that the crack is approximated as elliptical in the R6-analyses. Further it is concluded that the residual stresses are low and has small influence for the fracture of the PWHT dissimilar ductile weld. Uncertainty in the measured fracture toughness data is judged to be of largest importance for assessments of this weld.

3.5 SOME IMPORTANT OBSERVATIONS

In the ADIMEW experiment significant stable crack extension was observed along the fusion line, see Fig. 3.14. The crack extension was about 25 mm after initiation of growth before the test was stopped. The experiment was performed in displacement controlled load conditions and it is not expected that a similar amount of stable crack extension will occur in a real failure situation, since that in general will involve a mixed displacement and load controlled condition.

An interesting observation in the experiment is that the crack first grows toward the material interface, almost perpendicular to the pipe axis, the expected direction from a mixed mode evaluation, but then continues to grow along the fusion line. The crack grows along the fusion line, just inside the weld metal, see Fig. 3.14. This result indicates that the material close to the fusion line is weaker than both the bulk weld metal and the HAZ in the ferritic metal. A fracture path that includes modes I and II is preferred instead of pure modus I fracture. Due to experimental difficulties, no crack growth resistance curve (J-R) is available for the fusion line of the material.

The FEM analysis of the experiment shows that the load at initiation of crack extension can be verified numerically with good accuracy. Note however that significantly lower fracture toughness data were obtained with small subsize specimens compared with those from standard CT-specimens. Uncertainty in the measured fracture toughness data for the bimetallic weld is judged to be of largest importance for the assessment of this weld. For example it is hard to manufacture specimens with the crack tip exactly at a weld interface.

The FEM-analysis predicts that the amount of stable crack extension will significantly be reduced if loading conditions of the component are changed from displacement controlled to load controlled. At load controlled conditions the crack is predicted to become unstable already after 4.3 mm extension.

It is useful to have simplified assessment methods for routine engineering calculations of ISI-intervals. The results in section 8 show that the R6-method can be used to predict the critical defect size for the geometry considered within reasonable accuracy. This procedure has been implemented in the software SACC and has been extensively used in Swedish NPP to estimate appropriate ISI-intervals.

Note that when a crack is in the vicinity of a weld, the calculation of J and plastic collapse becomes much more complex, because the material near a weld and crack is inhomogeneous as it regards the tensile strength properties. There are weld material, heat affected zone material, and base material with mismatched stress-strain curves. Predictions are sometimes made using the base-metal stress-strain curve and the weld-metal J-resistance curve (J-R). This can lead to mispredictions depending on the ratio of strength for the base versus weld material.

The observations from the post-test analyses presented in this investigation show that:

Significant stable crack extension along the fusion line, around 25 mm, was obtained in the displacement controlled ADIMEW experiment before the test was stopped.

The FEM-analysis predicts that the amount of stable crack extension will be significantly reduced if the component is subjected to load controlled conditions. A calculation of J as a function of crack length predicts that unstable crack growth may occur at about 4.3 mm of crack extension in load controlled conditions.

The load at initiation of crack extension can be predicted from elastic-plastic FEM-analyses by using fracture toughness data obtained with laboratory specimens. However, uncertainty in the measured fracture toughness data is judged to be of largest importance for the assessment of the dissimilar metals weld.

The analysis shows that for the applied moment of the onset of crack extension from the defect in the buttering, the 316L parent pipe is at the same time subjected to extensive yielding.

The R6-method, option 1, results in a good determination of the critical defect size for initiation of crack extension in the buttering in this dissimilar metal weld.

The results indicate that it is very conservative to assume the lowest data of all involved materials when performing an R6-evaluation of the crack in the buttering. For a crack along the interface between HAZ and weld material it seems to be appropriate to use fracture toughness data of the weld material in order to evaluate the acceptable and critical crack size.

The axial weld residual stress is small at normal operating temperature 287 - 300 ˚C if an effective PWHT is assumed, and thus the influence from the weld residual stress is negligible. In general it is also reasonable to assume that weld residual stresses are of minor importance for the fracture behaviour of ductile material since relaxation of such stresses are expected to occur during crack extension. In practice this means that it is not necessary to know the exact levels and distributions of weld residual stresses in order to predict the critical crack size.

The small mixed mode character of the field at the inclined crack appears to have minor influence when assessing the fracture.

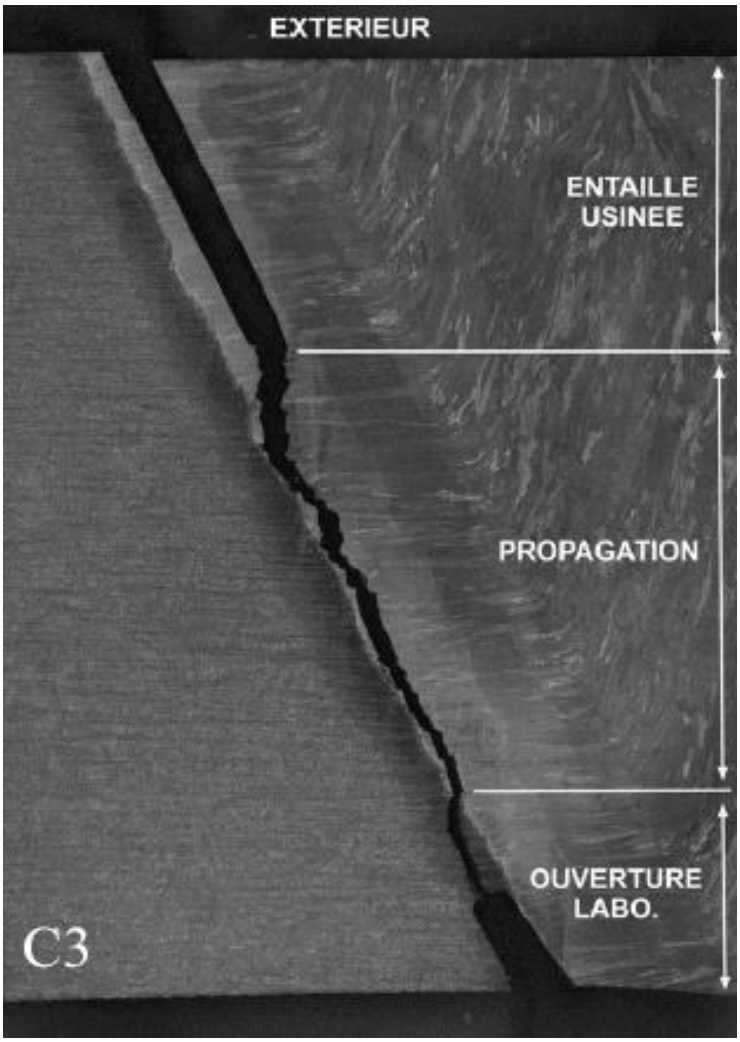

Fig. 3.14: A section through the crack that showed 25 mm stable crack propagated in the ADIMEW experiment.

4 The NESC-IV project

4.1 GENERAL ASPECTS

The NESC IV project is a coordinated experimental/analytical program that draws from major elements of the biaxial cruciform testing program conducted by the Heavy Section Steel Technology (HSST) Program at the Oak Ridge National Laboratory (ORNL) in USA. The NESC-IV project was formally approved at the NESC Steering Committee meeting held in Stockholm during September 2000.

That program has focused on modelling of postulated shallow flaws in heavy-section nuclear RPVs that are subjected to realistic multi-axial loading states produced by credible upset events such as PTS transients and normal operational pressure-temperature (P-T) transients. The NESC IV project consists of two phases that are focused on fracture toughness testing and model development for both shallow surface flaws and embedded flaws. The project includes six biaxial bend cruciform tests of through-clad semi-elliptic defects in a longitudinal weld from an RPV (Part A), and four uniaxial tests of extended sub-clad defects in RPV plate material (Part B). These tests were conducted at ORNL as a cooperative effort between the HSST Program and the NESC network. Additional work packages conducted by the European partners of NESC-IV included extensive material characterization, design/fabrication of the embedded-flaw specimens, residual stress measurements, and structural/fracture mechanics analyses.

A major objective of NESC-IV was to address the transferability of fracture toughness data from laboratory specimens to applications that assess the integrity of RPVs subjected to upset and normal loading transients. The "Master Curve" concept incorporated into ASTM E-1921 provides standardized testing and data analysis techniques for characterizing fracture toughness of RPV steels in the ductile-to-brittle transition region. The cruciform experiments performed within NESC-IV were intended to challenge applications of the Master Curve methodology to predict the behaviour of shallow flaws in RPV clad materials subjected to biaxial loading conditions in the transition region. The NESC-IV was conducted with the contributions from the following organisations:

Bay Zoltan Foundation, Hungary
British Energy, UK
CEA, France
DNV, Sweden
EON Kernkraft, Germany
Framatome ANP, Germany
IWM, Germany
KFKI, Hungary
MPA Stuttgart, Germany
NRI Rez, Czech Republic
Prometey Institute, Russia
Rolls-Royce plc, UK
Serco Assurance, UK
TWI Ltd., UK
VTT, Finland

Details of the activities conducted within the NESC-IV project are given in Refs [IV-1]-[IV-6].

4.2 CRACK GEOMETRY AND LOADING

Surface cracks in cruciform clad beams under biaxial loading

A total of six clad cruciform specimens containing shallow surface flaws were tested under biaxial bending in Part A of the project. The cruciform specimens have a nominal thickness of 102 mm and an austenitic cladding of 6 mm. The test section for the cruciform beams contained weld material below clad layer, in which the surface flaw was inserted. The length orientation of the flaw was parallel to the longitudinal weld and it extended in the weld through-thickness direction. After pre-cracking the final nominal dimensions of the flaw were 53.3 mm long and 19.1 mm deep (including the cladding).

The key experimental variable was the test temperature of the beam, the objective being to achieve cleavage failure in the non-linear region of the load-versus-CMOD curve. Furthermore, each set of

specimens should be tested at a single temperature to facilitate statistical analysis of the results. However selection of a suitable temperature was not straightforward. In the first test of the cruciform specimen with a target crack-tip temperature of -60˚C the specimen failed well within the elastic region of the load-versus-CMOD curve. As a consequence, the subsequent tests were performed at slightly higher temperatures, in the range –40 to –33˚C. Information on the geometry and test temperature of these tests are given in Fig. 4.1.

Embedded cracks in clad beams under uniaxial loading

Part B of the NESC-IV project was focused on fracture behaviour of embedded flaws. A total of four specimens containing embedded flaws were tested under pure tension. Two of the test sections included the surface clad layer, while the remaining two were without cladding. The test section for the uniaxial beams contained only plate material below the clad layer (i.e. no weld material). The embedded flaw was a 2D sharp notch extending through the entire specimen with a flaw depth of about 20 mm located 14 mm under the surface. The uniaxial specimens had a nominal thickness of 102 mm. Information on the geometry and test temperature of these tests are given in 4.2.

4.3 MATERIAL CHARACTERIZATION

The test material consisted of an A533 B pressure vessel steel from a reactor pressure vessel (PVRUF) with a single-layer stainless steel strip-clad overlay (100 mm wide and 7 mm thick) on the inner surface. The longitudinal welds present in the vessel were of the double-J configuration. They were submerged-arc welds with A533 B Class 1 filler metal. The plate material, clad overlay and welds were typical of a production-quality RPV. The shell had a nominal inner radius of 2210 mm and a thickness of 232 mm, which includes the clad overlay. The different materials to be characterised included were: A533 B plate, longitudinal weld, clad overlay, clad/plate HAZ, and clad/weld HAZ.

Test	T [^{o}C]
PVR-1	-40
PVR-2	-38
PVR-3	-41
PVR-4	-55
PVR-5	-33
PVR-6	-35

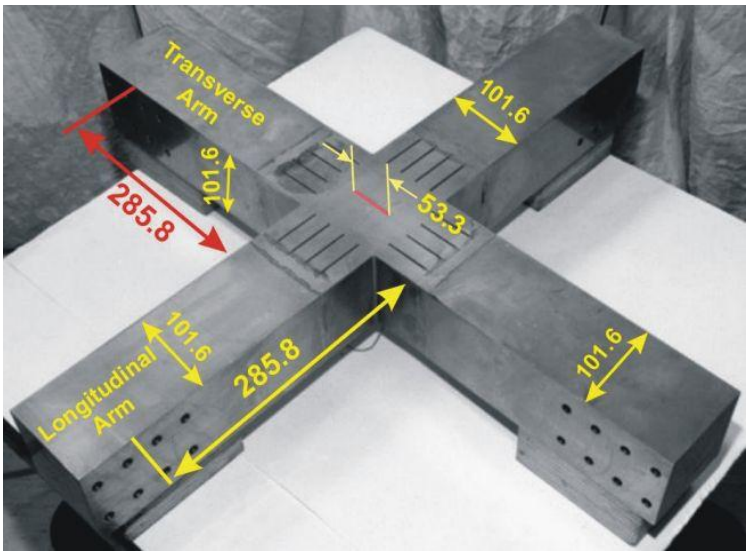

Fig. 4.1: Information on the geometry and test temperature of cruciform tests of NESC-IV.

Test	*T* [°C]	Remarks
4.1.1	-128	Unclad
4.1.2	-90	Unclad
4.2.1	-93	Clad
4.2.2	-77	Clad

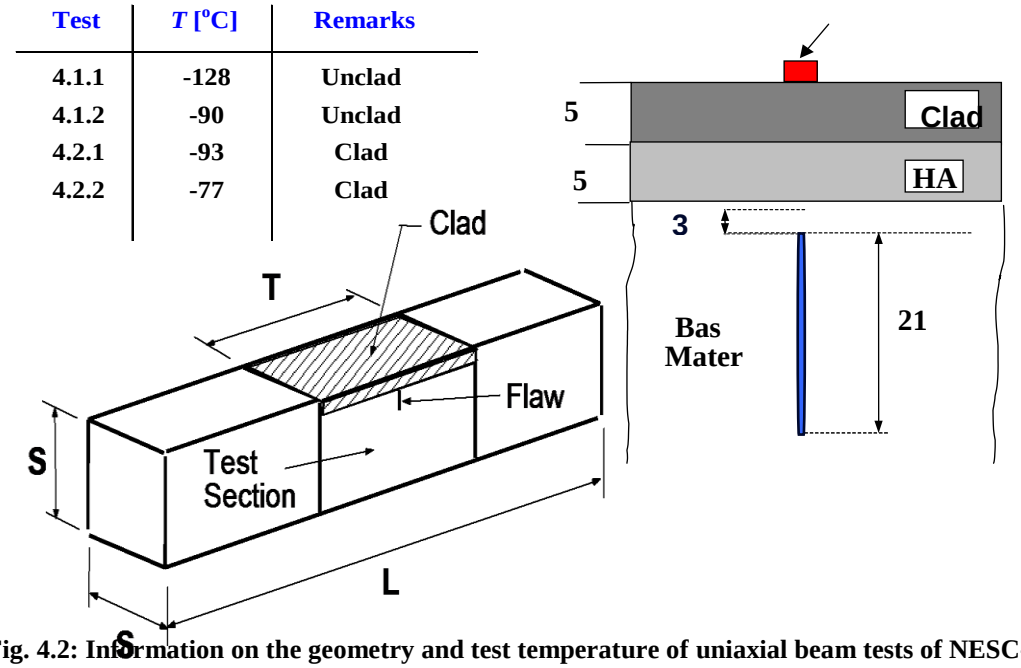

Fig. 4.2: Information on the geometry and test temperature of uniaxial beam tests of NESC-IV.

Tensile Tests

The scope of the tensile testing was to provide yield and tensile strength data as well as the full stress-strain curves for the various materials as input to the finite element fracture models. All tensile specimens were taken out in the circumferential direction. The temperature ranges covered by the tensile experiments were in the range of -100°C to room temperature. The temperature dependence of the yield strength and the ultimate tensile strength values are shown in Fig. 4.3 for the different materials. Table 4.1 shows the best-estimate values of the Ramberg-Osgood function parameters for the plate materials, the weld and the clad, taking the average estimates from the fitting of the tensile test results.

Table 4.1: Estimates of the Ramberg-Osgood parameters.

Material	N	α	εo
Weld	8.97	3.430	0.0030
Plate 100 & 200	6.65	3.587	0.0025
Clad	5.48	2.279	0.0025

Impact Testing

Several series of Charpy tests have been performed. All specimens were taken out in circumferential direction, implying crack propagation in radial direction. It was found to show a similar transition behaviour for Plate 100 and Plate 200. Drop-weight tests were performed by ORNL for the Plate 100, 200 and weld materials, resulting in T_{NDT} data. The reference nil-ductility transition temperature RT_{NDT} was not governed by the Charpy test results and was always equal to T_{NDT}. Table 4.2 summarises the key parameters obtained from the data.

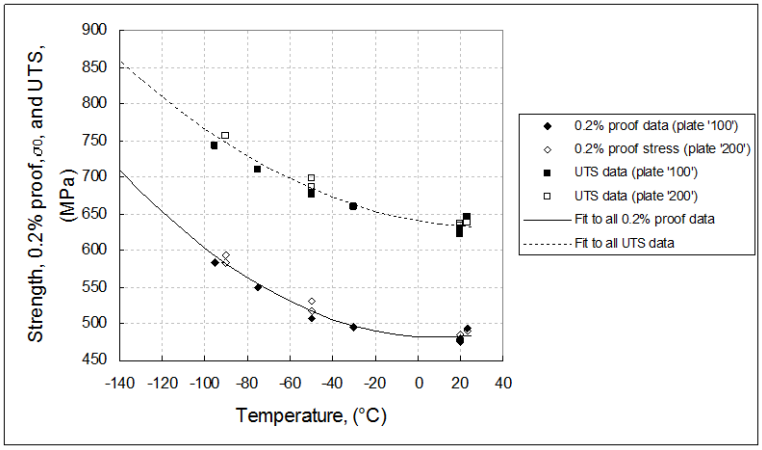

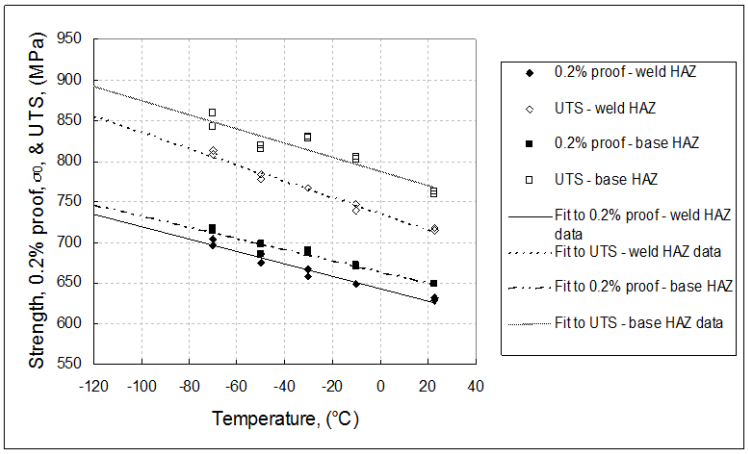

Fig. 4.3: Temperature dependence of Rp0.2% and UTS of the different materials.

Table 4.2: Summary of the impact, drop weight and RT_{NDT} parameters, [°C].

Material	Charpy T_{28J}	Charpy T_{41J}	Drop Weight T_{NDT}	RT_{NDT}
Plate 100	-55.1	-45.3	-30	-30
Plate 200	-68.6	-59.0	-35	-35
Weld	-35.3	-24.9	-35	-35

Fracture Toughness Testing

The scope of the fracture testing on the test materials was twofold:

- To obtain a "standard" estimate of the Master Curve T_0 parameter using standard deep notch (high constraint) specimens.
- To assess the shift in the transition curve for low constraint specimens.

Plate Fracture Toughness Data

The following test series have been performed on specimens from the Plate 100 material:

- IWM undertook tests on 25mm compact tension, C(T), specimens (a_0/W ~ 0.5).
- NRI tested 10×20 mm SEN(B) specimen having a_0/W ratios of ~ 0.5, ~ 0.2 and ~ 0.1.
- TWI performed a series of experiments on 10×20mm SEN(B) bars, with a_0/W ~ 0.1.

The K_{Jc} vs. test temperature data for the a_0/W ~ 0.5 specimens from Plate 100 are shown in Fig. 4.4. The SEN(B) and C(T) data were analysed separately because of the inherent difference in crack tip constraint between both types of specimens. Applying the Master Curve fitting procedure yielded to a T_0 value of -94.9°C for the SEN(B) tests and -99.8°C for the C(T) experiments.

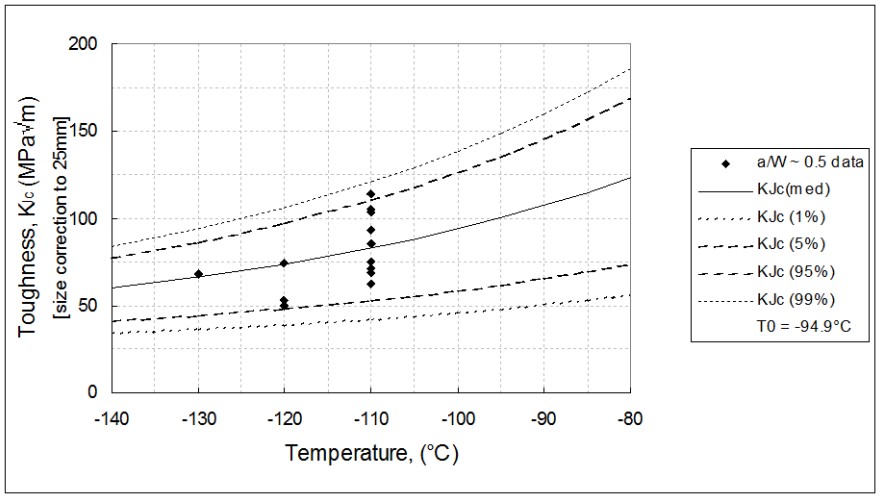

Fig. 4.4: Standard fracture toughness data and Master Curve fit for the Plate 100 material.

Figure 4.5 shows the analysis of the NRI low constraint SEN(B) a_0/W ~ 0.1 data, leading to a T_0 value of -120.4°C, which is 25.5°C lower than the figure obtained from the a_0/W ~ 0.5 experiments.

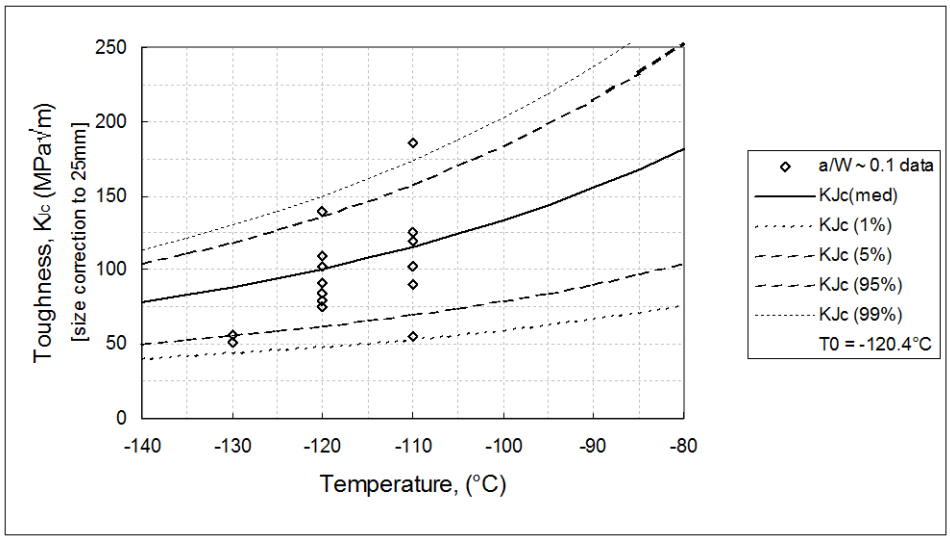

Fig. 4.5: Low constraint fracture toughness data for Plate 100.

Table 4.3 summarizes the T_0 values for the different plates, specimen types and a0/W ratios, which is indicative of the degree of constraint. Since the large scale embedded flaw bend specimens were fabricated from Plate 200, it will be necessary to use these data for the integrity analysis work and assume it will exhibit the variability of the Plate 100 specimen tests.

Table 4.3: T_0 estimates from the Plate 100 and 200 fracture toughness data.

Material	Crack size	Test temp. [°C]	Transition temp. [°C]
C(T), B=25 mm	$a_0/W \sim 0.5$	-50	-73.6
SEN(B)	$a_0/W \sim 0.5$	-100, -110, -120	-94.8
10 mm x 10 mm	$a_0/W \sim 0.1$	-120, -130, -140	-132.8

Weld Fracture Toughness Data

The K_{Jc} data for the deep notch SEN(B) specimens are shown in Fig. 4.6, together with the fitted Master Curve. When the IWM and ORNL C(T) data were compared, it was immediately apparent that the set of specimens tested by IWM possesses a markedly different and higher T_0 reference temperature when compared with the set tested at ORNL. Investigation indicated that this was probably due to the location of the pre-crack tips in the IWM specimens, which appeared to sample material close to the weld root region. Although details of the welding procedure have not been obtained, it is considered that the IWM data set is not appropriate to the large-scale specimens being tested in this project. The Master Curve fit to the VTT SEN(B) data produced a T_0 estimate of -94.8oC and the T_0 obtained from the ORNL C(T) experiments was equal to -73.6°C. Based on the above analysis, the estimate of the RT_{T0} parameter for the SEN(B) specimens is -75.4°C.

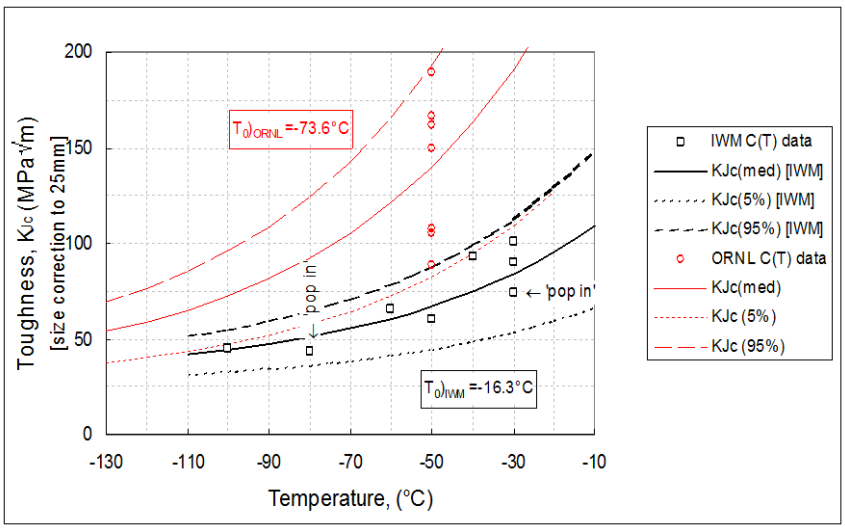

Fig. 4.6: Fracture toughness data and Master Curve fit for the weld material, from tests on C(T) specimens with a/W ~ 0.5.

4.4 FRACTURE ANALYSIS

The fracture analysis of the project was performed in two stages. In the first stage pre-test analyses were performed, leading to recommendations concerning the test temperature conditions for the biaxial cruciform tests. In the second stage, post-test analyses were performed on the basis of the Post-Test Problem Definition, which provided a unified presentation of all the input data required for structural post-test analysis. The post-test analyses are briefly discussed below.

Fracture analysis of surface-breaking flaws under biaxial loading

The post-test fracture analysis of the biaxial tests was not straightforward on account of the need to consider the impacting factors such as; the elasto-plastic behaviour of three distinct material zones (clad, HAZ and weld) and the residual stress induced by the mismatch between the materials. Five organisations performed finite element analysis on the cruciform specimens.

As an initial check on the performance of the FE models, the predicted applied moment vs. CMOD curves were compared with the data from the cruciform beam tests themselves, as shown in Fig. 4.7. All four models (DNV, ORNL, MPA and IWM) were found to provide accurate representations of the physical behaviour of the test pieces.

Concerning the crack tip behaviour, the focus in the first instance is on the stress intensity factor K_J. The cracked-body FE analyses show that K_J value in the HAZ region is greater than that at the root or apex of the crack. Fig. 4.8 shows the predicted increase in K_J at the two positions as the applied moment is increased.

To compare the results of the different FE analyses, two locations have been selected: the middle of the HAZ and the deepest point or apex of the flaw. The average values for these locations are reported in Table 4.4. The variation is modest, with a standard deviation at the highest bending moment level of 16 MPa√m.

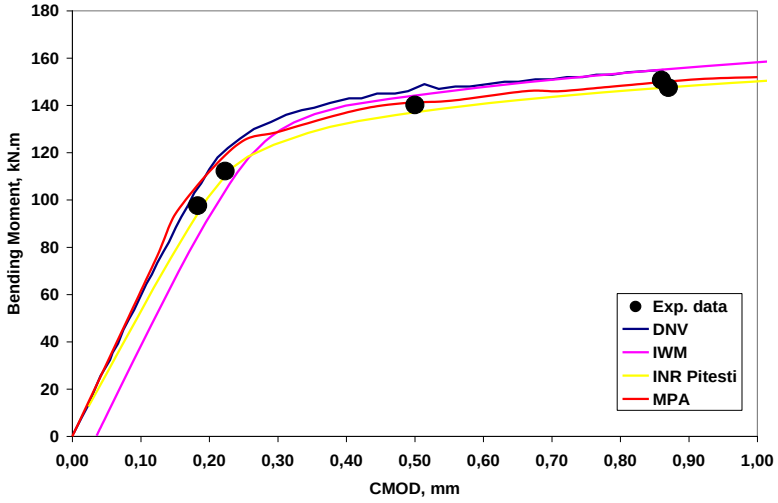

Fig. 4.7: Comparison of the experimental load- *CMOD* curves with FE predictions.

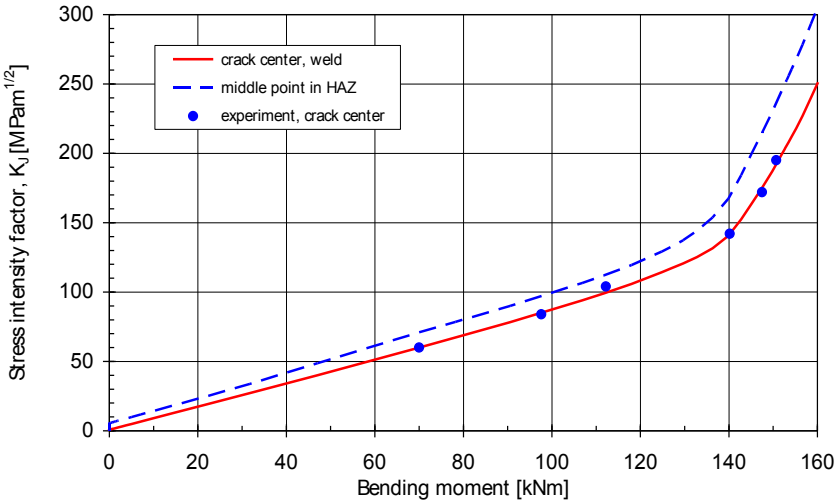

Fig. 4.8: Increase in *K* with load at the HAZ and deepest points, from the IWM analysis.

Fig. 4.9 compares the results of cruciform tests with the reference temperature transition curves determined according to the RT_{NDT} and RT_{To} parameters determined for the weld materials (-35o and -74°C respectively). The experimental data points are based on the average K_J values reported in Table 4.4. All the points fall above the reference curves, confirming their conservatism.

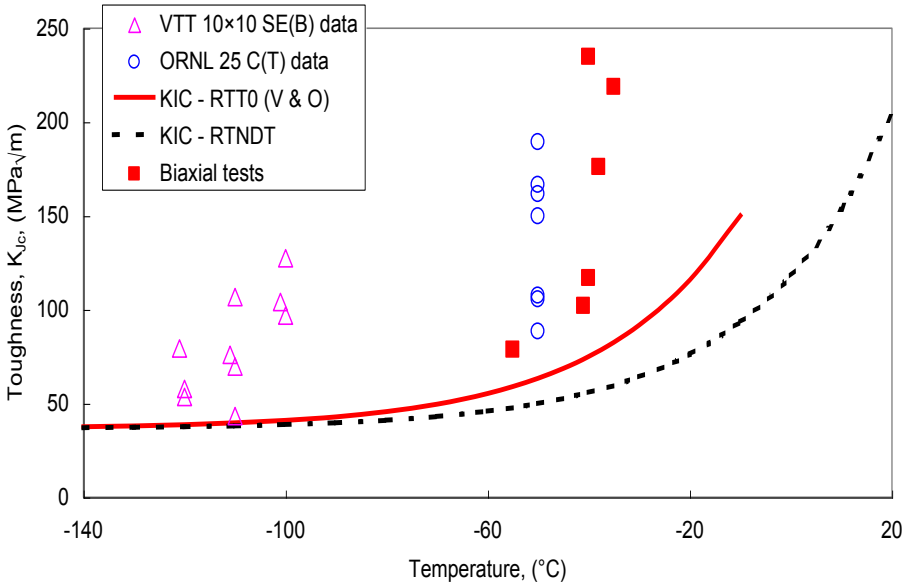

Fig. 4.9: $K_{j,max}$ from the biaxial tests compared with the RT_{NDT} and RT_{To} reference curves.

Fig. 4.10 compares test data with the 5, 50 and 95% cleavage probability Master Curves, based on the standard high constraint T_o estimate of -74°C. The data points lie within the band determined by the 5% and 95% Master Curves. Considerable scatter is observed. For test PVR-4 which failed at the lowest load, the K_J value falls just inside the 5% Master curve. On the other hand the values for tests PVR-5 and PVR-6, which exhibited the highest bending moment, lie on or slightly above the 95% Master curve. Overall the results provide evidence that the biaxial loading counteracted the shallow flaw, constraint loss effect.

Fracture analysis of embedded flaws under uniaxial bending

As an initial check on the performance of the FE models, the predicted applied moment vs. CMOD were compared with the data from the uniaxial beam tests. In general all the models provided accurate representations of the physical behaviour of the test pieces.

Concerning the crack tip behaviour, the focus in the first instance is on the stress intensity factor K_J. The majority of the FE analyses considered only the clad and un-clad specimens tested at approximately –90°C (4.1.2 and 4.2.1). Table 4.4 gives the values reported by the different analyses at the fracture bending moment for both the near surface (shallow) and deep tips. The variation between the analyses is modest, with a standard deviation of 20 MPa√m.

Fig. 4.11 compares the results of the K_{Imax} values from the tests with the 5, 50 and 95% cleavage probability Master Curves, based on the standard high constraint T_o estimate of -88°C. With the exception of the test performed at –128°C (almost in the lower shelf), the data lie well above even the P_f (95%) Master Curve, indicated that substantial constraint loss occurs at both crack tips.

The constraint parameter Q is expected to provide a more accurate estimate of constraint level than the T-stress at loads for which elastic-plastic conditions prevail. DNV, NRI and JRC studied the variation of the Q parameter for both the upper and lower tips for a nominal test temperature of –90°C. In all three cases the formulation of Q used was based on the crack opening stress, The DNV values at K_J = 100 MPa√m at different crack configurations are summarized in Table 4.5. All these results are in good agreement with each other and indicate that constraint loss occurs at both tips, with the effect being particularly pronounced for the shallow tip.

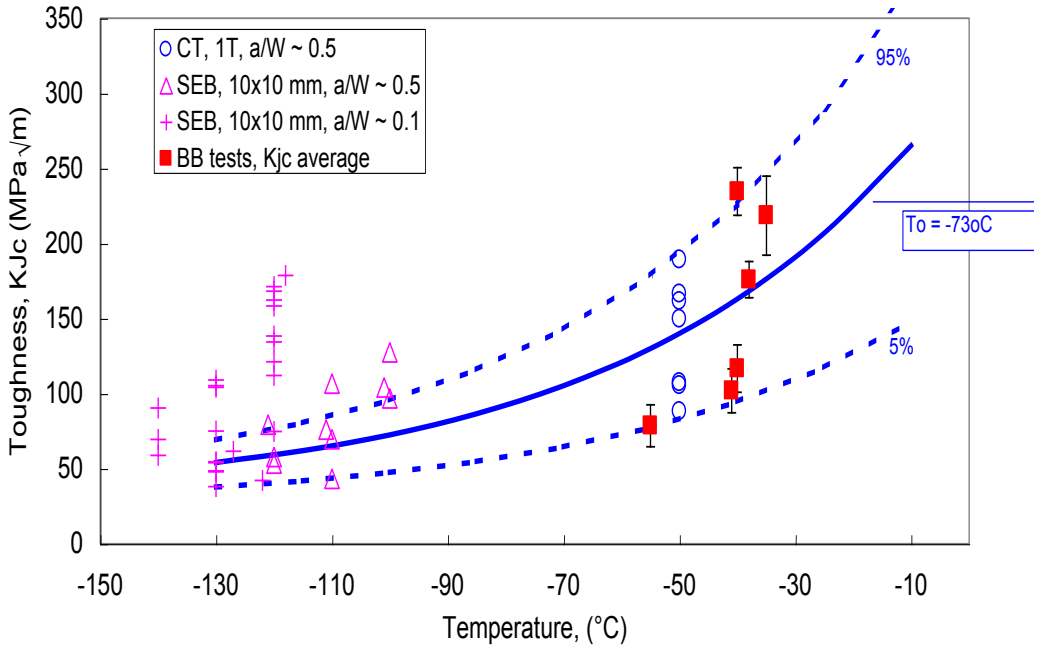

Fig. 4.10: Average calculated values of maximum K_J (HAZ position) compared with the standard MC.

Table 4.4: Comparison of the K_J values [MPa√m] calculated for the embedded flaw beams.

Test	T (°C)	DNV	JRC	NRI	IWM	ORNL	FANP	mean	st. dev
Unclad 4-1-2	-95.4								
Shallow tip		225	219	-	240	281	239	243	23
Deep tip		175	164	-	173	213	175	178	21
Clad 4-2-1	-93.2								
Shallow tip		186	147	170	195	195	178	181	14
Deep tip		133	108	128	133	128	123	127	7

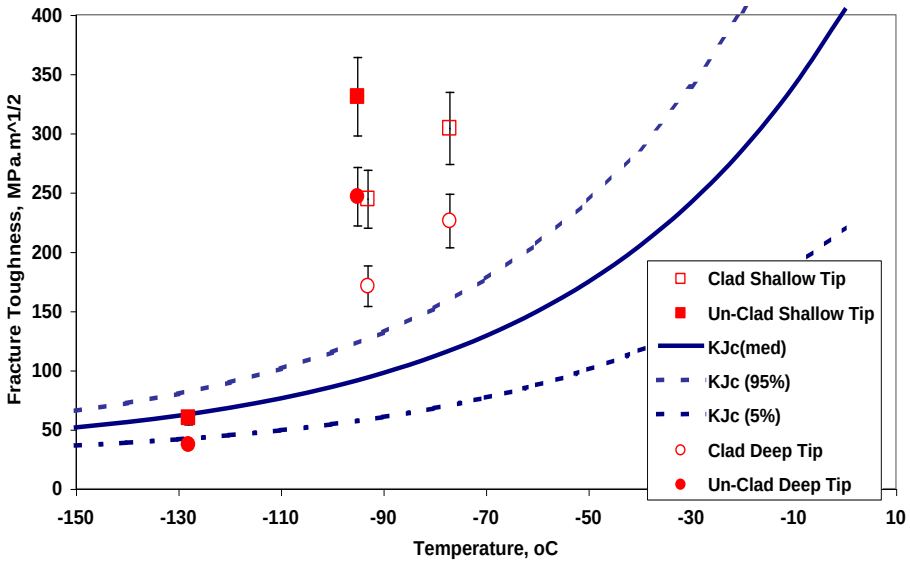

Fig. 4.11: Average values of *K* at fracture compared with the Master Curve (5%, 50% and 95%).

Table 4.5: *Q*-values for different crack configurations in the base material.

Case	*Q*
SEN(B), a/W= 0.50	+ 0.05
SEN(B), a/W= 0.20	- 0.34
SEN(B), a/W= 0.10	- 0.68
Embedded flaw, deep tip	- 0.35
Embedded flaw, shallow tip	- 1.05

4.5 SOME IMPORTANT ISSUES

Calibration of the Master Curve

The capability of the Master Curve to represent the transition behaviour and the calibration of T_o parameter is the fundamental basis for the subsequent evaluation of transferability of the methodology to more complex flaw geometries and loading conditions. The ASTM E-1921 procedure was successfully applied to the fracture data for weld, Plate 100 and Plate 200. Fig. 4.12 shows the compete data set for high-constraint C(T) and SEN(B) type specimens, plotted as function of T-T_o, where the T_o value corresponds to that for each data set. It is evident that for all three materials the mean Master Curve is consistent with the observed transition behavior in the range T_o ±25°C, and that data points fall with the limits defined by the 5% and 95% fracture probability curves.

Concerning the T_o estimates for the different specimen types and test conditions, a bias +8°C is expected between SEN(B) and C(T) specimens types due to differences in constraint. However in the case of the weld, the T_o value from the C(T) tests was 21°C higher than that from the SE(B) tests. Overall it appears that, even if a common test standard is applied, some caution is needed in interpreting fracture test data from different data sets of limited size and scope.

It is noted that the reference temperature RT_{To} values determined from the T_o estimates for the weld, Plate 100 and Plate 200 materials is consistently lower than the corresponding RT_{NDT} value. This trend is consistent with that observed in the NESC-I and NESC-II projects on RPV steels and underlines the importance of using direct measurements of fracture toughness for best-estimate assessments.

Experimental Evidence for Constraint Loss

The NESC-IV project considered two specific situations in which very different constraint conditions arise. In the case of the clad cruciform specimens, the testing conditions covered both a relatively shallow-flaw with biaxial bending load. For the embedded flaw beams, although the global loading was uniaxial, the situation of sub-surface crack tip at a highly loaded ligament was simulated. The influence of these features on the fracture behavior has been assessment in the first instance by comparison of the computed crack tip stress intensity values with the transition fracture behavior as represented by the Master Curve.

Considering firstly the biaxial beam tests, the test results fell within the standard high-constraint 5% and 95% Master Curves for the weld material (with T_o determined from C(T) specimens tested at a similar temperature). Since no uniaxial tests were performed, it is not possible to explicitly quantify the separate biaxial and shallow flaw effects). However it is clear that the results do not provide evidence of a substantial constraint loss effect and this leads to the hypothesis that the biaxial loading suppressed such effects, in particular at lower load levels. The results are therefore consistent with those from other biaxial test series reported in the literature (mostly also from the HSST program). Fig. 4.13 compares data from the NESC-IV biaxial tests with those published data from HSST Plate 14, ORNL 533B weld and Vocalist material A. All the data points fall within the 5% and 95% bounds and are reasonably distributed about the mean (50%) curve. As to whether biaxial loading can actually reduce the fracture

toughness below that predicted by a standard high constraint Master Curve, the limited NESC-IV biaxial data set is insufficient to allow conclusions to be drawn in this respect.

In summary, while the NESC-IV experiments did not explicitly test the Master Curve crack-front size dependence, however application of the standard correction in some cases increases the consistency of the results with constraint-based Master Curve models.

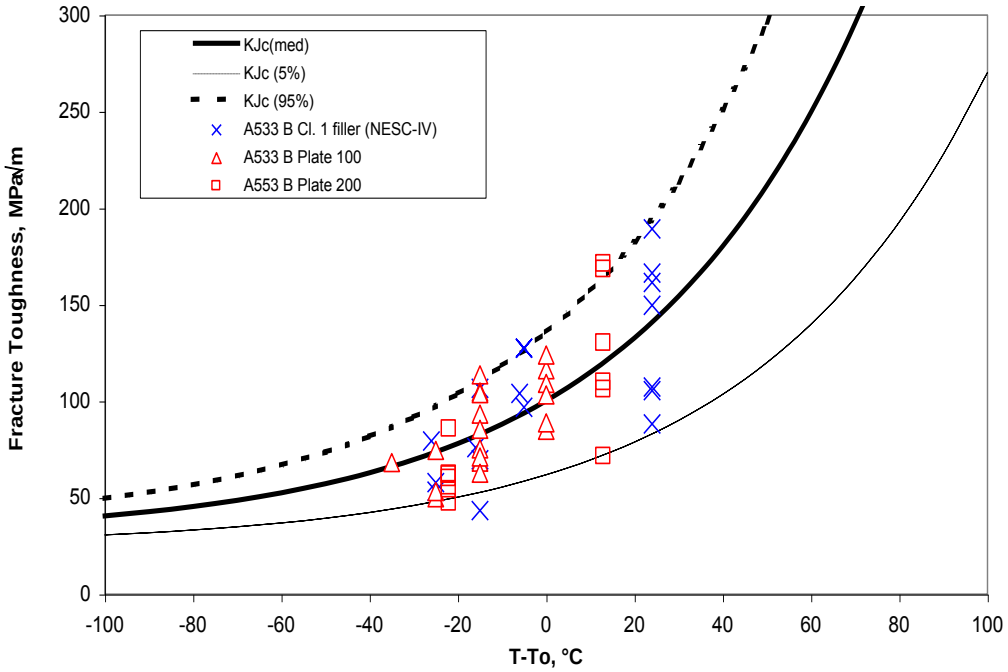

Fig. 4.12: Master Curve fits to the high constraint fracture data for the plate and weld materials.

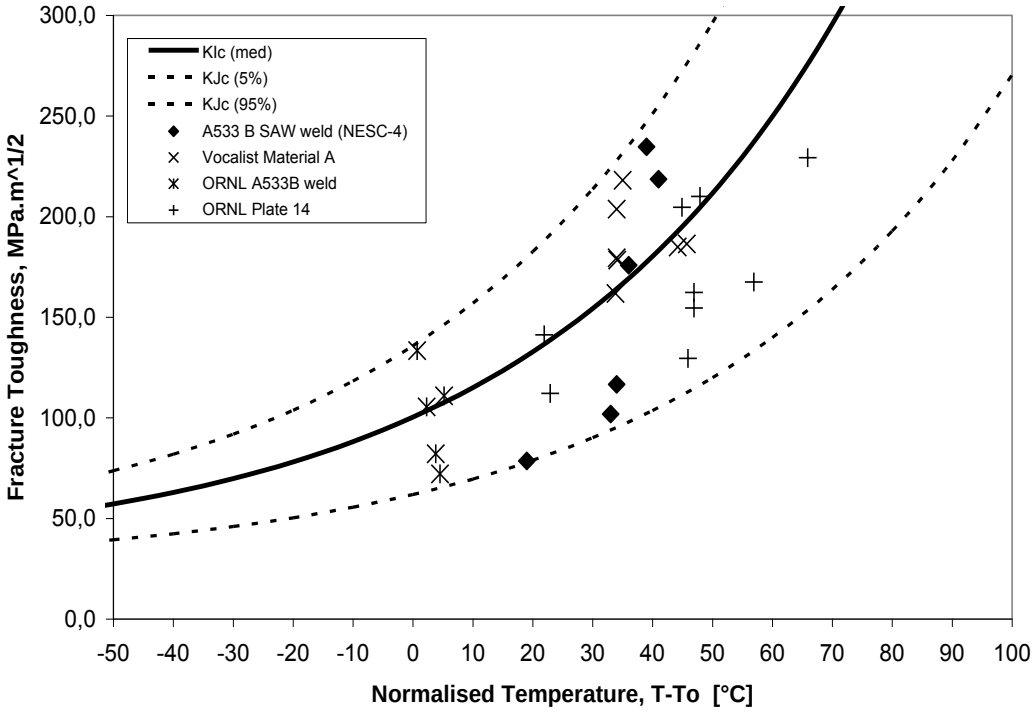

Fig. 4.13: Comparison of the NESC-IV biaxial test results on shallow flaw test pieces and other tests with the standard Master Curve.

Engineering constraint-based assessment methods

From the analyses conducted within the NESC-IV project, it was clear that the R6 constraint methodology can be very successful in predicting the observed behaviour during the embedded flaw beam tests, given appropriate material and structural constraint data. However, the lack of fully representative fracture toughness data meant that relevant data have been inferred using the Master Curve methodology, in an attempt to include the effects of temperature, crack front length, constraint, and plate-to-plate variability. There are four key areas where its applicability was examined:

1. Does the Master Curve provide an adequate description of the effect of temperature on transition toughness under high constraint conditions, for the materials used? If it does, then the difference in test temperature between the embedded flaw beams and many of the fracture toughness specimens is not an insuperable problem.

The general ability of the Master Curve to match the temperature variation of transition toughness in RPV steels is well established. As discussed in section 6.1 above, the Master Curve is considered to provide a reasonable description of the effect of temperature on fracture toughness for Plate 200 material under high constraint conditions.

2. Is its methodology for size-correction appropriate? Most of the test specimens were 10mm thick, and the fracture toughness data from these specimens were size-corrected to 25mm. The test beams were 100 mm thick.

Size correction to B = 25mm from a smaller test specimen thickness is a fundamental part of the Master Curve procedure, and must be considered reasonably well established over the modest corrections usually employed. Thus a further size correction from B = 25mm to B = 100 mm is not unreasonable. That said, there are no specific data available to judge its validity, since no 100 mm thick deep-cracked specimens were tested. It is noted that the B = 100 mm i.e. size-corrected, assessments do provide a slightly better correlation with the test results.

3. Can the effect of constraint loss in fracture toughness specimens be adequately described by a shift in T_o?

The ability of the Master Curve to describe fully the effect of constraint loss on transition toughness over the relevant temperature range has also to be considered. During the post-test analyses, only fracture toughness data of a/W=0.1 specimens from plate 100 over a temperature range from -130°C to -110°C. Subsequent additional tests performed at -80°C towards the end of the project provided evidence that the T_o shift established for the lower temperatures was also valid for higher values.

4. Is it reasonable to use the Master Curve to transfer plate 100 data to plate 200?

Comparison of the fracture toughness data for Plates 100 and 200 at a/W=0.5 shows that there is very little difference between the two plates at this constraint level. It is thus reasonable to assume that the same will hold at other constraint levels.

5 The NESC-V project

5.1 GENERAL ASPECTS

In nuclear plant piping systems thermal fatigue damage can arise at locations where there is mixing of different temperature flows. The severity of this phenomenon is difficult to assess via plant instrumentation and analysis. In Europe and elsewhere, there have been instances of thermal fatigue damage and over the last 10 years several recent R&D programs have been devoted to developing better understanding of the induced thermal loads and associated damage mechanisms. To exploit this work, in 2003 the Network for Evaluation of Structural Components (NESC) set up a project involving both utilities and R&D organizations. Its aim was to develope a consensus methodology for assessing high cycle thermal fatigue in piping components, with special attention to turbulent mixing phenomena at mixing tees in light water reactor systems. It has involved the collaboration of over 10 organisations from 5 European countries. All have participated on an 100% in-kind basis. The work program focused on the below main aspects:

a) Creating a database of service and mock-up data for better understanding thermal fatigue damage mechanisms. Common trends in the most severe cases, i. e. those leading to leakage and rupture, were sought for.

b) Developing a European multi-level thermal fatigue damage procedure, which should reflect the multi-disciplinarity of the phenomenon (thermo hydraulic, material, strain evaluation through FEA, damage analysis, fracture mechanic, ISI performance).

c) Selecting suitable cases from the database in order to validate the proposed procedure.

Additionally, several aspects on thermal fatigue are discussed. Existing procedures and expertise, not only in Europe but in USA and Japan are discussed. A main problem with thermal fatigue is to assess the thermal load and its transfer to the structure. Hence an entire section is devoted to shortcomings and possibilities with different ways of load determination.

Moreover, general fatigue assessment issues such as choice of fatigue curves and fatigue correction factors are discussed and general recommendations are provided. The need for the inclusion of additional environment factors has been debated, as the data used in the construction of the original design curves were often not obtained in control of environmental effects. The key parameters to be considered for environmental effects are described.

Details of the activities conducted within the NESC-V project are given in Ref. [V-1].

5.2 CRACK GEOMETRY AND LOADING

This NESC project has had a broad scope where systematic collection and appraisal of existing knowledge has been a key task. Looking in the back mirror on past experience in a systematic way has also been important. Hence, no specific experiment was carried out within the project. The emphasis was put on field operation and a database was set up. The project created a database of thermal fatigue damage cases, 45 of which relate to operational components and 5 to laboratory simulation tests. The cases were provided by the project participants. The vast majority of cases are pipe components, especially tee junctions where cracks emerge in the tee or in its neighborhood or valves. Apart from the database a separate list of significant cases from the literature was set up. A large number of field cases of thermal fatigue could be identified in the common literature. It is noted that much of the international efforts in thermal fatigue are initiated by these cases. A list of reference cases from the literature is shown in Table 5.1. A list comprising all the cases from the NESC database is given in Table 5.2.

The failure cases examined in the database essentially fall into two groups, as observed in other thermal fatigue studies:

1) In the first group the loading is characterized by turbulent mixing (or striping), with or without stratification. Typical components affected by this process are Tees without internal mixers. It is noted that none of the through wall cracking cases can be attributed to turbulence alone. However, the observed damage is not just superficial, and cracks penetrating to more than 50% of the wall thickness were observed in a few cases.

2) In the second group the thermal loading is predominantly stratification or similar types of large scale instabilities. Damage caused by stratification appears much more likely to cause leakage, and almost all the cases of through-wall cracking referred to in the present report are associated with this phenomenon. The combination of a low flow rate in at least one of the fluids and a high temperature difference controls the damage evolution. It is clear that different forms of stratification exist, the most harmful being the case with a moving interface between a stratified and a non-stratified state.

The largest separate data set on damages in Tees came from EDF. Operational data for three different geometries have been studied. These fourteen cases are well documented, and are operated under fairly similar conditions. The variable load ranges from 80°C to 180°C, with a rather accurate registration on the distribution of time spent on each load level. Hence, these cases enable a unified view on thermal fatigue of mixing tees subjected to turbulent mixing. The Tee geometries and the observed crack patterns are shown in Figures 5.1 - 5.3. The Tee itself is similar in each of the geometries; however the adjacent components may be different. It is noted that the cases also cover three different loading conditions in terms of flow directions.

It is of interest that the cracks appear within short operational times. All cracks appear within six months and all the components were run with quite large variations in operational conditions. The Civaux through wall cracking case (No.14 in Table 5.2) occurred within two months of operation. In this case turbulent mixing has been cooperating with a large scale instability to create both rapid initiation and crack propagation.

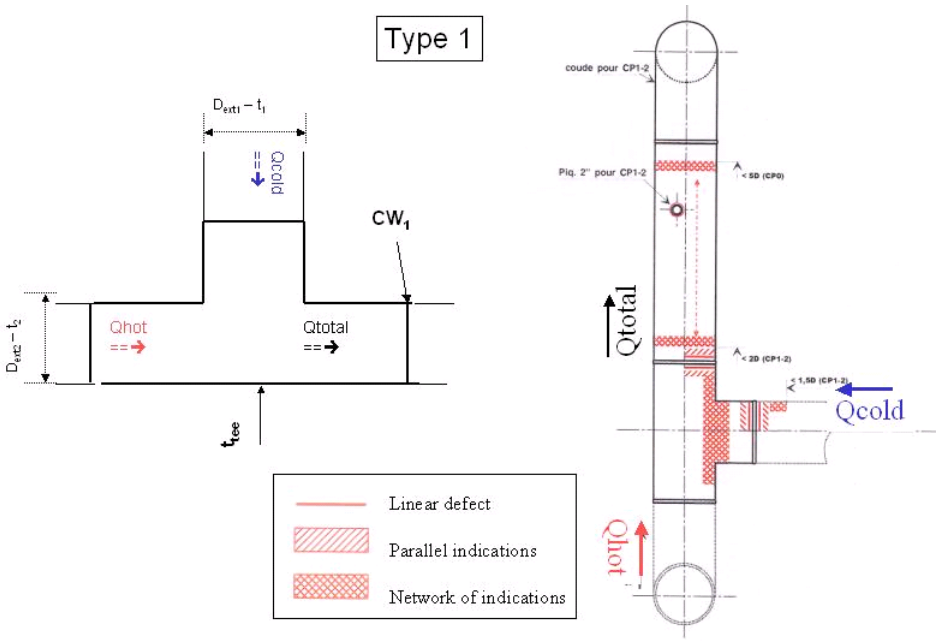

Figure 5.1: Location of cracks in a Type 1 Tee, from the EDF generic dataset.

Table 5.1: Damage cases (list of cases from the common literature).

Plant	Location	Size
Crystal River 3	Check valve body near the valve-to-safe end weld	140-degreecircumferential crack; two crack initiation sites: one on the inside surface and one on the outside surface
Obrigheim2	Weld between a 90-degree elbow and a nozzle	Crack extended 70 degrees circumferentially at the inside surface, 12-mm long at the outside surface
Farley 2	Heat affected zone of elbow-to-pipe weld	Crack extended 120 degrees circumferentially at the inside surface, 25-mm long at the outside surface
Tihange 1	Elbow base metal	89-mm long at the inside surface, 41-mm long at the outside surface
Genkai 1	Heat-affected zone of elbow-to-pipe weld	Crack extended 97 mm circumferentially at the inside surface, 1.5-mm at the outside surface
Dampierre 2	Check valve-to-pipe weld and base metal of straight portion of pipe	Crack extended 110 mm circumferentially at the inside surface, 25 mm at the outside surface
Loviisa 2	Pressurizer auxiliary spray line control valve body	Crack extended 80 mm along the horizontal surface and 25 mm along the vertical surface of the valve body
Biblis-B	Base metal of a straight portion of the pipe	Crack extended 50 mm axially at the inside surface, 20 mm at the outside surface
Three Mile Island 1	Weld between a 90-degree elbow and a 51-mm diameter horizontal line	Crack extended 51 mm circumferentially at the inside surface, 14 mm at the outside surface
Dampierre 1	Base metal of a straight portion of the pipe	Crack extended 80 mm circumferentially at the inside surface, 22 mm at the outside surface
Loviisa 2	Weld between a T-joint piece and a reducer	65-degree circumferential crack
Oconee 2	Safe-end to pipe weld	Crack extended 360 degree circumferentially at the inside surface, about 77 degree circumferentially on the outside surface
Civaux 1	Longitudinal weld in an elbow	180-mm long through wall crack

Table 5.2: The NESC-TF database of operational damage cases.

ID	Location	Size	Event	Load type	ΔT (°C)
1	Internal BWR part pipe connection with labyrinth type sealing	Through wall crack at the sealing at a base material part of the sealing with 5 mm thickness.	Operational	Transient	226
2	BWR part pipe connection with labyrinth type sealing	See ID1.	Operational	Transient	See ID1.
3	BWR mixing tee.	Through wall crack at 16 mm thickness.	Cold water from leaking pump	Stratification	210
4	BWR mixing tee.	8.6 mm axial crack in at base material thickness 14.5 mm.	Not known	Stratification/ Turbulence	280
5	BWR pipe mixing tee with inner sleeve	Axial and circumf. 2-3 mm cracking in a previous weld repair. Wall thickness	Intermittent inlet of cold water	turbulence	90 intermitently 200
6	BWR mixing tee.	Axial 11 mm cracking in the base material of wall thickness 14 mm.	Turbulent mixing under normal conditions	turbulence	64, intermittently 170
7	BWR nozzle in vessel with sleeve as thermal barrier	Through cracking in the base material of the sleeve	instable flow due to leakage, …	Instability	226
8	BWR pipe (Cone at pipe attachement)	Base material surface cracks at thickness 63 mm	operational events,	Transient	226
9	BWR pipe (Cone at pipe attachment)	Secondary cracking in supporting plate due to ID9	operational events,	Transient	--
10	BWR heat barrier sealing at a pump	Base material surface crack at thick section	Instable flow (leakage in sealing)	Instability	226
11	BWR pump	Base material surface crack at thick section	Instable flow	Instability	140
12	BWR pump thermal barrier	Surface crack at thick section.	Instable mixing cold and hot water	Turbulence	100-40
13	BWR pipe mixing tee with inner sleeve	Base material axial cracks in pressure bearing shell in contact with labyrinth sealing.	Possibly un-tight sealing	Instability	90

ID	Location	Size	Event	Load type	ΔT (°C)
14	PWR tee with connecting reducer	Circumferential through wall crack in weld between tee and reducer, thickness 5.5 *(mm)*	Incomplete tightness of valve	Stratification	70
15	PWR mixing tee with elbow	Through wall axial crack at elbow longitudinal weld. Thickness 9.6 mm.	Turbulent mixing, operational	Turbulence or large scale instability	160
16	PWR mixing tee	Through wall axial crack at pipe part with thickness 6 mm	Valve leakage	Stratification	230
17	PWR mixing tee	Cracking (net-work-type) in base material	Valve leakage	Turbulence or stratification	180
18-31	PWR mixing tees	Partial penetration cracks in base material and welds	Operational	Turbulence	80 and larger
32	BWR straight pipe after mixing tee	Axial through-wall crack in pipe, base material of 12.5 mm. Crack may have initiated in weld.	Valve leakage	Stratification	200
33	PWR elbow (Civaux 1 in table 5.1)	Through-wall Axial crack in axial weld in the elbow, thickness 9.6 mm	Operational	Large scale instability directly after turbulent mixing in a tee	80 and larger
34	PWR valve (Z-type geometry valve) (Loviisa 2 in Table 5.1)	Axial through wall crack at the base material, variable thickness larger than 10 mm	Leakage	Stratification	65 and intermittently higher
35	PWR elbow near tee at check valve (Tihange 2 in Table 5.1)	Longitudinal through-wall crack of about 45 mm length on the outside surface in the base metal of the last downstream elbow. Thickness 18 mm.	Leakage	Stratification	270
36	BWR pipe elbow	Through wall crack at longitudinal weld back side of elbow. Thickness 12 mm.	Leakage	Stratification	120
37	BWR pipe reducer near tee.	Through wall crack at circumferential weld of a reducer. Thickness 12 mm.	Leakage	Stratification	150

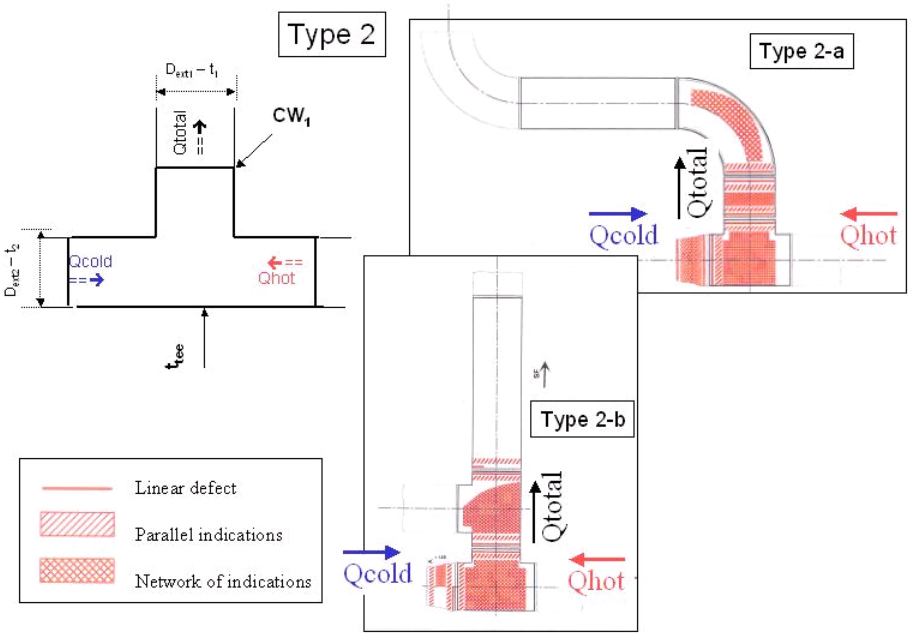

Figure 5.2: Location of cracks in a Type 2 Tee, from the EDF generic dataset.

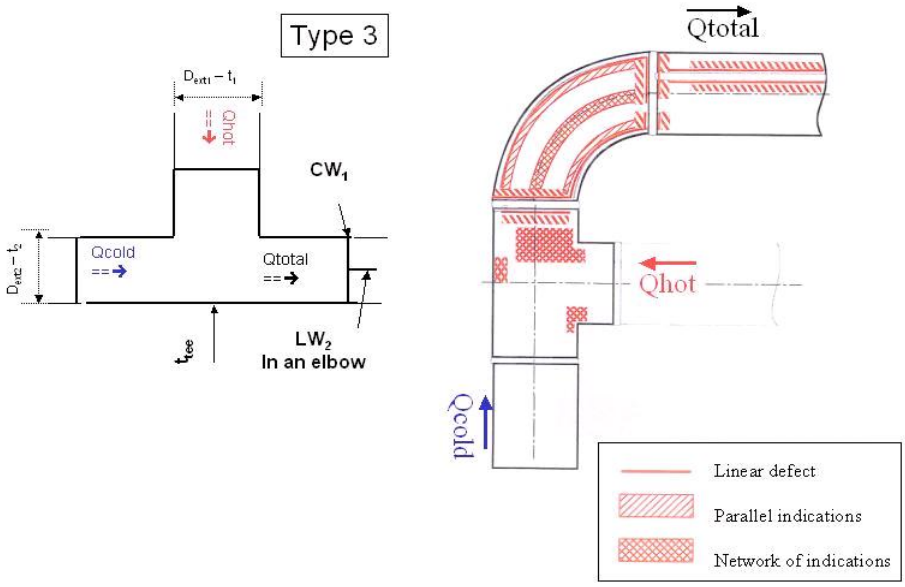

Figure 5.3: Location of cracks in a Type 3 Tee, from the EDF generic dataset.

Feature tests i.e. tests involving simulated thermal fatigue performed under laboratory conditions, have an important role to play for verification of assessment procedures and for establishing transferability of standard fatigue curves to component-life situations. For NESC-TF five cases have been brought together in an experimental case database. All of these experiments were different and had rather different scope. The principles for these mock-ups are shown in the figures below. Detailed information form each test has been collected in a separate dedicated report. Specifically the FAT3D is dedicated to the study of three dimensional effects with an accurately controlled load, whereas the Fatherino 2 test aims at turbulent mixing in a tee. All five experiment set-ups are shown in Figs. 5.4 - 5.8.

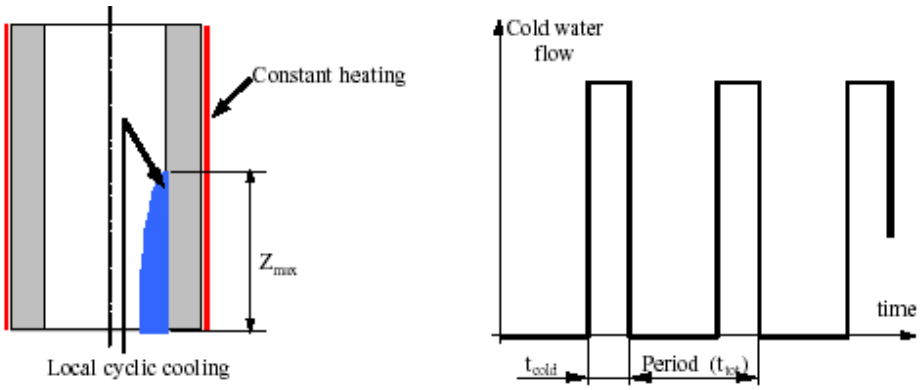

Fig. 5.4: Principle of the CEA FAT3D test.

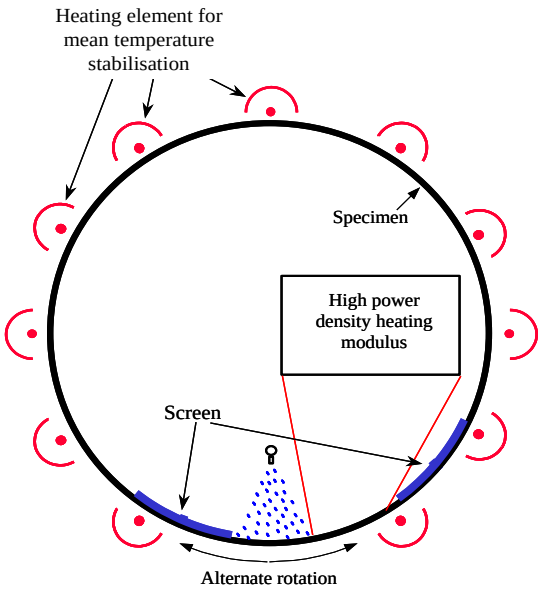

Figure 5.5: Principle of the INTHERPOL thermal loading device.

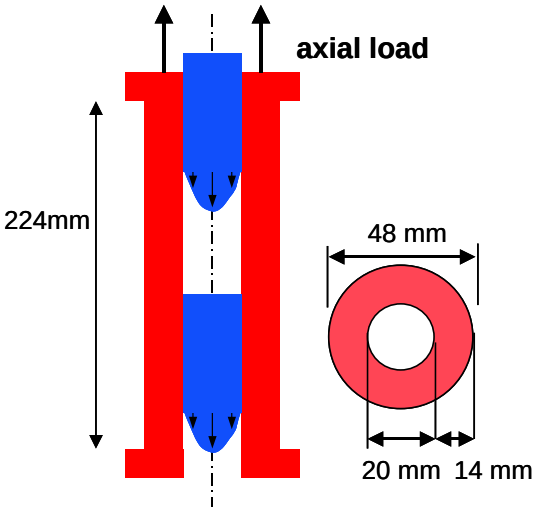

Figure 5.6: Principle of the JRC thermal cycling device.

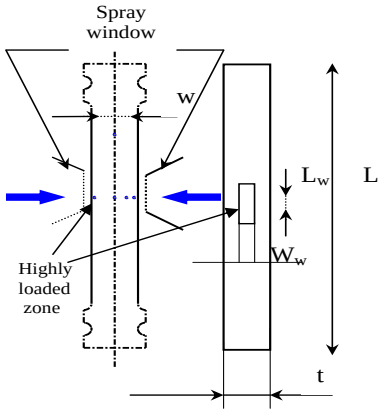

Fig. 5.7: Principle of the SPLASH facility.

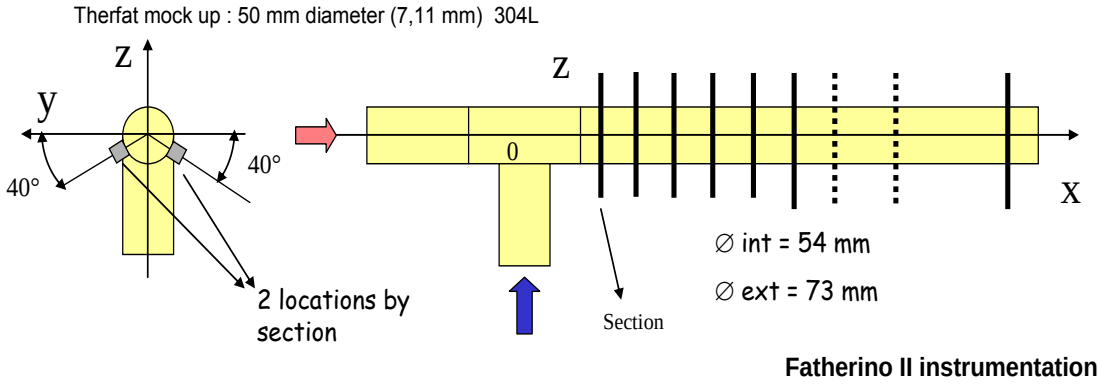

Fig. 5.8: Schematic of the FATHERINO 2 test set-up.

5.3 MATERIAL CHARACTERISATION

Since the database contains numerous components and experimental set-ups no specific material characterization is possible. The material types used in the studied experiments are collected in the table below. It is evident that all experiments used the material type stainless steel 304/316.

In fact, the same holds for the operational damage cases. Almost without exceptions, the damaged component was made of 304/316 type stainless steel. This will by necessity impose some limitations on the conclusions. The experience of thermal fatigue in carbon steel and other materials is hence very limited. This is of course a limitation, but also indicates that nuclear carbon steel components are less exposed to thermal fatigue. A main reason for this may be that carbon steels are seldom chosen for components in operation subjected to fluctuating thermal loads. The material types studied in this project are given in Table 5.3.

Table 5.3: Material types studied in NESC-V.

Experiment	Material
FAT3D	316 L
JRC Cyclic Down-Shock Tests	316L
EDF INTERPOL Test	304L
CEA SPLASH Tests	AISI 304L, 316L, 316NG
CEA FATHERINO Test	304L

5.4 FRACTURE ANALYSIS

A European Procedure for Assessment of Fatigue Damage under Turbulent Mixing was developed and used for analysis in this project. This procedure is so far limited to turbulent mixing in tees. The main reason for this limitation is the simplification of the stress state, since no special effects on the stress distribution is observed.

A multi-level approach is proposed for the procedure, which follows the French model and recognizes that despite recent R&D work on measurement and simulation of mixing conditions at Tee junctions, the description and quantification of the associated thermal loads remains a difficult task. The first level contains a screening criterion for turbulent mixing. For stainless steel (304, 304L, 316 and 316L), no specific fatigue analysis or fabrication improvements are necessary if $\Delta T_{nom} = |T_{run} - T_{brach}| \leq 80^{o}C$, see Fig. 5.9.

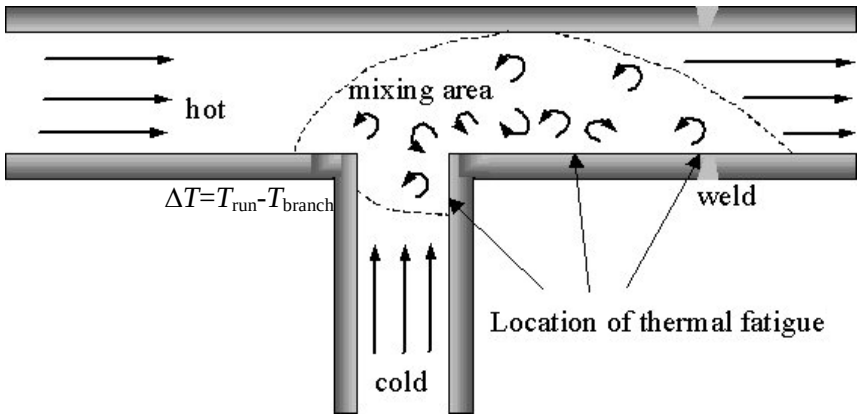

Figure 5.9: Turbulent mixing at a Tee.

The second level relies on the basic assumption that the temperature variation is described as sinusoidal. The total analysis includes the following four basic steps.

1) Thermal analysis with heat transfer between fluid and component by convection and conduction through the pipe wall. The temperature in the fluid is sinusoidal $T = \Delta T / 2 \cdot \sin(2\pi f \cdot t)$. ΔT is the local temperature range, *f* is the frequency to be determined and *t* is time. This analysis is repeated for different temperature variations and frequencies.

2) The time dependent temperature distribution is used directly as input to an elastic stress analysis. The resulting stress or strain variation as function of the frequency is determined.

3) Appropriate reduction factors are then applied on the stress/strain variation.

4) The number of cycles for a specific ΔT is determined from the computed stress/strain variation and appropriate fatigue curves. The frequency, *f*, which gives the shortest life (in duration) is selected. This procedure is repeated for different temperature variations resulting in a curve which gives the fatigue life (in duration) versus temperature variation. The fatigue usage factor can be directly determined from the ratio between duration of the thermal load and the computed fatigue life at this temperature.

These calculation steps will lead to a fatigue reference curve, Fig. 5.10, where the duration is given for each ΔT. An example of this curve is shown in the below figure. In case of a variable ΔT a pseudo type Miner sum is performed.

The SIN method was applied for the EdF mixing tee cases, presented above. Both design analyses and best estimate analyses of these cases were attempted. The method is quite sensitive to parameter variations. The usage factors should ideally not deviate too much from unity. The computed usage factors are on the low side. However, with the appropriate factors in a design curve the predictions will be conservative, see Fig. 5.11.

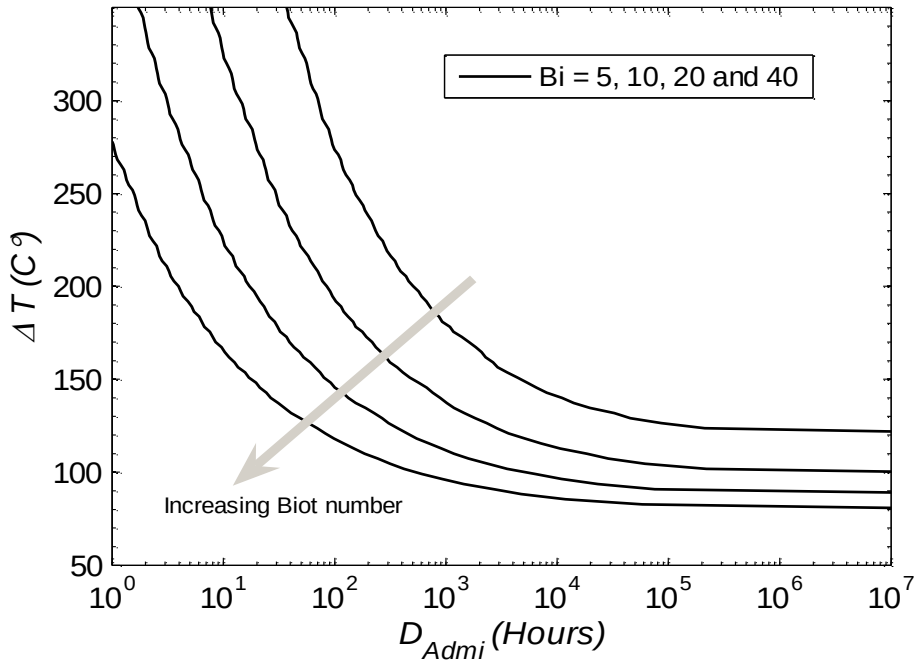

Figure 5.10: Example of a fatigue reference curve.

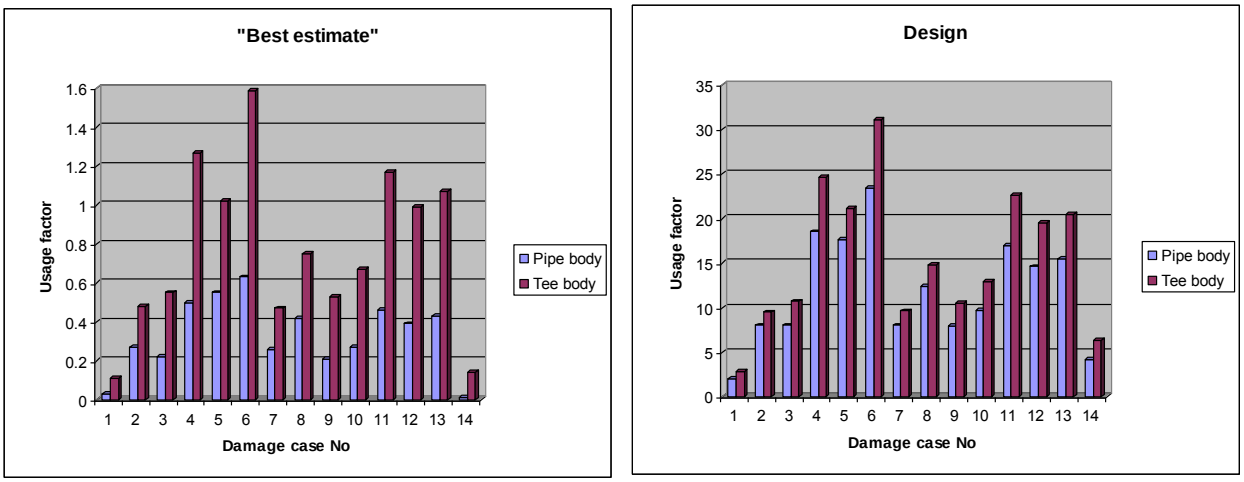

Figure 5.11: usage factor of the SIN-method. Analyzed with a mean fatigue curve and a design curve.

Despite the limitations and simplifications, the SIN-method seems to provide reliable results. Reliable margins, i. e. usage factors well above unity, prevail if a design curve is used. It is, however, important to emphasize that the SIN methods is only attuned for cases of turbulent mixing. Load cases with a three dimensional special distribution such as stratification should not be analyzed with the SIN-method.

5.5 SOME IMPORTANT ASPECTS

An important issue in this study concerns the evidence to support the use of screening criteria at mixing Tees, based on the nominal temperature difference between flows, i.e. to establish if there is a threshold below which no significant fatigue damage occurs. In this regard EDF have proposed a threshold value of ΔT=80°C at mixing Tees fabricated in stainless steels /5.13/ and this concept has been taken up in the proposed European procedure . The Swedish study, which collected a substantial dataset of temperature difference values for damaged components , shows a small number of cases (2 with ΔT=55°C, 1 with ΔT=56°C and 3 with ΔT=60°C) below the 80oC level. However, when an attempt was made to examine these in more detail, only limited information was found; at least one case had a nominal temperature difference above 60oC and the component was occasionally operated with a considerably higher temperature difference. The project's own database was also evaluated to verify this approach. The EDF cases for mixing Tees, which all show some damage, were operated with nominal temperature differences higher than 80oC for most of the time. For all the other cases in the NESC database, the number of damages cases for increasing nominal ΔT values is summarised in Fig. 5.12. The distribution is similar to that for the Swedish cases in Fig. 5.13. Hence the support of a thermal fatigue threshold at ΔT=80°C finds fair support in the NESC database.

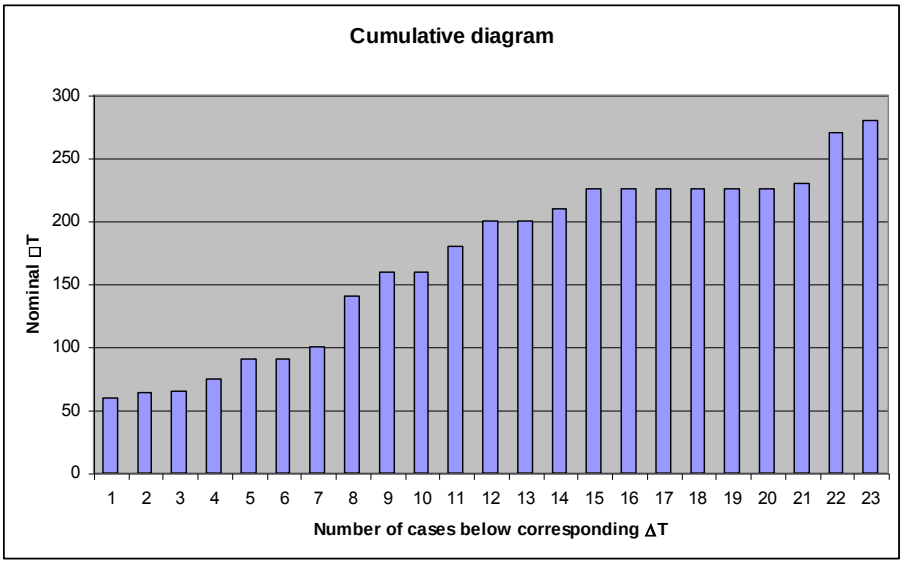

Figure 5.12: Number of NESC-TF operational database cases below a given ΔT.

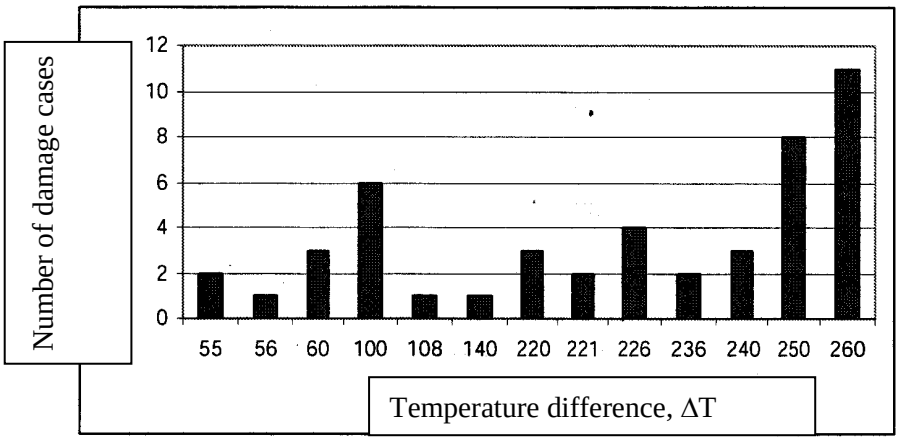

Figure 5.13: The distribution of temperature ranges from the investigation of piping failures in Sweden.

There are several instances in which thermal fatigue damage has developed within short times, even less than a year. These cases are generally associated with the turbulent mixing in tees and underline the importance of reliably representing the actual operating conditions in the damage assessment process. Hence the common classification of thermal fatigue as an ageing process (implying that its probability increases progressively with time) is potentially misleading.

It is instructive to distinguish between high frequency turbulent loading and three dimensional loads with relatively low frequency. This load is often related to large scale instabilities of the fluid. Although this categorization is simplified it is effective for the understanding of thermal fatigue. Turbulent mixing mainly causes skin stresses and hence rather shallow cracks, generally in a network pattern.

The three dimensional nature of the load will exhibit larger and deeper stresses. Hence, these loads are inclined to create deep cracks, that eventually lead to through wall cracking. The experiment FAT3D above shows a case where through wall cracking was induced in the laboratory. The experiment was conducted with a tight control of the thermal load and was designed to study the conditions for through wall cracking with three dimensional loads. The thermal load imposed high membrane stresses and explained both the through wall cracking and the axial orientation of the crack. The time for the crack to penetrate the wall was even shorter than the time to initiation.

The damage case survey shows that stratification in combination with thermal cycling is a major cause of through wall cracking. Stratification may typically occur in conjunction with turbulent mixing in dead legs, see Fig. 5.14. Here, the movement of the interface between the stratified and non-stratified fluid may cause large stresses. Simultaneously, and in another frequency domain, turbulent mixing may add to the crack initiation, while the three dimensional load is responsible for the crack driving mechanism.

A main risk scenario is hence a combination of turbulent mixing and a large scale instability where rapid crack initiation is followed by rapid crack growth.

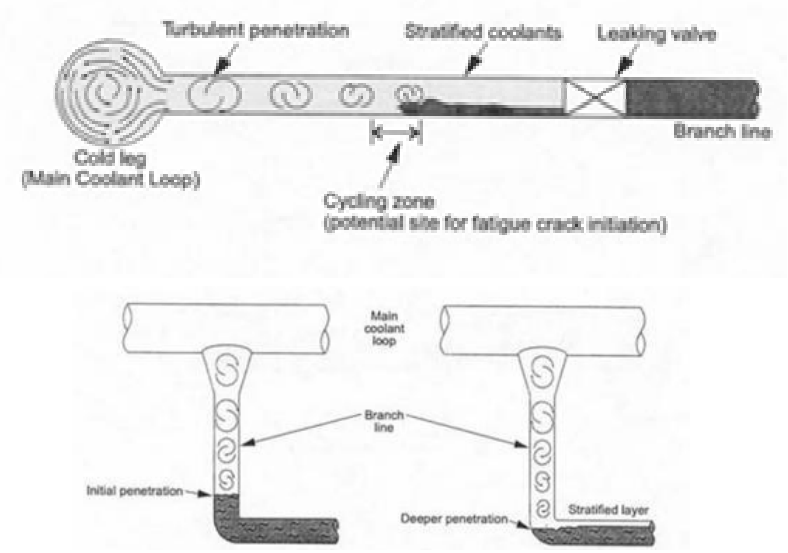

Figure 5.14: Thermal cycling in a straight pipe and an elbow

6 The NESC-VI project

6.1 GENERAL ASPECTS

For light water reactors the integrity of the reactor pressure vessel (RPV) has to be demonstrated for severe overcooling transients, considering also that crack-like flaws could be present in the vessel wall. For safety assessment purposes such postulated flaws are generally assumed to be surface breaking, located on the inner clad surface and of semi-elliptical form. Studies on actual defect distributions indicate that actual RPV flaws, if present at all, are more likely to be sub-surface. This has prompted a series of studies aimed at optimising the fracture mechanics procedures for evaluating brittle fracture initiation at such flaws. Such procedures need however to be properly validated against experimental data and several previous NESC projects have included sub-clad flaws (NESC-I, NESC-II, NESC-IV). NESC-VI focuses on the role played by the stainless cladding at the inner surface of a VVER-type vessel if fracture were to initiate at a postulated sub-surface flaw. The NESC-VI project can be considered as an extension to the NESC-IV project to study the transferability of fracture toughness data between different crack configurations.

The 6th project of the NESC organisation deals with the fracture mechanics analysis of a set of 3 tests on beam specimens with simulated sub-surface flaws, which were performed by NRI Rez plc for the PHARE project "WWER Cladded Reactor Pressure Vessel Integrity Evaluation (with Respect to PTS Events)". The objectives were as follows:

1) To assess the capability to predict whether the cracks propagating into the cladding arrest or cause full fracture, and

2) to assess the capability to predict the location of first initiation: near-surface or deep crack tip

The project was launched in December 2006 and completed in 2008. It brought together a group of 10 organisations from the NESC organisation to perform comparative analyses of selected tests, based on a comprehensive datapack prepared by NRI.

Details of the activities conducted within the NESC-VI project are given in Ref. [VI-1].

6.2 CRACK GEOMETRY AND LOADING

Semi-large scale test specimens represented bars for four-point bending with cross-section nominal dimensions 85 x 85 mm with cladding. Scheme of the test specimens is given in Fig. 6.1. Inserts from archive materials with the length of 200 mm were welded together with the arms to obtain final required length of the test specimens 670 mm.

Specimens with two types of through-cracks were tested in NRI:

- 8 specimens (named "normal specimens") with embedded type cracks, with the crack depth of 15 mm, their upper tip located 3 mm under the fusion line of the cladding, both crack tips are sharp (fatigue cycled). Specimens are marked by 1E2, 1E3, 1E4, 1E5, 1E9, 1E10, 1E11 and 1E12.

- 3 specimens (named "abnormal specimens") with embedded type cracks, with the crack depth of 40 mm, their upper tip located 3 mm under the fusion line of the cladding, only upper crack tip is sharp, lower crack tip was artificially blunted (drilled out). Specimens are marked by 1E6, 1E7 and 1E8.

Test temperature during all tests was equal to the room temperature, i.e. in the range betwee19 and 23 °C. The following procedure has been applied during the tests:

1. Identification of the specimen, identification of loading and fracture parameters, measurement of the specimen.

2. Assembling of the specimen in the test equipment, pre-loading up to approx. 5 kN (precise value is measured and typed during the experiment), installation of measuring devices.

3. Fracture test was realised by slow quasi-static loading up to specimen fracture or pop-in (if pop-in occurred, the test was interrupted for some time and necessary documentation - photos were taken), and then the loading continued up to specimen fracture (residual central force being smaller than 20 kN). All measured parameters were continuously recorded. Fracture test usually lasted between 10 and 40 minutes.

4. If necessary, further loading of the specimen was applied till full fracture (fracture through of the specimen), but without any further measurements.

5. Conservation of fracture surfaces against corrosion, identification and marking broken arms, cutting-off fracture surfaces and fractography.

   Database of raw measured parameters was created - data are archived on CD as files marked in similar manner as the specimens.

A total number of 8 normal and 3 abnormal specimens were tested in NRI. Three of normal specimens, sustaining maximum applied load, failed suddenly (fractured through) after initiation of brittle fracture, while the five remaining normal specimens exhibited pop-ins with crack arrest in cladding (close to cladding/base material interface) and in base material close to specimen bottom; the appropriate values of force just before pop-ins for these specimens were lower than in case of specimens that fractured through. During the subsequent loading, additional pop-ins as well as ductile tearing were observed before the final specimen failure. All 3 abnormal specimens exhibited initiation of brittle fracture (pop-in) from the upper crack tip, crack arrest in the cladding (with no crack propagation from crack bottom hole) and some amount of ductile tearing into cladding during subsequent loading before the final specimen failure. For evaluation of the test within NESC, the following three specimens were selected:

1) 1E2 – normal specimen with pop-in

2) 1E4 – normal specimen with sudden fracture through

3) 1E7 – abnormal specimen with pop-in

The main features of these three tests are given in Table 6.1. The experimental results on load versus load-line-displacement (LLD) for these tests are shown in Fig. 6.2.

Table 6.1: Main fracture test experimental results

Spec No.	Specimen Type	Average crack depth (mm)	Test temp. (°C)	Max. force (kN)	Force after 1st pop-in (kN)	Ductile tearing before pop-in (mm)	Failure features
1E2	normal	13,8	20,5	259,7	110	0,045	pop-in 1 **mm** to cladding
1E4	normal	14,7	20,5	339,4	-	0,133	sudden fracture through
1E7	abnormal	39,7	19,5	205,5	162	0,342	pop-in to cladding,

Test	T [°C]	Remarks
1E2	20.5	Pop-in
1E4	20.5	Fracture
1E7	19.5	Pop-in

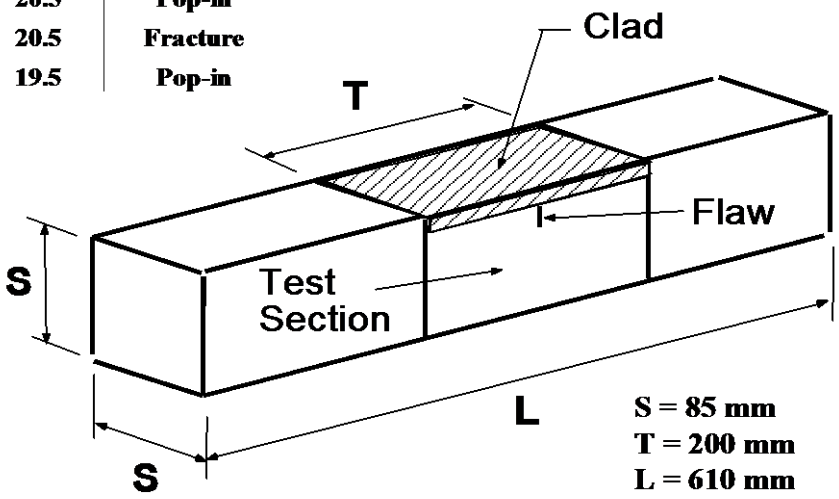

Fig. 6.1: Scheme of the test specimens.

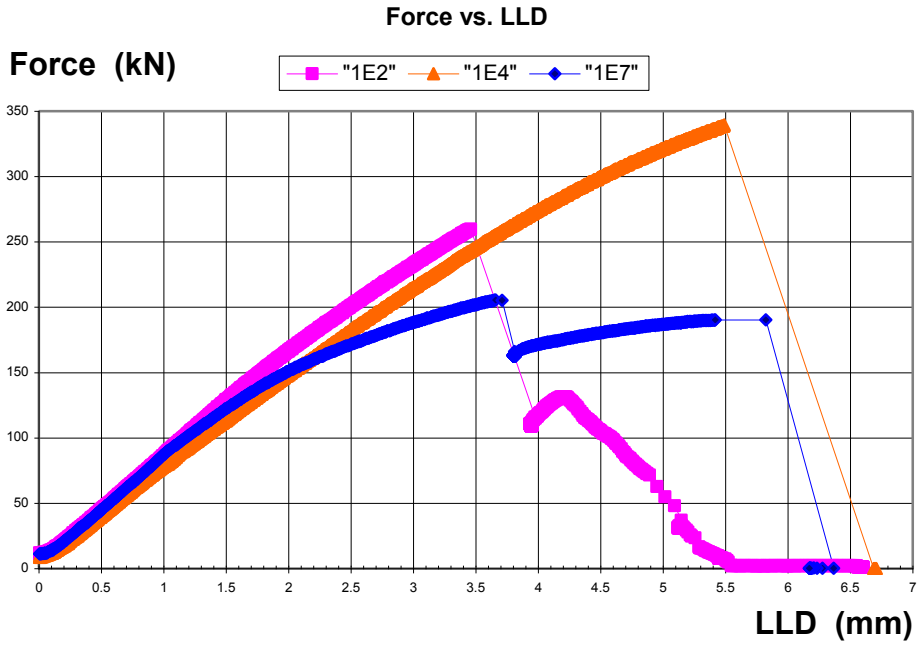

Fig. 6.2: Experimental force vs. LLD curves for tests 1E2, 1E4 and 1E7.

6.3 MATERIAL CHARACTERISATION

The test material was intended to be representative of that used for WWER-440 reactor pressure vessels. Thus real archive materials from decommissioned reactor pressure vessel were chosen. The base metal (BM) and the cladding had both been manufactured with the same technology as vessels in Dukovany NPP. Blocks of dimensions of approximately 500x1000 mm were mechanically cut from the vessel – these blocks contained also full thickness austenitic cladding. The blocks were then heat treated by a special procedure to obtain a similar degree of embrittlement (defined by the ductile-to-brittle transition temperature) as an RPV at the end of its design lifetime.

Tensile properties

For both the thermally treated (aged) base material and cladding, three tensile tests were performed on small round tensile specimens with diameter 4 mm at room temperature. Results obtained from one selected tensile test (for each of the two materials) were mathematically treated to obtain the true stress - true plastic strain curve Overview of the mechanical properties of the heat treated (aged) BM and heat treated cladding is as follows:

Base material**:** $R_{P0.2}$ = 887.8, R_m = 984.1 MPa , E =211 GPa

Cladding (second layer of cladding): $R_{P0.2}$ = 337.9, R_m = 593.9 MPa, E =162 GPa

Fracture Toughness

Master Curve reference temperature T_0 was determined for the aged BM, based on samples taken from two locations: 3 mm below BM–cladding interface and 18 mm below BM–cladding interface. Pre-cracked Charpy specimens loaded by three-point-bending were used. The respective T_0 values together with their standard deviations as determined according to ASTM-1921 are:

For location 3 mm below the interface: $\mathbf{T_0 = 22.8\ °C,}$ σ = 5.43 °C

For location 18 mm below the interface: $\mathbf{T_0 = 19\ °C,}$ σ = 5.67 °C

The *J-R* curves were determined for both 1st and 2nd layers of cladding (ss-1 and ss-2). Three specimens for each layer were tested. The following lower bound curves were established for the cladding material, [*da* in mm and *J* in $kJ.m^{-2}$]:

For 1st layer, at BM: $J = 590.da^{0,5}$

For 2nd layer, at RPV inner surface: $J = 180.da^{0,7}$

6.4 FRACTURE ANALYSIS

Nine organisations contributed results of stress and fracture analyses. Here contribution from Inspecta is briefly presented.

Both 2D and 3D analyses are used to predict the fracture events tests 1E4 ad 1E7. Constraint parameters T_{stress} and Q are evaluated for both crack tips of each test. The finite element program ABAQUS is used for the analyses. The responses of Load-Line-Displacement in the FEM analyses agreed very well with the test results. The crack driving forces and T_{stress} are calculated as a function of load for both tests. Constraint results of the tests indicate substantial loss of constraint at the shallow tips. Prediction of fracture events of the tests by using the standard Master Curve methodology gives conservative results. Considering the constraint values at the crack tips and making correction of the loss of constraint in the Master Curve methodology significantly improve the prediction of the fracture events in the tests.

Comparison of the results from different participants

Basic information about the FE calculations performed by the individual partners is given in Table 6.2.

Comparison of Force vs. LLD (CMOD) curves

Comparisons of calculated Force vs. LLD or Force vs. CMOD curves for individual partners were made for specimens 1E2, 1E4, 1E7. It was observed that all partners results show good agreement between experimental and calculated records in case of Force vs. LLD curves, see Fig. 6.3. However, in case of Force vs. CMOD curve (abnormal specimen 1E7), the 2D calculation clearly overestimates values of

force compared to the appropriate experimental force values. But in case of 1E7, also in two 3D calculations some overestimating of calculated values of force is seen (or may be deduced) compared to experimental values of force.

Table 6.2: Basic information on the analyses from different participants.

	Dimension of FE model	FE code	Model of crack front	Type of FE calculation	Specimens evaluated
AREVA NP	3D	ABAQUS	straight	elastic-plastic	1E2
BZLOGI	3D	MSC.MARC	straight, real	elastic-plastic	1E2, 1E4, 1E7
INSPECTA	2D, 3D	ABAQUS	straight	elastic, elastic-plastic	1E4, 1E7
IWM	2D	ABAQUS	straight	elastic-plastic	1E2, 1E4
ORNL	3D	ABAQUS	straight	elastic, elastic-plastic	1E2, 1E4, 1E7
TRACTEBEL	2D	SYSTUS	straight	elastic-plastic	1E2, 1E4, 1E7
VTT	3D	ABAQUS	real	elastic-plastic	1E7
NRI	3D	SYSTUS	real	elastic, elastic-plastic	1E2, 1E4, 1E7

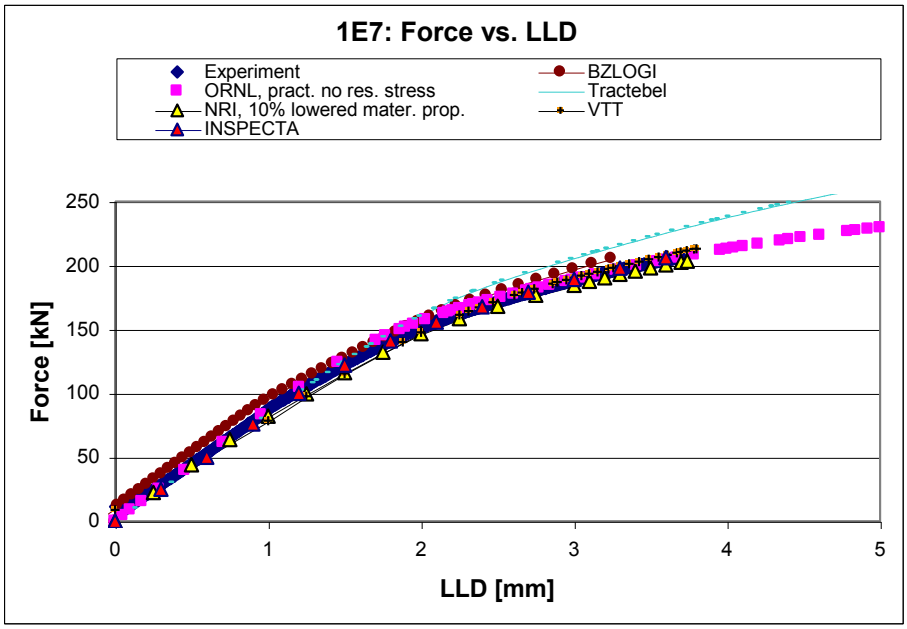

Fig. 6.3: Calculated Load vs LLD compared with the experiments.

Comparison of K_J development

Fig. 6.4 shows development of elastic-plastic stress intensity factor K_J (determined based on J) with loading. In these figures it may be clearly seen that ORNL, AREVA GmbH, INSPECTA and

TRACTEBEL did not model residual stresses, since their K_J-values start from zero (for zero bending load). In contrast to this, BZLOGI, IWM and NRI modelled residual stresses, their K_J-values are different from zero for zero bending load, and the only difference between these three partners results is that NRI assigned artificially negative values of K_J to those load levels when residual stresses dominate above the bending loading, i.e. closing of crack due to residual stresses prevails over opening the crack by bending loading.

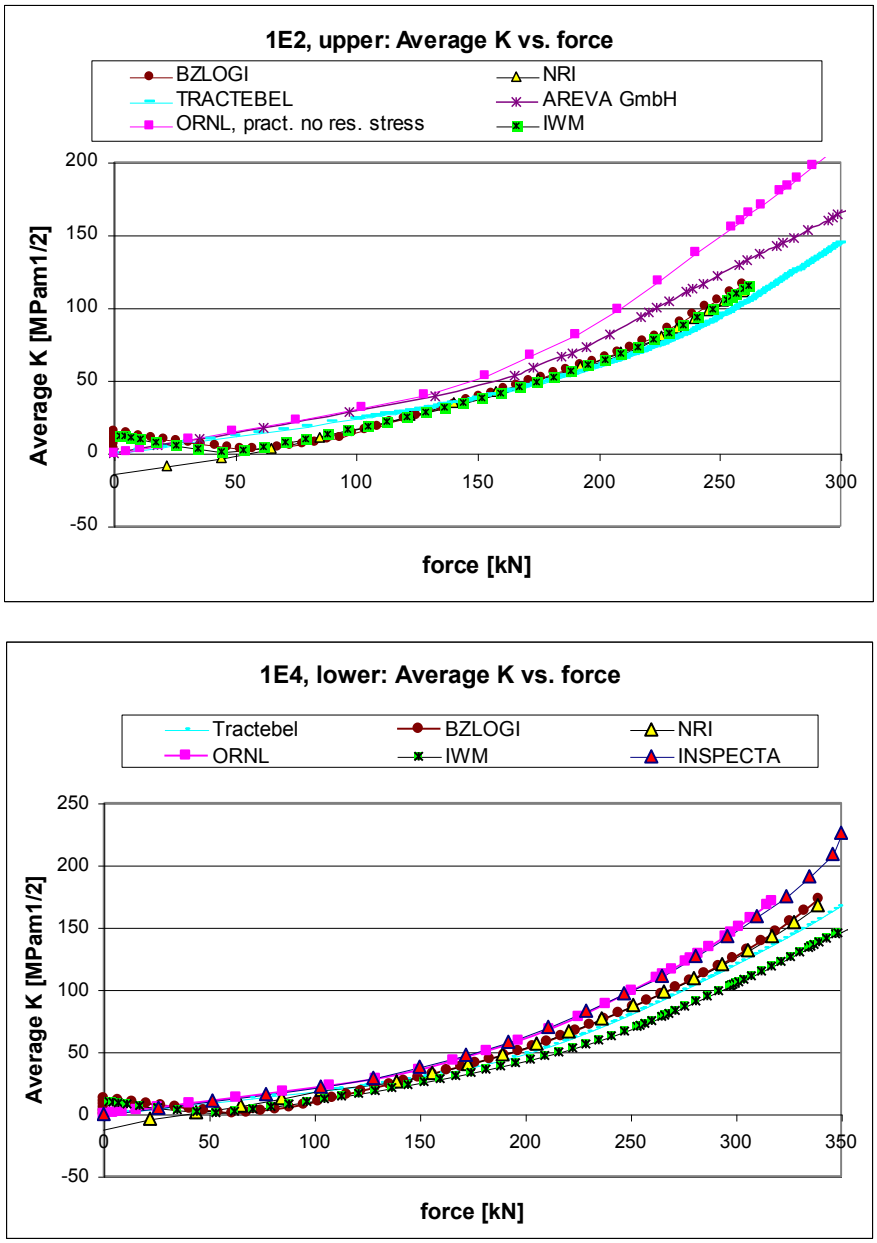

Fig. 6.4: comparison of K vs load obtained from different calculations.

Comparison of variation of K_J along crack front

Comparisons of variations of K_J along crack front are seen in Fig. 6.5. The results show basically decrease in J near the flank (free) surface, in some cases there are indications about small increase in tight vicinity of flank surface, which is of minor effect comparing to prevailing decrease of J when approaching the flank surface. The variation of J is, as expected, depending on whether real or straight

crack front was modelled, in case of straight crack front, the J-integral does not vary too much in the middle part of crack front. In case of modelling real crack front, J-integral varies moderately in dependence on real shape of crack front.

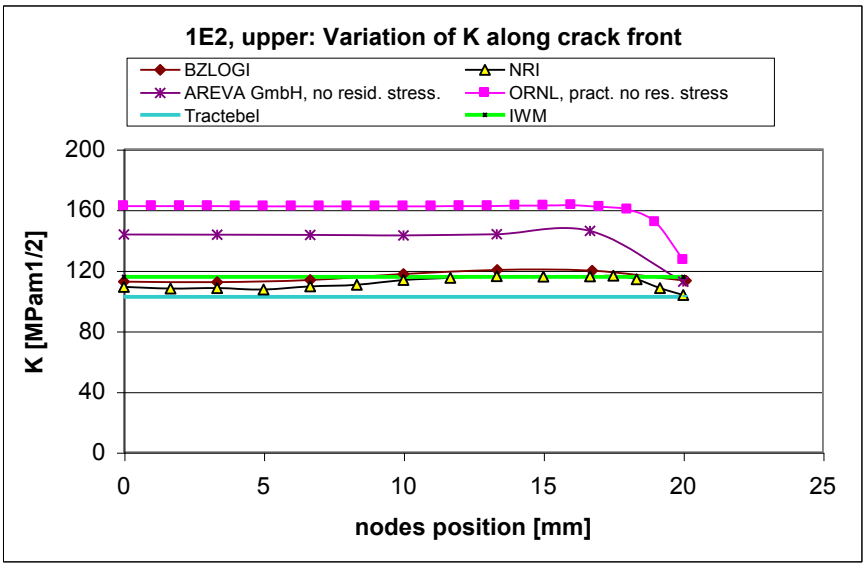

Fig. 6.5: Variation of K along the crack front obtained from different calculations.

6.5 SOME IMPORTANT OBSERVATIONS

Sensitivity of K_J to Modelling Assumption

Different parameter studies have been performed for K_J, allowing assessment of effects such as 2D vs.3D models, and straight vs. real crack fronts. 2D models produce lower values of K_J compared to 3D models (3D models are in general more precise), so, using 2D models as approximation of 3D ones is non-conservative. Modelling real crack front is more accurate than modelling straight crack front, but since model with straight crack front produces higher values of J than model with real crack front (which is conservative), it may be used as a conservative approximation of a model with real crack front.

Modeling residual stresses has also significant (non-negligible) effect on J-values, so, it is advisable to include them into the FE analysis. In the examined configuration (material properties, geometry of crack, loading conditions, etc.), omitting residual stresses in the model produced higher values of J compared to the case when they are modeled, and consequently, this approach was conservative with respect to prediction of J. However, in general (under different conditions), omitting residual stresses could be non-conservative.

Application of Master Curve Approaches for Fracture Initiation

Fracture initiation: the Master Curve (without constraint adjustment) provides a conservative prediction for fracture at upper tip; this confirms the presence of a constraint loss effect. The integrated Master curve approach for variable K_J should be checked.

Engineering Assessment Methods

Two types of assessment were carried out with the R6 FAD methodology:

- Predictions of expected behaviour – using a median or 50% value of the fracture toughness to calculate K_r. For this analysis, the point where the load line and the failure assessment curve intersect represents the expected or "average" failure load which would result if a series of identical buried defect specimens had been tested.

– Predictions of lower bound behaviour – using a lower bound, 2%, value of fracture toughness to calculate K_r. Here, the intersection of the load line and failure assessment curves provides a lower bound, conservative value for the failure load. In a conservative, R6 safety assessment, the specimen may be "unsafe" (at risk of cleavage) at the predicted lower bound load.

The conclusions were as follows:

- We need to add all the remaining PHARE tests to get statistical significance
- 1E4 and 1E7 appear to have failed at the collapse cut-off
- Constraint effects appear to be active at the upper tips of 1E4 and 1E7
- 1E2 has failed below the mean
- Need to compare R6 CDF with cracked body analyses
- Need to test Gao and Dodds approach

For assessments based on lower bound toughness values the lack of a constraint-modified toughness is a problem and the margins on constraint-modified assessments look a little slim. Fig. 6.6 shows the conventional and constraint-based R6 assessments of the tests.

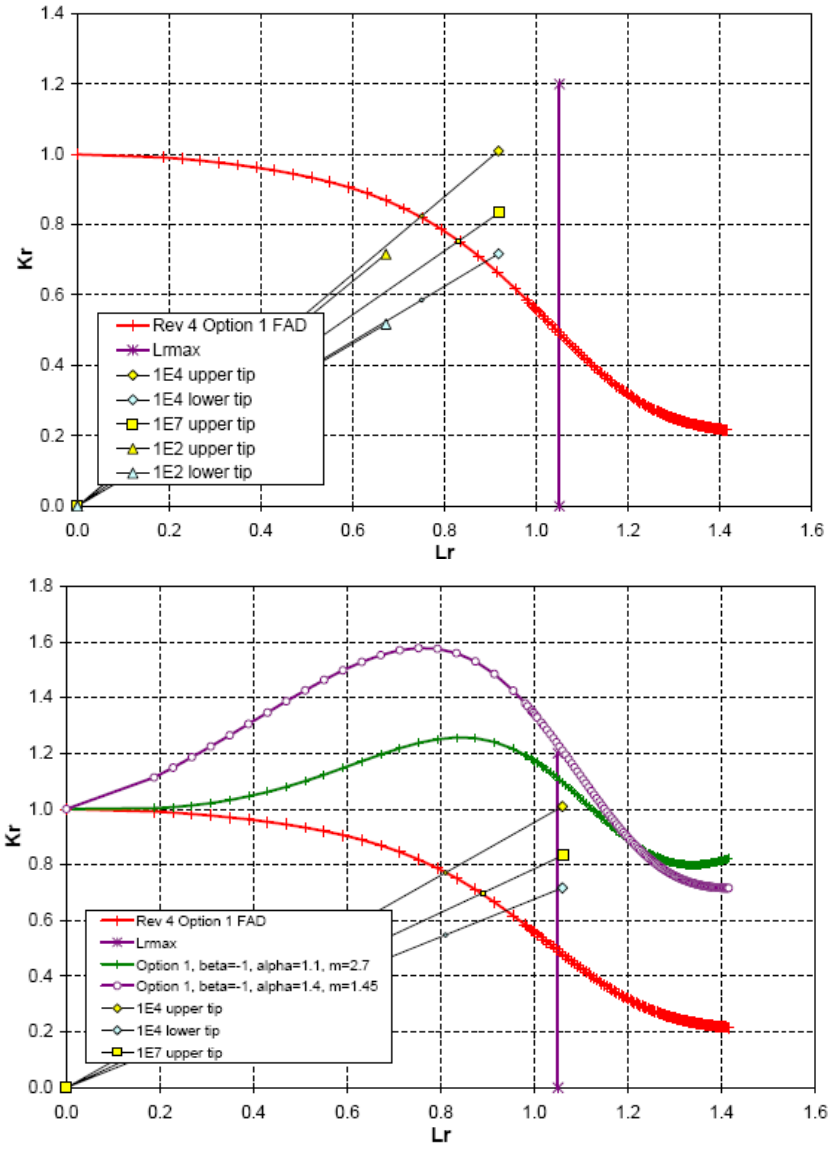

Fig. 6.6: Conventional and Constraint-modified R6 analyses of the tests.

7 Conclusions and recommendations

The NESC-I project

1. NESC-I has been a large scale project to evaluate the reliability of the entire process of structural integrity assessment, by examining all the key components including inspection accuracy and reliability, material properties data requirements, test measurement techniques, and the appropriate levels of complexity for thermal/*structural* analysis and fracture assessments. The experiment was designed to simulate selected conditions associated with an ageing, flawed reactor pressure vessel (RPV) subjected to severe pressurised thermal shock (PTS) loading.

2. The NESC-I test has demonstrated that, for the specific conditions considered, defects of up to 74 mm depth in material related to that of an ageing RPV would not propagate to cause catastrophic failure under a severe PTS-type thermal shock. This outcome was fully in line with the pre-test analysis forecasts.

3. Strict application of nuclear safety codes for the in-service assessment of the defects in the NESC-I spinning cylinder would typically allow defects with a maximum depth in the range of 1 to 9 mm. This is shown by the test outcome to include an apparently large margin of conservatism, and is attributed to the use of substantial safety factors as well as a lower bound representation of material fracture toughness.

4. The large through-clad defect produced several millimetres of ductile tearing, which proceeded the triggering of a local cleavage event at one end of the defect just below the cladding HAZ at 216 seconds into the PTS transient. This result further demonstrates that stable tearing consistent with small scale testing behaviour can occur in a thick component prior to cleavage fracture in the transition regime.

5. In the case of the large sub-clad defect no cleavage occurred, although it was found to have grown along the entire initial crack front. Fractographic investigations determined that a major part of this growth was by an unanticipated and as yet unexplained intergranular fracture mode.

6. The small amount of defect growth found in the three smaller sub-clad defects was also found to be intergranular in nature. The remaining defects, all below 12 mm in depth, showed no evidence of extension.

7. The results demonstrate the beneficial effect of the cladding in inhibiting cleavage initiation in the near-surface regions of the NESC-I cylinder. Comparison of the results with those from a previous spinning cylinder test, which did not contain cladding, demonstrates that it requires relatively higher loading to obtain cleavage fracture with cladding present.

8. The inspection trials undertaken without knowledge of what defects were present showed that the detection and sizing performance with ultrasonic techniques was good. In general, the detection performances achieved were better than the results obtained in the comparable PISC II trials a decade earlier, demonstrating the lessons learned and the good progress made.

9. The crack driving force estimates were found to vary by ±10% in the case of the detailed 3-D finite element analyses. In the case of the simplified analyses, considerable spread in maximum predicted CDF values was found.

10. It is recommended that the inspection system and personnel should be suitably qualified. In applying inspection procedures, precautions should be taken to reduce the incidence of human error as far as possible. This aim will be enabled by well-written, unambiguous procedures both for data acquisition and data analysis, good quality control and training (including on-the-job training) of the inspection personnel.

11. Where at all possible, fracture toughness data should be used for determining the reference temperature for the ductile to brittle transition behaviour. Indeed, it may be the only means to adequately describe behaviour in critical locations such as the thin near-surface region, for which formulations such as the ASME RT_{NDT} parameter cannot be applied due to the inability to obtain appropriate test data required by that parameter.

The NESC-II project

1. The NESC-II project considered two large-scale PTS tests on thick-walled cylinders fabricated of a 17 MoV 8 4 mod steel with a two-layer austenitic cladding on the internal surface. The base material was heat-treated to produce a low toughness, high transition temperature condition, as could occur in an end-of-life RPV.

2. The results of the NESC-II tests underline the inherent conservatism of existing defect assessment procedures for shallow RPV flaws and indicate the resistance of even degraded material containing simulated flaws to severe thermal shock loading.

3. The Master Curve method was used to describe the fracture toughness transition of the 17 MoV 8 4 mod steel, although its shape was found to be not particularly well suited for this type of low upper shelf material.

4. The code-based assessment routes considered indicated that a limiting defect size one order of magnitude below that used in the NP tests, underlining the value of the results in demonstrating the resistance to crack initiation of this material condition under PTS loading. The need for such procedures to be able to consider credible defect geometries, material characteristics and loading conditions was stressed, as in NESC-I.

5. Further work is needed to resolve the issue of size corrections to the standard Master Curve, in which T_o is referenced to a crack front of 25 mm. This was highlighted by the analyses of the large crack front length (~1370 mm) in test NP2.

6. The intergranular fracture mechanism observed in the NP2 test for the sub-clad defect needs further investigations.

The NESC-III project

1. This project studied the accuracy of structural integrity assessment procedures for defects in dissimilar welds of pipes. The NESC-III project was built around the conducted ADIMEW project to share its overall objectives.

2. The R6-method, option 1, can conservatively be used to estimate appropriate ISI-intervals.

3. The FEM-analysis predicts that the amount of stable crack extension will be significantly reduced if the component is subjected to load controlled conditions. The loading conditions in most structures are somewhere between the extremes of load control and displacement control. It is therefore conservative to use fracture toughness data corresponding to initiation of crack extension in order to calculate appropriate ISI- intervals. In case of judgements of real defects, an analysis of stable crack growth, e.g. based on J-Resistances curves, may be used in order to investigate if further safety margins exist.

4. The analysis shows that for the applied moment of the onset of crack extension from the defect in the buttering, the 316L parent pipe is at the same time subjected to extensive yielding. The results also indicate that it is very conservative to assume the lowest data of all involved materials when performing an R6-evaluation of the crack in the buttering. For a crack along the interface between HAZ and weld material it seems to be appropriate to use fracture toughness data of the weld material and the strength properties of the austenitic stainless steel pipe in order to evaluate the acceptable and critical crack size.

5. Weld residual stresses are in general of minor importance for the fracture behaviour of ductile material since relaxation of such stresses is expected to occur stable tearing. The results in this report indicate however that it is not necessary to know the exact levels and distributions of weld residual stresses in order to predict the critical crack size. On the other hand, weld residual stresses are still important in driving sub-critical crack growth due to stress corrosion. For estimation of appropriate ISI-intervals it is sufficient to use best-estimate weld residual distributions based on FE-solutions.

The NESC-IV project

1. The NESC-IV project has addressed the transferability of fracture toughness data from laboratory specimens to its use in integrity assessment methods for reactor pressure vessels subject to upset and normal loading transients, considering in particular the Master Curve approach.

2. A series of six biaxial bend feature tests on weld material specimens containing a shallow semi-elliptical surface flaw were successfully conducted, to produce cleavage fracture in the tests. A substantial database of mechanical and fracture properties data has been established for the PVRUF weld and plate materials and is available as an Excel workbook file.

3. The feasibility of generating fracture data for simulated embedded flaws was successfully demonstrated in a demonstration series of four uniaxial bend beam tests on plate material. All the tests ended in a brittle fracture event and it proved impossible to determine experimentally whether initiation had occurred first at the near surface tip or the deep tip.

4. The Master Curve provided an adequate description of the transition toughness under high constraint conditions for the materials used. In the case of the weld material, the bias in the To estimates between SEN(B) and C(T) specimens was greater than expected. This underlines the desirability of having fracture data as close as possible to the assessment conditions for best-estimates analyses.

5. Size correction to B = 25mm from a smaller test specimen thickness is a well established part of the Master Curve procedure. While NESC-IV did not produce specific data to judge the validity of applying the same correction procedure to longer crack lengths, it is noted the size-corrected assessments correlate slightly better with the test results and those not applying size correction.

6. The data from shallow-flaw SEN(B) specimens indicate effect of constraint loss in fracture toughness specimens can be described by a shift in To. The extent to which this effect is valid over a wider temperature range than that used in the tests themselves was shown in the case of the Plate 100 material to span a temperature range of To-35^{o}C to To+15^{o}C.

7. The RTTo reference temperature was found to be 10°C or more lower than the RTNDT value for all the materials considered and underlines the benefits of using direct measurement of fracture toughness for best-estimate analyses.

8. Detailed finite element analysis proved essential to analyzing both the feature tests. With measured stress-strain curves for the relevant materials over the relevant temperature range, it was possible to accurately predict the overall force-deformation of the test pieces. The estimates of KJc were generally within ±10%, which is similar to the inter-team consistency observed in the previous NESC-I and NESC-II projects.

9. Quantification of crack-tip constraint loss was studied principally via the T-stress and Q parameters. In the case of the uniaxial embedded flaw beams, both parameters predict increasing constraint loss with increasing load. In general, caution is essential before applying any constraint effect model to a geometry/loading regime for which its applicability has not been satisfactorily established.

10. The application of the R6 constraint modified procedure and the Wallin T-stress model were verified for the embedded flaw beam tests. The prediction that the load carrying capacity at temperatures in the range of To is increased by over 30% is supported by the experiment results. The Wallin model has a major advantage in the fact that no calibration data is needed; however its assumption that constraint loss is directly proportional to T-stress is not supported by the NESC-IV

data for T-stress/σy values in the range -0.4 to 0, i.e. for low applied loads and when the constraint loss effect is modest.

11. The local approach Beremin model using the Weibull stress was successfully calibrated from fracture data for the SEN(B) a/W = 0.5 and a/W = 0.1 geometries by applying the G-R-D procedure, although the value of the Weibull parameter m proved sensitive to whether the Weibull stress term was defined in terms of the crack opening stress or the hydrostatic stress.

The NESC-V project

1. The work of NESC-V aims at preparing the foundation of a European procedure for the handling of thermal fatigue of NPP components. It is evident that the common standards (such as ASME etc) provide only vague guidance, especially for high cycle fatigue. It has been a main ambition that the groups work should reflect the multi-disciplinary character of the subject. The work is primarily based on existing knowledge. The systematic collection and analysis of field experience aims at providing an overall picture of the important parameters. Experience from experimental work throughout Europe has also been gathered. These experiments normally highlight a specific issue of thermal fatigue.

2. Several aspects of thermal fatigue are covered in the report. Load handling, cyclic plasticity, fatigue curves and correction factors are a few examples. Two parts are, however, central. One such part considers previous field experience of thermal fatigue problems. A database of failure cases was set up. The other consists of the development and evaluation of a model for the analysis of thermal fatigue at turbulent mixing. The model is used for predicting the time to crack initiation in tee junctions and also provides threshold values on the nominal temperature values. The model is based on a simplification of the highly complex load state at turbulent mixing. Other load states, such as thermal cycling at stratification, are possible to analyse with CFD.

3. Thermal fatigue is governed by some dominating damage parameters which are examined in the report. An important result is the discussion about conditions for deep cracking. Thermal fatigue in general leads to surface cracking with arresting cracks. However, under certain conditions cracks can penetrate a wall within relatively short time. It is argued that three dimensional thermal distributions that are due to large scale instabilities at low frequencies are important. This type of load arises for example with thermal cycling of non-symmetric temperature distributions such as stratification. High risk locations are to be found were turbulent mixing combine with large scale instabilities. On example is turbulent penetration in a pipe section with nominally stagnant fluid.

4. No rigorous instructions for the solution of thermal fatigue problems are given. This has yet to be done due to the complex nature of the subject. Load assessment is the main difficulty. It is clear that the perspective on thermal fatigue will differ between countries and a common view is not at hand. Therefore room is given for the outline of the different national approaches.

5. The report summarizes a vast experience and many aspects on thermal fatigue. It is hoped that the report will provide valuable guidance and support for the handling of thermal fatigue. A significant outcome is the observation that almost all thermal fatigue failures are due to unforeseen causes. Hence there is an increased need for an improved risk analysis where risk locations can be identified, along with quantification of the level of risk. Further work should provide an even more comprehensive basis for assessing the different aspects of thermal fatigue damage assessment and mitigation measures. An important task would be the analysis of low frequency phenomena, such as stratification to support better understanding of these phenomena. The coupling between the thermal load and the structural load is a key question for future studies.

The NESC-VI project

1. Development of K_J with loading represents a certain problem – minor discrepancies were found that were not explained (within this conclusion we disregard one reason of discrepancies in K_J consisting in different input conditions - modeling/not modeling residual stresses, which is a separate issue). In

general, a particular conclusion may be drawn that 2D FE model underestimates K_J values, and thus it is not recommendable to be applied (it is not conservative). On the other side, modelling straight crack front appeared to be an acceptable conservative approximation.

2. Quantification of crack-tip constraint loss was studied principally via the elastic *T*-stress, elastic-plastic *T*-stress and *Q* parameters. All three parameters predict increasing constraint loss with increasing load. Using of all three constraint parameters showed large difference in constraint states between the upper (shallow) and lower (deep) crack fronts.

3. The application of the R6 constraint modified procedure was verified.

4. Modelling residual stresses has non-negligible effect, in the examined case omitting residual stresses in FE model represents a conservative approach (with respect to prediction of *K*) , but in general conditions it need not be the case. Thus modelling residual stresses is a more precise approach and recommendable.

5. Using local approach (similarly as using two-parameter fracture mechanics approach mentioned above) showed large difference in constraint states at lower and upper crack fronts – significantly higher loss of constraint was found at the upper (shallow) crack front than at the lower (deep) one. This finding is evidently correct and corresponds to behaviour of specimens during experiments.

6. As a success in the evaluation of the results may be considered the fact that the backgrounds of determination of elastic *T*-stress at individual partners were elucidated, and after the appropriate clarification of circumstances under which the elastic *T*-values were determined, the elastic *T*-stress values have become quite close each to other. Also, the attention of the partners was attracted to the problem arising in combination of elastic *T*-stress with results of elastic-plastic calculation (and experiment), and a consensus on solution of this problem is expected. This consensus may be also considered as an outcome of the current NESC VI project.

REFERENCES

[I-1] Sattari-Far, I and Dahlberg, L., (1998), “Pre-test fracture assessment of the NESC-I spinning cylinder under a PTS transient”, Int. Jour. Pres Ves & Piping, Vol. 75, pp. 203-212.

[I-2] NESC DOC DEAG, (1999), “Description of the Defects Present in the NESC-I Cylinder”, NESC DOC DEAG (99) 01.

[I-3] Schofield, J.S. and Swan, D.I., (1999), Probabilistic assessment of the NESC-I spinning cylinder experiment, NESCDOC TG3 (99) 06.

[I-4] Rimtamaa, R. and Planaman, T., (1999), “NESC-I spinning cylinder test- Evaluation report of matrial characterization”, NESCDOC TG2 (99) 03.

[I-5] NESC-I Project, (2000), “Thermal and structural analysis of the spinning cylinder”, NESC DOC TG3 (99) 10, JRC, European Commission.

[I-6] Keim, E., et al, (2000), “NESC I Spinning Cylinder Project: Residual Stress Measurement”, EUR 19649/EN , JRC, European Commission.

[II-1] Taylor, N., (2000), “Summary of NP2 Pre-Test Analysis”, NESC DOC TG3 (2000) 03.

[II-2] Sattari-Far, I., (2000), ”Fracture mechanics analysis of NESC-II experiments”, RSE R&D Report No. 2000/04, Det Norske Veritas, Stockholm, Sweden.

[II-3] Stumpfrock, L. et al, (2003), “Brittle crack initiation, propagation and arrest of shallow cracks in clad vessel under PTS loading”, Report EUR 20696 EN, European Commission DG-JRC/IE, Netherlands.

[II-4] NESC-II Project, (2003), “Brittle crack initiation, propagation and arrest of shallow cracks in clad vessel under PTS loading”, NESC DOC MAN (02) 07, JRC, European Commission

[III-1] Andersson, M. and Gunnars, J., (2004), Residual stresses in heat treated bi-metallic pipe weld, NESC III /ADIMEW, RSE R&D Report No 2004/07, rev 0, DNV.

[III-2] GILLES, P., Framatome ANP, (2004), “ADIMEW Project: Framatome-ANP, Post-Test Analyses, Ductile tearing analysis of a cracked 16” Dissimilar Metal Weld junction, Minutes of the 7th NESC-III Project meeting.

[III-3] Minnebo, P., (2004), Materials Characterisation Activities, TG2 Summary JRC, Minutes of NESC-III Project Meeting, Annex 3, p.16-19.

[III-4] Gros, X., N. Taylor, C. Faidy NESC III, (2005), Project Overview (First draft), JRC-Petten, European Commision.

[III-5] NESC-III Project, (2006), “Assessment of Dissimilar Weld Integrity, Final Report of the NESC-III Project, European Commission JRC, EUR 22510 EN.

[IV-1] Nilsson, K-F. and Bass R., (2001), “NESC-IV Pre-Test Problem Definition Document”, NESCDOC TG3 (2001) 01.

[IV-2] Bass, B R et al, (2002), "Biaxial bend fracture tests on a forged ferritic steel", Vocalist and NESC-IV Test Report.

[IV-3] Nilsson, K.-F. et al, (2002), “NESC-IV Post-Test Problem Definition Document”, NESCDOC TG3 (2002) 05, July 2002

[IV-4] NESC-IV, (2004), “NESV-IV Database Version 7.1”.

[IV-5] Sattari-Far, I., (2004), Post-Test Analysis of Uniaxial And Biaxial Tests of NESC-IV (Final FEM and R6 analyses), Annex 1, Minutes of the NESC-IV Progress Meeting, Lymm (UK), January 2004, NESC DOC (04) 01.

[IV-6] NESC-IV Project, (2005), “An investigation of the transferability of master curve technology to shallow flaws reactor pressure vessel application”, NESC-IV Report No. 4 (05), JRC, European Commission.

[V-1] M. Dahlberg, K.-F. Nilsson, N. Taylor, C. Faidy, U. Wilke, S. Chapuliot, D. Kalkhof, I. Bretherton, M. Church, J. Solin, J. Catalano, Development of a European Procedure for Assessment of High Cycle Thermal Fatigue in Light Water Reactors: Final Report of the NESC-Thermal Fatigue Project, EUR 22763 EN, 2007.

[VI-1] Pistora, V., Lauerova, D. and Taylor, C., (2008), Benchmarkanalysis for fracture mechanics methods for assessment of sub-clad flaws, (First draft of final report), JRC-Petten, European Commision.

2011:05

The Swedish Radiation Safety Authority has a comprehensive responsibility to ensure that society is safe from the effects of radiation. The Authority works to achieve radiation safety in a number of areas: nuclear power, medical care as well as commercial products and services. The Authority also works to achieve protection from natural radiation and to increase the level of radiation safety internationally.

The Swedish Radiation Safety Authority works proactively and preventively to protect people and the environment from the harmful effects of radiation, now and in the future. The Authority issues regulations and supervises compliance, while also supporting research, providing training and information, and issuing advice. Often, activities involving radiation require licences issued by the Authority. The Swedish Radiation Safety Authority maintains emergency preparedness around the clock with the aim of limiting the aftermath of radiation accidents and the unintentional spreading of radioactive substances. The Authority participates in international co-operation in order to promote radiation safety and finances projects aiming to raise the level of radiation safety in certain Eastern European countries.

The Authority reports to the Ministry of the Environment and has around 270 employees with competencies in the fields of engineering, natural and behavioural sciences, law, economics and communications. We have received quality, environmental and working environment certification.

Strålsäkerhetsmyndigheten
Swedish Radiation Safety Authority

SE-171 16 Stockholm
Solna strandväg 96

Tel: +46 8 799 40 00
Fax: +46 8 799 40 10

E-mail: registrator@ssm.se
Web: stralsakerhetsmyndigheten.se